UNIVERSITY OF BIRMINGHAM

HUMAN LOWER LIMB MOVEMENT PREDICTION BASED ON OPTIMAL CONTROL

by

WEIDA WANG

A thesis submitted to

The University of Birmingham

for the degree of

DOCTOR OF PHILOSOPHY

Department of Mechanical Engineering

School of Engineering

College of Engineering and Physical Sciences

University of Birmingham

June 2024

Abstract

The movement behaviour of the human body can be predicted by solving an optimal control problem, however, many limitations exist, for example, only certain movement behaviour such as level walking has been undertaken, and these predictions are often limited to able-bodied individuals. This thesis aims to advance existing predictive simulation studies, using optimal control theory to achieve prediction for both disabled individuals and able-bodied individuals.

There are significant technical challenges in predicting sit-to-stand motion for people with lower limb amputations, making it rare for researchers to delve into this field. The predictive study of sit-to-stand motion for the unilateral transtibial amputees completed in this thesis is the first in this field. This study not only modelled seat contact, but also created a novel "free fall method" to determine the initial and final postures of the motion, which is key for successful predictions. On this basis, using the established simulation framework, the motion behaviour under nominal prosthetic stiffness was first predicted, and then the effects of changing prosthetic stiffness were studied. Finally, several scientific conclusions were drawn.

Limited ankle dorsiflexion is a common problem due to ankle injuries and surgical operations, greatly affects our mobility. This thesis is the first to complete the predictive study on the sit-to-stand movement behaviour for people with ankle dorsiflexion limitations. The prediction of sit-to-stand motion was formulated as an

optimal control problem and solved by the direct collocation method. Subsequently, the effects of different levels of ankle dorsiflexion limitation were studied, revealing the corresponding biomechanical compensation strategies. The nature of no experimental data required as input makes our predictive study eliminate the lengthy tests in the laboratory or clinical settings, with great potential to benefit the development of new interventional treatment for people with ankle joint impairments.

The objective function is the important component of the optimal control problem. However, the weights of different terms in the objective function are often adjusted manually, imposing a substantial burden in terms of time and labour. To address this problem, this thesis integrated the inverse optimal control method with the muscle-driven musculoskeletal dynamics model to investigate muscle coordination during the transition from squatting to standing. A nested bilevel optimisation algorithm was proposed to solve the inverse optimal control problem. The proposed bilevel optimisation algorithm effectively addressed the complex muscle coordination problem during human motion, providing a new approach for studying muscle coordination patterns.

The new model and algorithm proposed in this thesis effectively fill various gaps in the existing human lower limb predictive simulation studies and have great potential in the customisation of rehabilitation programs, design of assistive devices and development of bionic robots. In addition, the achievements in this thesis have important reference significance for predicting movements in other scenarios.

Dedication

I dedicate this PhD thesis to my parents, for their selfless love and encouragement behind me.

Acknowledgements

I would like to express my sincere gratitude to my supervisor Dr. Ziyun Ding for her great guidance and selfless help during my doctoral studies. From the selection of scientific research direction to paper writing skills, Dr. Ding gave me many valuable opinions and suggestions, which benefited me a lot. To promote my academic progress, Dr. Ding extensively mobilised various resources and built an academic exchange platform to enrich my academic thoughts. When I was accidentally injured and in extreme physical and mental pain, Dr. Ding warmly encouraged me to be tenacious and overcome the disease. At the same time, considering my mobility difficulties, Dr. Ding specially opened the online meeting channel for me to provide academic guidance and communication, which enabled me to overcome numerous difficulties and pressures and finally complete my PhD studies successfully.

I would like to thank my second supervisor, professor Duncan ET Shepherd, for his enthusiastic guidance and help in my academic research and life.

I would like to thank all my colleagues in the research group for their support and help: In my research project titled " Muscle-Driven Simulation of the Transition from Squatting to Standing Using Inverse Optimal Control ", Dr. Jiayu Hu and Mr. Qingyao Bian helped me collect experimental data and provided relevant suggestions for the project; Mr. Khalid Alsayed also gave me enthusiastic care and help in my daily life. At the same time, I would like to express my sincere gratitude to all the subjects who

participated in the experiment!

When I started learning the optimal control theory of human movement, I had exchanges and discussions with several scholars in the field, which enabled me to quickly consolidate the basic knowledge and master the relevant concepts. For this, I would like to express my sincere gratitude to professor Kui Xiang, professor Biwei Tang, professor Muye Pang, Dr. Size Zheng and other scholars.

Pursuing a PhD is a challenging journey in life. I am grateful to my parents for their selfless dedication and support. I would like to express my special gratitude to my father. When I was stuck in a difficult situation in scientific research, he used philosophical thinking to inspire my academic thoughts, relieve my confusion and pressure, and gave me endless motivation for scientific research. These became the golden keys that helped me open the door to success.

During my doctoral studies, I received funding from the School of Engineering at the University of Birmingham for tuition fees and support from the China Scholarship Council for living expenses. Without these financial support, I would not have been able to complete my PhD studies. Here, I would like to express my sincere gratitude to them!

The academic research achievements of many predecessors in the field of human movement biomechanics have provided me with rich academic nutrition and laid a solid foundation for completing related research projects. Here, I would like to express my deepest respect to them!

Last but not least, the examiners have put in hard work to review this thesis and provided valuable suggestions for future research. Here, I would like to express my deepest respect and gratitude!

Table of Contents

List of Illustrations

List of Tables

Academic Output

[1] Weida Wang, Jiayu Hu, Biwei Tang, Duncan Shepherd and Ziyun Ding. Muscle-Driven Simulation of the Transition from Squatting to Standing Using Inverse Optimal Control. IEEE Transactions on Biomedical Engineering. (Under review)

[2] Weida Wang, Ziyun Ding, Anthony Bull and Duncan Shepherd. Sit-to-stand Optimal Control Prediction Considering Seat Contact for the Unilateral Transtibial Amputee: a Novel Optimisation Framework Based on Direct Collocation. Proposed journal for submission: Nature or Science Robotics. (In preparation)

[3] Weida Wang, Ziyun Ding. Predictive Simulation of Sit-to-stand Movement for People with Ankle Movement Impairments Using Optimal Control. Proposed journal for submission: IEEE Robotics and Automation Letters. (In preparation)

Chapter 1. Introduction

1.1 Research background and motivations

The health level of the lower limbs is closely related to the person's mobility. Abnormal lower limb function will seriously reduce the person's mobility. Studying lower limb movement behaviour through biomechanical theory can not only deepen our understanding of movement mechanisms, but also provide valuable references for clinical medicine, rehabilitation training, and assistive device design. The emergence of computer simulation technology has greatly accelerated the development of the field of human movement biomechanics. However, traditional simulation studies often use experimental measurement data as calculation input, which greatly limits the scope of research. Experimental measurements usually consume a long period of time and are difficult to carry out in many cases. In contrast, predictive simulation research is conducted from the perspective of motor control and optimal control theory, making it possible to generate new motion behaviours without experimental data. The strong superiority demonstrated by predictive simulation has attracted increasing attention from biomechanical scholars in recent years. Unfortunately, its high technical barriers often discourage researchers, resulting in limited research and several unresolved issues in this field. For example, existing predictive simulation research focuses more on the normal walking behaviour of the human body, with less attention paid to other common activities of daily living; the

research subjects are usually healthy people, and there are few studies on the movement behaviour of amputees and other lower limb dysfunctions patients. In addition, the weights of different objective function terms in predictive optimal control problems are often adjusted through inefficient manual trial and error, so there is an urgent need to develop more efficient and accurate adjustment methods. The bilevel optimisation method established in this thesis can meet this requirement well. Therefore, based on optimal control theory, this thesis conducts predictive research on human lower limb movement behaviour, in order to fill the research gaps in this field and make up for the shortcomings of existing research.

1.2 Research objectives and significance

Based on the optimal control theory, this thesis conducts a series of research work around the predictive simulation of human lower limb movements. The specific research objectives and significance are as follows:

1) To develop a simulation framework for predicting the sit-to-stand motion behaviour of unilateral lower limb transtibial amputees considering seat contact. The "free fall method" proposed in this simulation framework is the first of its kind and has pioneering significance in inspiring similar simulation studies.

2) To explore the effect of changes in prosthetic stiffness on the dynamic behaviour of sit-to-stand motion in unilateral transtibial amputees. This is the first study to explore the effect of changes in prosthetic parameters on the sit-to-stand

movement behaviour of lower limb amputees through predictive simulation. It breaks the traditional research method that relies on continuous trial and error in the laboratory and has great potential in prosthetic design and other fields.

3) To develop a predictive simulation framework for predicting the sit-to-stand movement of people with unilateral ankle dorsiflexion limitation, and to explore the effect of different levels of ankle dorsiflexion limitation on dynamic behaviour. This is the first predictive study on the movement behaviour of people with unilateral ankle dorsiflexion restriction, providing a new approach to studying pathological behaviour after ankle injury and valuable reference for clinical medicine and rehabilitation treatment.

4) To develop a novel optimisation simulation framework to alleviate the burden of manually adjusting the weights of objective function terms in the optimal control problem of human motion prediction. This is the first study on the inverse optimal control problem of muscle-driven movement from squatting to standing, which achieves accurate prediction of human motion trajectories. It is of great significance for understanding muscle coordination during the squat-to-stand motion and inspiring the design of bionic robots.

1.3 Overview of this thesis

The subsequent chapters of this thesis are organised as follows:

The literature review in Chapter 2 summarises the relevant theories and

research progress of human motion biomechanical simulation. The focus is on summarising the modelling methods of multi-body dynamics, the research progress of predictive simulation, and the algorithms for solving optimisation problems.

Chapter 3 conducts a predictive study on the sit-to-stand motion behaviour of the unilateral lower limb transtibial amputee considering seat contact. A novel predictive simulation framework is established in this chapter and verified by comparing with experimental data. Subsequently, based on the established simulation framework, the effects of varying prosthetic stiffness on the patient’s dynamic behaviour are further explored.

Chapter 4 conducts a predictive study on the sit-to-stand movement behaviour of people with unilateral ankle dorsiflexion limitation. A predictive simulation framework is established, and the effects of different levels of dorsiflexion restriction on the patient's dynamic behaviour are subsequently investigated.

Chapter 5 conducts research on the inverse optimal control of muscle-driven human movement from squatting to standing. An inverse optimal control simulation framework is established and the muscle coordination patterns during the motion are explored.

Chapter 6 summarises the research work of this thesis and provides prospects for future research directions.

Chapter 2. Literature Review

2.1 Introduction

Common software used for simulation research on human motion biomechanics include OpenSim [1–3], Anybody [4, 5], BoB [6], Freebody [7], and so on. As an open-source software developed and continuously maintained by Stanford University's Biomechanics Laboratory, OpenSim has powerful simulation capabilities and a large amount of learning resources, making it widely adopted by many scholars in the field of biomechanics. All OpenSim modellers can share models and datasets underpin the model on the platform. In addition, OpenSim has added new modules and continuously improved them in recent versions, which can realise the prediction of human motion. Therefore, the OpenSim simulation platform was chosen to carry out the research work in this thesis. In order to ensure a good connection with the research work in the following chapters, this chapter focuses on describing the relevant progress related to OpenSim while taking into account the comprehensiveness of the review.

2.2 Multi-body Dynamics Model and Related Theories

2.2.1 Topological Structure of the Biomechanical Simulation Model

For biomechanical research on human movement, the deformation of the human

skeleton can be ignored, and rigid body dynamics theory is usually used for computational analysis. In OpenSim, human body segments are modelled as multiple rigid bodies with certain mass and inertia, and joints are established between different bodies to achieve mutual connection. Joints are responsible for achieving relative motion and force transmission between different bodies. The selection of joint types is usually based on the degrees of freedom required for human movement. Various types of forces can be simulated by force elements in the model, which can be divided into active and passive types according to their characteristics. The active force elements can actuate joints to perform active movement, and the passive force elements can be used to simulate the passive forces and contact forces. Figure 2.1 schematically illustrates the topological structure of a multi-body dynamics model used for simulating walking.

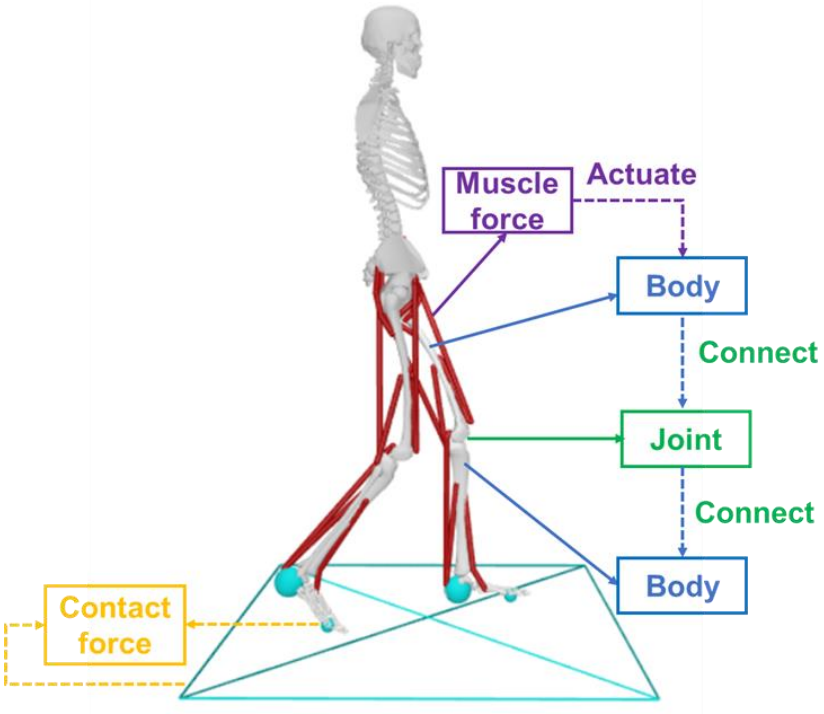

Figure 2.1. Topological structure of a multi-body dynamics model in OpenSim.

2.2.2 Driving Methods of Model Motion

The lower limb joints mainly perform rotational movements, and their kinematic behaviour is affected by the torque acting on them. The driving methods of multi-body dynamics models can be divided into two types: torque driven and muscle driven.

Torque driven

The torque actuator directly outputs torque to drive the joint rotation. The output torque can not only simulate the total joint moment contributed by the relevant muscle groups, but also represent the motor torque in the exoskeleton device. When establishing a simulation model, if we focus on analysing human kinematics and the total joint moments without caring about the dynamic behaviour of specific muscles, the torque driven method is a good choice. Compared with the muscle driven method, torque driven can significantly reduce the number of actuators in the model, while avoiding the calculation of complex muscle dynamics equations. Therefore, it can greatly improve the efficiency of simulation calculations and reduce the difficulty of convergence.

Muscle driven

In the muscle-driven method, the movement of the skeleton is driven by the tension generated by the attached muscle-tendon actuators. Furthermore, changes in the position of the skeleton will in turn change the kinematics of the muscle-tendon

actuators, thereby affecting the actuation forces. This driving method can not only simulate the force situation of the human body in more detail, but also obtain the contribution of each muscle to the movement. Obviously, the mechanical model of the muscle-tendon actuator plays an important role in muscle driven simulation.

In 1989, Zajac *et al.* [8] published a milestone paper on the Hill-type muscle model (see Figure 2.2). In this paper, the macroscopic and microscopic structures of muscle were first explained in detail. Subsequently, the force-length and force-velocity relationship curves of muscle fibres were presented, and a muscle contraction dynamics model composed of three elements was discussed. The activation dynamics model was abstracted as a first-order differential equation that converts input muscle excitation into muscle activation. As the bond between muscles and bones, the mechanical properties of tendons can affect the performance of muscle-tendon actuators, so they also proposed a mechanical model for tendons. Finally, they investigated the static and dynamic properties of the muscle-tendon actuator. Overall, this paper comprehensively discussed the relevant concepts and calculation methods of the Hill-type muscle model, laying a solid foundation for subsequent scholars to conduct muscle driven simulation research.

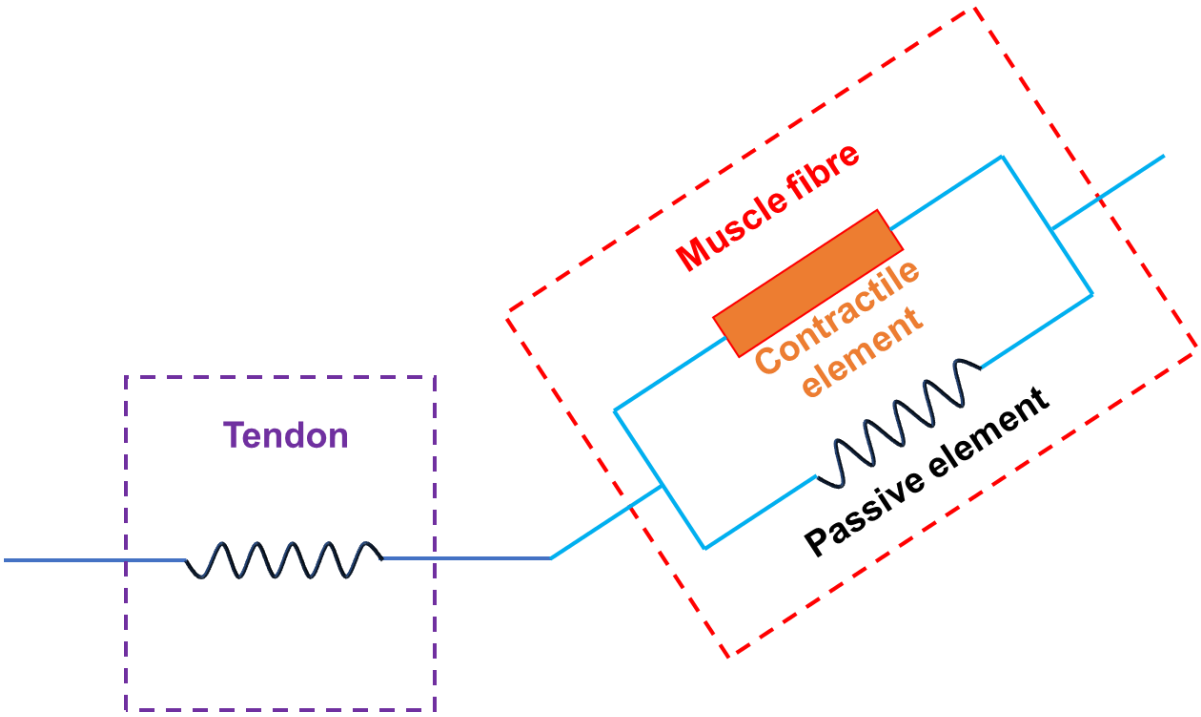

Figure 2.2. Hill-type muscle model. Adapted from [8].

For muscle-driven simulation studies, researchers often make appropriate modifications to the classic Hill-type muscle model based on the characteristics of the research problem and the need for computational efficiency. Millard *et al.* [9] developed two variants based on the classic Hill-type muscle model and evaluated the computational accuracy and efficiency of these models under different conditions. In the first variant model, damping force was added to the muscle fibres, which enhanced the numerical stability during the calculation process and improved the calculation speed compared to the classic model. The second variant assumed that the tendon length could not be changed, resulting in a more significant improvement in computational efficiency. However, the application scope of this variant is relatively limited, and acceptable calculation accuracy will only be achieved when the tendon

slack length is shorter than or equal to the optimal fibre length. These research results can provide some guidance for the selection of muscle models. The classic and variant muscle-tendon actuator models in their study have been integrated into OpenSim, and researchers can select appropriate models as needed to carry out their own simulation research.

To improve the robustness of solving optimal control problems through direct collocation method, Groote *et al.* [10] proposed a modified muscle-tendon actuator model based on the Winters' activation dynamics model [11, 12] and the Hill-type contraction dynamics model [8]. They first smoothed the transition between muscle activation and deactivation in the activation dynamics model. The muscle force-length, muscle force-velocity, and tendon force-length relationship curves were subsequently modified to enhance their differentiability, which facilitates gradient-based optimisation calculations. On this basis, four formulations of contraction dynamics were constructed through pairwise combinations of different types of dynamic equations and state variables. Specifically, the dynamic equations can be expressed in explicit and implicit formats, and the state variable can be selected from the normalised tendon force and the normalised muscle fibre length. In addition, they introduced additional control variables to the implicit dynamic equations. They found that when the muscle contraction dynamics equation is expressed in an implicit format, the solution to the optimal control problem can converge robustly. In contrast, expressing the equation in an explicit format may not achieve convergence in some

cases. The muscle-tendon actuator model, which was improved by them, makes it more efficient to solve the muscle driven optimal control problem through the direct collocation method.

2.2.3 Contact Model

The human body will inevitably interact with the external environment during movement, such as possible contact between feet and the ground, as well as contact between buttocks and the chair. In the absence of experimental data on external forces, it is necessary to reflect these contact forces by establishing contact models.

Two classic compliant contact force models (see Figure 2.2) are implemented in OpenSim [2]. The first model is called the Hunt-Crossley force model. This model is mainly based on Hertz contact theory [13] and Hunt-Crossley theory [14], and is suitable for contact force calculation between simple geometric shapes such as spheres and planes. The normal component of the contact force can be obtained by the sum of two terms. The first term reflects the effect of the Hertz contact force, which is related to the material properties of the contact pair and the depth of mutual penetration. The second term represents the Hunt-Crossley dissipation force, which can be determined by the materials' dissipation properties, the penetration velocity, and the Hertz contact force. The tangential component of the contact force reflects the friction between the contact pairs, which can be calculated based on the Stribeck friction curve and the normal contact force [15].

The Hunt-Crossley model has strict restrictions on the geometric shape of the contact pair. The second contact model, which is based on the elastic foundation theory [16, 17], can break this limitation. In this model, the geometries in the contact pair can be presented as arbitrary shapes. After discretizing the surfaces of the contacting geometric bodies into several triangular meshes, a spring can be placed at the centroid of each mesh to generate contact force.

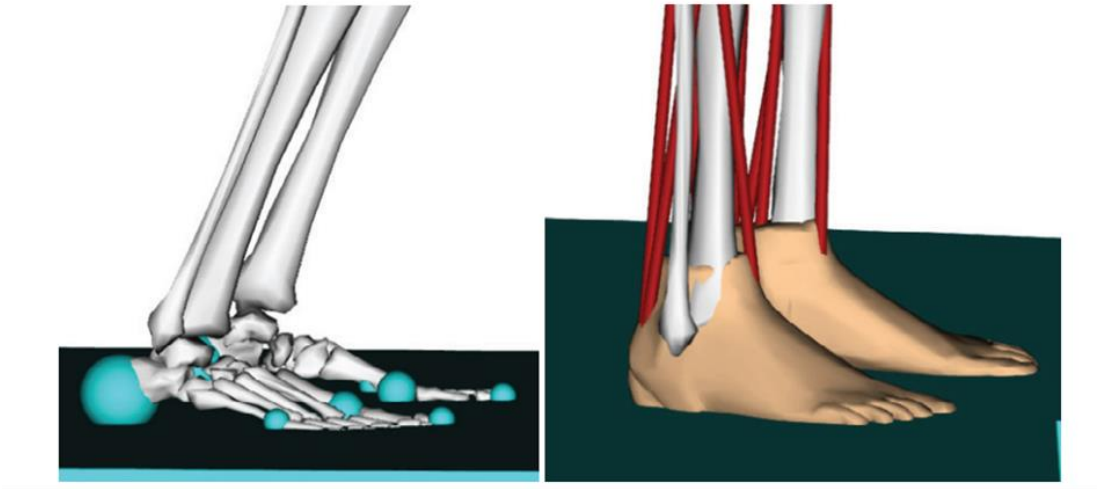

(a) (b)

Figure 2.3. Two classic compliant contact force models [2]. (a) Hunt-Crossley model. (b) Elastic foundation model.

Foot-ground contact and buttocks-chair contact can be simplified to the contact problem between the sphere and half-space, which is suitable for solving through the Hunt-Crossley force model. However, at the position where the contact sphere just leaves the surface of the half-space, there is a problem that the normal contact force curve is not differentiable. In addition, the original Stribeck curve used to solve the friction coefficient is not smooth. Since the solution of gradient-based optimisation is

very sensitive to the differential characteristics of the curves, the existence of the above problems will have adverse effects on the application of this model in gradient-based optimisation problems. To address these issues, Serrancolí *et al.* [18] smoothed the normal contact force curve and the Stribeck curve to obtain a smooth Hunt-Crossley force model, which can improve the numerical stability of the gradient-based optimisation solution process.

2.3 Classification and Methods of Simulation Problems

In-silico simulation is an important approach for conducting biomechanical research on human motion. For a specific research problem, choosing an appropriate simulation method is particularly critical. Simulation problems can be roughly divided into two categories: one is simulation based on experimental data; the other is predictive simulation of motion, which can be completely independent of experimental data. The commonly used solution methods and related research progress for these two types of simulation problems will be discussed in detail below.

2.3.1 Simulation Based on Experimental Data

Some important mechanical variables, such as joint moments and muscle forces, are difficult to measure directly through experimental instruments during human movement. However, for these variables of interest, we can solve them indirectly by combining other available relevant experimental data with multi-body dynamics theoretical calculations.

Inverse kinematics

The generalised coordinate values (usually joint angles) of the human body during movement can be obtained through inverse kinematics calculation. During the experiment, several reflective markers are attached to the bony landmarks of the human body, and the movement trajectories of these markers can be captured by infrared cameras at a certain frequency. Virtual markers corresponding to the experimental positions are placed on the human body simulation model, and the spatial coordinates of these virtual markers can vary with changes in generalised coordinate values. Therefore, inverse kinematics can be formulated as a mathematical optimisation problem [1]: at each time frame, the generalised coordinate values are solved to minimise the weighted sum of squared differences between the experimental measurement positions and the positions of the virtual markers on the human simulation model.

Inverse dynamics

Inverse dynamics can be used to solve the generalised forces exerted on the degrees of freedom of each joint during the motion process. The generalised force acting on a rotational degree of freedom is also known as joint moment, which represents the sum of the moments contributed by the relevant muscles actuating that degree of freedom. In addition to collecting kinematic data of the human body, external forces (usually ground reaction forces on both feet) also need to be

measured through force plates or sensors in the experiment. The kinematic quantities of each segment in the human body can be calculated in advance through inverse kinematics. Starting from the distal position of the human body model, force analysis is performed on each body in sequence towards the proximal position, and then the joint moment can be obtained through dynamic equations.

Force sharing problems

In muscle-driven simulation, the problem of solving the force of each muscle based on the pre-prescribed human kinematics and external forces is called the force sharing problem. In this problem, the total moment acting on each rotational degree of freedom can be uniquely determined by inverse dynamics. However, due to the fact that each rotational degree of freedom is driven by several muscles, solving the muscle force inversely from the total moment yields an infinite number of solutions. This type of problem can be formulated as a mathematical optimisation problem for solution, which can be specifically divided into two categories: static optimisation and optimal control.

1) Static optimisation

Static optimisation refers to solving optimisation problems separately at each time frame, so that the results at different time frames are independent of each other. As a computationally efficient and easy to implement method, static optimisation has

been widely used to solve muscle forces in walking motion [19–21].

2) Optimal control

The objective function of the optimal control problem is the integration of muscle-related mechanical variables over the entire duration, taking into account the continuity and integrity of the movement. Due to technical difficulties, there are fewer studies using optimal control to solve force sharing problems. Recently, Clancy *et al.* [22] used optimal control to simulate cycling. The experimental data included human kinematics and pedal reaction forces collected from sixteen healthy subjects while cycling under a wide range of cycling cadences and power outputs. A three-dimensional musculoskeletal model containing eighty muscles was employed to investigate the effect of muscle coordination patterns on tibiofemoral compression forces. Two different dynamic optimisation problems were formulated and solved using the advanced MocoInverse tool. The first problem served as the benchmark, and its objective function consisted of terms related to the actuators' controls and the derivatives of normalised tendon forces. In contrast, an additional term was added to the objective function of the second problem to penalise excessive tibiofemoral forces. The solution results showed that the tibiofemoral compression force obtained by solving the second problem was effectively reduced compared to the benchmark problem. It was found that the reduction in tibiofemoral compression force could be attributed to changes in muscle coordination patterns. In addition, they presented a

linear fitting expression between peak tibiofemoral force and cycling power.

Tracking problems

The essence of the tracking problem is to calculate a set of muscle controls that can drive the musculoskeletal model to produce motion consistent with experimental data. In the aforementioned force sharing problem, the experimental data is only used for calculating joint moments, and the kinematics of the model will not be changed by simulation. However, the multi-body dynamics equations are included in the calculation of the tracking problem, which allows for deviations between simulation results and experimental data.

1) Computed muscle control

As a classic algorithm, the computed muscle control was first proposed by Thelen *et al.* [23] for tracking a given motion. In this algorithm, forward dynamics calculation is combined with the static optimisation algorithm. To test the ability of the algorithm, they tracked average experimental data from cyclists using a 2D musculoskeletal model. The simulated pedal angle and reaction forces were very close to the experimental values, which means that the algorithm can achieve good tracking performance. Additionally, the muscle excitations calculated by the computed muscle control were compared with the results obtained by the simulated annealing algorithm and the experimental electromyography data, and it was found that the

muscle activities obtained by the three methods were relatively similar.

The above-mentioned computed muscle control algorithm incorporates the effects of muscle activation dynamics and contraction dynamics, but does not take into account the phenomenon of muscle force generation lagging behind muscle excitation. This may cause problems when tracking walking data, so Thelen *et al.* [24] improved the computed muscle control algorithm to consider the lag in muscle force generation. Furthermore, the residual elimination algorithm was used to improve the dynamic consistency between the experimental data of kinematics and ground reaction forces. The improved computed muscle control algorithm was subsequently used to generate tracking simulations for walking. The experimental data of joint angles and ground reaction forces were well tracked, and the calculated lower limb muscle activations were similar to the electromyography data reported in other literature.

2) Optimal control

The tracking problem can also be formulated as an optimal control problem for solution. In the objective function of the optimal control problem, deviations between experimental variables and simulation variables are usually directly penalised to achieve good tracking performance.

In 2017, Lin *et al.* [25] used optimal control theory to track both walking and running movements. They established a three-dimensional musculoskeletal model

driven by sixty-six muscles in OpenSim, and simulated foot-ground contact using the Hunt-Crossley force model. The objective function of the optimal control problem in their study consisted of two terms. The first item penalised muscle activations, and the second term was used to minimise deviations between simulated and experimentally measured ground reaction forces. The system dynamics equations were converted into equality constraints using the trapezoidal collocation method, and then the optimal control problem was solved in MATLAB. The tracking simulation results of both motions were highly consistent with the experimental data, proving the feasibility of using the direct collocation method to solve the tracking optimal control problem.

In summary, this section provides a comprehensive discussion on simulation problems based on experimental data and their solutions. Although these methods have been widely applied in biomechanics research, their limitations are also very obvious: when experimental data are difficult or impossible to obtain, simulation research cannot be carried out.

2.3.2 Predictive Simulation

Predictive simulation studies can generate new motions without experimental data, which is undoubtedly a huge advantage. Due to the high technical difficulty of solving predictive problems, the number of related studies is far less than that of simulations based on experimental data. To gain a more comprehensive

understanding of the technological progress of predictive simulation and the shortcomings of existing research, the review in this section will cover predictive studies on various movements of human lower limbs, which are not limited to the movements studied in this thesis. The classification of human lower limb movements in daily life is shown in Figure 2.4.

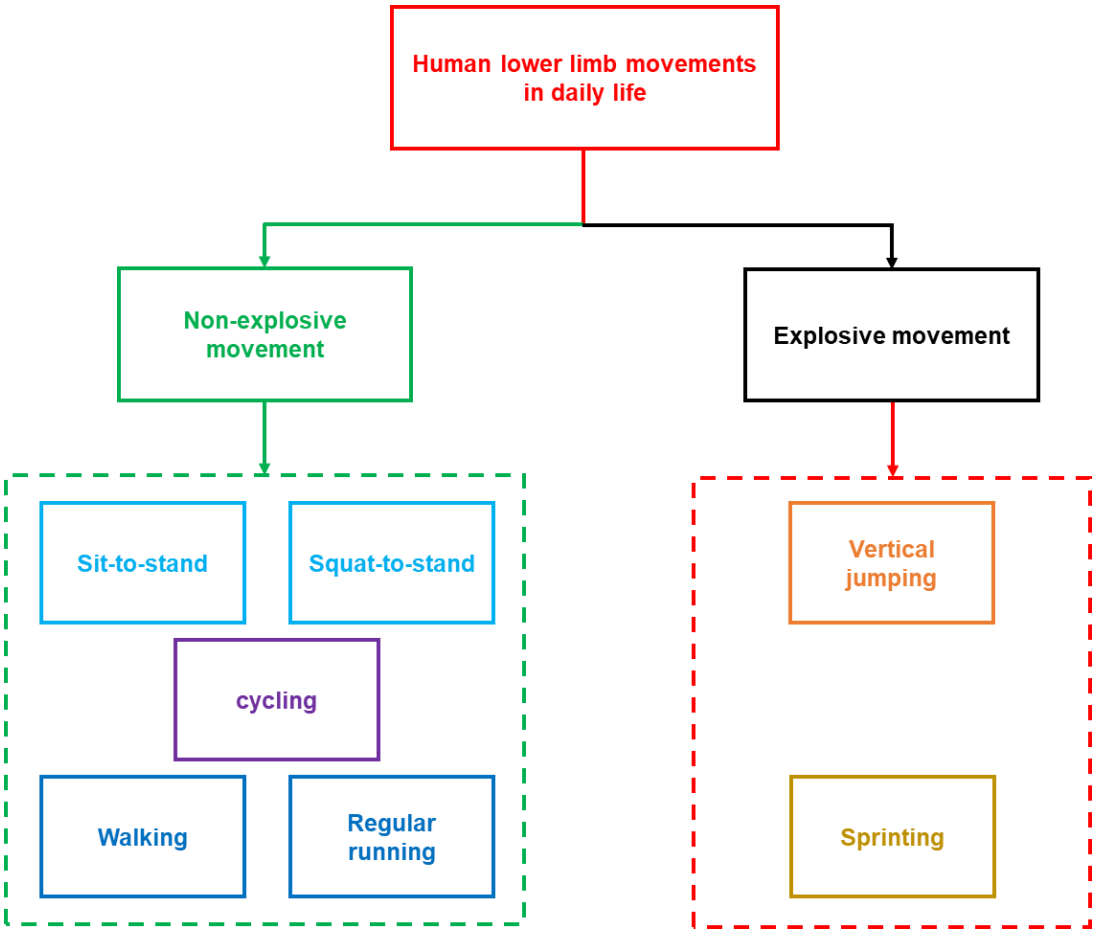

Figure 2.4. Classification of human lower limb movements in daily life.

It is generally believed that human movement is the optimal result determined by the central nervous system after considering one or a combination of multiple criteria.

Therefore, the predictive simulation can be formulated as an optimal control problem for solution. Different from the tracking optimal control problem, there is no tracking term in the objective function of the predictive problem.

Sit-to-stand and squat-to-stand are common movements in human daily life. The main difference between these two movements is whether there is contact between the human body and the seat. Pandy *et al.* [26] used a two-dimensional model driven by eight muscles to predict the behaviour of healthy individuals from squatting to standing and from sitting to standing. They first proposed five objective functions representing different motion goals, all of which were then used to predict human motion from squatting to standing. It was found that the results predicted by most of the objective functions had certain discrepancies with the experimental data. Subsequently, objective functions related to muscle stress and derivative of tendon force were used to predict the sit-to-stand motion. The results showed that using these two objective functions separately cannot fully capture the main characteristics of the sit-to-stand motion. However, by combining these two objective functions into one, the predicted dynamic behaviour obtained better agreement with the experimental data.

Aging can lead to the decrease in muscle strength, which can make it difficult for the elderly to complete the sit-to-stand motion. Kumar *et al.* [27] predicted the effect of muscle strength decline on sit-to-stand movement using a planar human model driven by eight muscles. The decrease in human muscle strength was simulated by

simultaneously reducing the peak isometric forces of all muscles. The optimal control problem was solved by the single shooting method. When muscle strength decreased to 20% of its original level, the model was unable to successfully perform the sit-to-stand task. In this situation, by applying a force to the centre of mass of the torso to simulate external assistance, the successful completion of the movement could be achieved. Their research provided some insights into the reasons for the failure of sit-to-stand movement, and could also provide some insights for how to apply external assistance.

Cycling can provide sufficient exercise for the lower limb muscles of the human body. Gidley *et al.* [28] predicted cycling motion using a two-dimensional musculoskeletal model driven by eighteen muscles. A tracking problem was first solved, and the cycling motion was then predicted using five different objective functions. The objective functions of different predictive problems were related to factors such as metabolic energy, derivative of tendon force, muscle stress, and muscle fatigue. The tracking problem and all predictive problems were solved using the simulated annealing algorithm. Due to the absence of tracking terms in the objective functions of predictive problems, the predicted results are generally not as close to the experimental values as those obtained by solving the tracking problem. Among the five predictive simulations, the objective function related to muscle fatigue best reflected the trend of experimental data. However, there were still some differences from the experiment.

As the most important activity in human daily life, walking has been extensively studied in its predictive problem. Anderson *et al.* [29] predicted normal human gait using a 3D musculoskeletal model driven by fifty-four muscles. Their objective function consisted of two terms: the first term was used to minimise metabolic energy consumption, and the second term penalised hyperextension of the joints. After assuming the symmetry of the relevant variables in both legs, only half of the gait cycle was simulated to reduce computation time. The simulation results were then compared with the experimental values. Although there are some deviations, the main motion characteristics of walking can be predicted, which indicates that the objective function used has certain rationality. Their study has laid a good foundation for gait prediction, but it also has certain limitations. For example, the knee joint was modelled as a rotational joint with one degree of freedom, which cannot fully reflect its anatomical features.

To better predict knee contact forces, Lin *et al.* [30] used a detailed knee joint model with six degrees of freedom that is capable of simulating joint contact. In their study, the human musculoskeletal model was driven by eighty muscle-tendon actuators. The tracking problem was first solved to provide the initial guess for subsequent predictive simulations. Subsequently, the direct collocation method was used to predict the gait behaviour of a subject at different speeds. The predictive problem aimed to minimise energy consumption. It was found that the computational time consumed by the predictive problem was much greater than that of the tracking

problem. Their study provides a new method for predicting the knee joint contact force during human walking.

Disorders within the human body may cause gait abnormalities. Conducting predictive simulation research on abnormal gait will not only help us enhance our understanding of the etiology, but also bring certain inspiration to rehabilitation treatment. Based on a two-dimensional musculoskeletal model driven by eighteen muscles, Ong *et al.* [31] predicted the effects of different pathological manifestations of ankle plantarflexion muscles on human walking behaviour. The objective function of the optimal control problem comprehensively considered multiple factors such as metabolic energy consumption, risk and stability during movement. The normal gaits were first predicted through the single shooting method, and the feasibility of the model was verified by comparing the simulation results with the experimental data. Different pathological states of the plantarflexion muscles were simulated by adjusting the parameters of the musculoskeletal model. Specifically, muscle weakness can be simulated by reducing the peak isometric force, and muscle contracture can be simulated by reducing the optimal fibre length. Their study can provide some reference for discovering the causes of abnormal gait.

Walking on a treadmill is a good way to improve one's physical fitness. Pariser *et al.* [32] were the first to achieve prediction of walking behaviour on a treadmill. In order to simulate the interaction between the foot and the treadmill belt during walking, a simple toy model was first established for preliminary simulation

exploration. Based on the experience gained from the simple model, a planar musculoskeletal model was subsequently developed to predict human treadmill gait at three different speeds. The cubic sum of muscle controls was penalised in the objective function. Their prediction results effectively reflected the changes in human gait behaviour with speed, verifying the predictive ability of the model. The model they established can speed up the selection of treadmill walking-based exercise plans.

As the speed gradually increases, walking will transition to another common activity in daily life - running. Miller *et al.* [33] completed predictions of running at normal speed using a planar musculoskeletal model in which each leg was driven by nine muscles. Similar to the approach used in predictive simulations of healthy human walking, bilateral symmetry of the legs was assumed to save computation time. Three different predictive optimal control problems were solved to study the feasibility of different optimisation criteria. The objective function consisted of four terms, the first of which could be selected from cost of transport, muscle activation or muscle stress. The remaining three terms remained unchanged in different predictive simulations, two of which were used to encourage the periodicity of the running motion, and one was used to penalise excessive passive joint moments. The simulated annealing algorithm was used to solve the optimal control problem. It was found that the results predicted using the criterion of minimising muscle activation were in good agreement with the experimental data, indicating that the commonly

used criterion of minimising cost of transport may not be the most appropriate criterion for predicting regular running.

The movement in which a person's running speed increases continuously until reaching a limit is called sprinting. Miller *et al.* [34] used predictive simulation to study the effect of modifying the parameters of the muscle mechanics model on sprint performance. The musculoskeletal model used was similar to the one used in regular running predictive simulation [33], but the optimisation objective of the optimal control problem was different. The objective function not only maximised the horizontal speed of the human body's centre of mass, but also included several penalty terms that were beneficial to simulation calculations. The results of their study showed that increasing the maximum muscle shortening velocity and the shape factor of the muscle force-velocity relationship curve can significantly improve the maximum sprint speed. Their study demonstrates the unique advantages of predictive simulation, as modifications to specific muscle properties are difficult to accomplish experimentally.

The study by Miller *et al.* [34] has pioneering significance in using predictive simulation to study sprinting. However, the model they used was highly simplified. To further explore the effects of modifying muscle parameters on sprint performance, Lin *et al.* [35] employed a more detailed musculoskeletal model, which includes eighty-six muscle-tendon actuators and upper limb joints. Different from another sprint study [34], the objective function used did not directly maximise speed, but included terms related to stride length and stride frequency to comprehensively reflect the stride

speed. In addition, a penalty term for avoiding inappropriate movement patterns was also included in the objective function. Their results showed that increasing optimal isometric muscle force can lead to a significant improvement in maximum sprint speed. Their study demonstrates the potential of predictive simulation in guiding athlete training.

Vertical jumping has a clear motion goal, so its behaviour is suitable to be predicted by optimal control theory. Pandy *et al.* [36] used a musculoskeletal model driven by eight muscle to predict the vertical jumping behaviour of the human body. The objective function of the optimal control problem was to maximise the vertical position of the centre of mass. The muscle excitations obtained by a numerical method were shown in the form of bang-bang control. The human kinematics, ground reaction forces, and muscle activations predicted by simulation showed similar patterns to experimental measurement results reported by others, validating the predictive model's credibility. Their research paves the way for subsequent predictive studies on vertical jumping motion.

The efficiency of solving predictive problems limits the complexity of the multi-body dynamics models used. Porsa *et al.* [37] predicted the vertical jumping motion of the human body using a direct collocation method and a shooting method, respectively. The objective function of the optimal control problem was consistent with the previous study [36], but the musculoskeletal model used was driven by 48 muscles, resulting in a significant increase in the complexity of the multi-body

dynamics model. The results showed that the computational efficiency of the direct collocation method is more than a hundred times higher than that of the shooting method. In addition, they combined the direct collocation method with the multi-body dynamics model established in OpenSim for the first time, providing a new approach for solving the problem of human motion prediction.

The vertical jumping performance of the human body can be enhanced through assistive devices. Predictive-based simulation can aid in the design of assistive devices. Ostraich *et al.* [38] used optimal control theory to predict the vertical jumping performance of the human body when wearing a passive exoskeleton. The lower limb of the 2D human model used had a total of three rotational degrees of freedom, each of which was driven by two actuators with direct torque output. The effects of different types of exoskeleton design schemes and factors such as exoskeleton mass on the maximum jumping height were explored. The optimal control problems were solved by OpenSim Moco using the direct collocation method. The results obtained can be used to guide the design of exoskeletons, which can help save the cost and time of research and development.

From the above discussion, it can be seen that the goals of explosive movements such as vertical jumps and sprints are relatively clear. However, most of the movements in human daily life are non-explosive, and there is no unified objective function when formulating their predictive optimal control problems. That is to say, the determination of the objective function for the predictive problem of non-

explosive motion is still an open problem, which currently mainly relies on the experience of researchers. In addition, the weight distribution between different objective function terms is often determined through manual adjustment, resulting in low research efficiency.

In recent years, the bilevel optimisation technique has been applied to the field of human motion prediction. This technique can automatically adjust the weight distribution between different objective function terms, freeing researchers from the tedious manual trial and error. Nguyen *et al.* [39] developed a bilevel optimisation method for determining the objective function of the optimal control problem for predicting walking. In the lower-level optimisation problem, a planar musculoskeletal model driven by eighteen muscles was used to predict walking behaviour. The objective function reflected factors such as muscle fatigue, stability and smoothness of movement. After the lower-level problem was solved by the direct collocation method, the simulation results were passed to the upper-level optimisation. The upper-level optimisation evaluated the deviations between the experimental data and the predicted results, and then updated the weights of the objective function terms through the genetic algorithm. The bilevel optimisation algorithm they established was able to predict gait behaviour with a small difference from experimental data.

Tang *et al.* [40] proposed a novel bilevel optimisation method to determine the weights of different objective function terms in the predictive optimal control problem. In the lower-level optimisation, a human model driven by four torque actuators was

used to predict human lifting motion. The objective function comprehensively considered the effects of energy consumption, motion stability, and fatigue in the lumbar joint. The weights of different terms were adjusted through the particle swarm optimisation algorithm used in the upper-level optimisation. The method they proposed can provide some inspiration for accurately predicting human lifting movements.

In this section, a detailed review has been provided of the research progress on predicting the movement of the human lower limbs. It can be seen that there are many predictive studies on walking, but relatively few predictive studies on other common daily life activities; there are many studies on predicting normal movement behaviour in healthy people, but relatively little research on predicting pathological movement behaviour in patients. In addition, bilevel optimisation methods used in existing studies on predicting human lower limb movements have the disadvantage of high computational resource consumption, which needs further improvement.

2.4 Algorithms for Solving Optimisation Problems

According to section 2.2, most simulation methods can ultimately be transformed into solving mathematical optimisation problems. This section will review the relevant optimisation solution algorithms involved in human motion simulation.

2.4.1 Common Optimisation Algorithms

According to whether gradient information of the objective function is required during the optimisation calculation process, relevant algorithms can be divided into two types: gradient-based algorithms and derivative-free algorithms.

Gradient-based algorithms

Nonlinear programming problem is a common mathematical optimisation problem, with the existence of nonlinear functions in its objective function or constraints. The mathematical expression is shown in Equation (2.1):

$$\begin{aligned} &minimise\ f(\boldsymbol{a}) \\ &subject\ to\ \boldsymbol{E}(\boldsymbol{a}) \leq \mathbf{0} \end{aligned} \tag{2.1}$$

where $\boldsymbol{a}$ is the vector to be optimised, f is the objective function, and $\boldsymbol{E}$ is the vector function related to the constraints.

The commonly used algorithms for solving nonlinear programming problems include interior-point methods [41], sequential quadratic programming methods [42, 43], etc. For large-scale nonlinear programming problems, the open source software IPOPT [44] or the commercial software SNOPT [45] can be used to solve them.

Derivative-free algorithms

When the differential properties of the objective function are poor, it is difficult to solve optimisation problems through gradient-based algorithms. Fortunately,

derivative-free algorithms can work in such situations.

Inspired by the metal annealing process, Kirkpatrick *et al.* [46] proposed the simulated annealing algorithm. The calculation starts with an initial vector and tries to reduce the objective function at each iteration. Interestingly, they utilised knowledge of statistical mechanics to introduce randomness during the iteration process, resulting in a certain probability that the solution obtained in the new round of iteration would cause the objective function to become larger. The introduction of randomness enables the solving process to explore a wider range within the feasible region, improving the likelihood of obtaining the global optimal solution.

The genetic algorithm [47, 48] imitates biological evolution in the optimisation calculation process. Several initial vectors are first given, which form a population. Each vector in the population can be considered as a chromosome, and each component of the vector can be considered as a gene. By performing operations such as crossover and mutation on chromosomes in the population, a new set of chromosomes can be obtained. After evaluating their quality, the population in the next generation can be determined. The computational iteration process continues until the convergence criterion is met. Genetic algorithm evaluates multiple sets of solutions in each iteration, greatly increasing the amount of information that can be utilised.

Kennedy *et al.* [49] proposed the particle swarm optimisation algorithm inspired by bird flock. Multiple vectors representing particles are gathered together to form a

particle swarm. In each iteration, the optimal positions of each particle itself and the entire particle swarm are first identified. The velocity vector of each particle is then calculated and combined with the current position to get the updated position. Compared with the genetic algorithm, the process of generating a new population in particle swarm optimisation is more convenient and easier to implement through programming. Particle swarm optimisation has been widely used in the field of optimisation computing, laying a solid foundation for subsequent research on swarm intelligence algorithms.

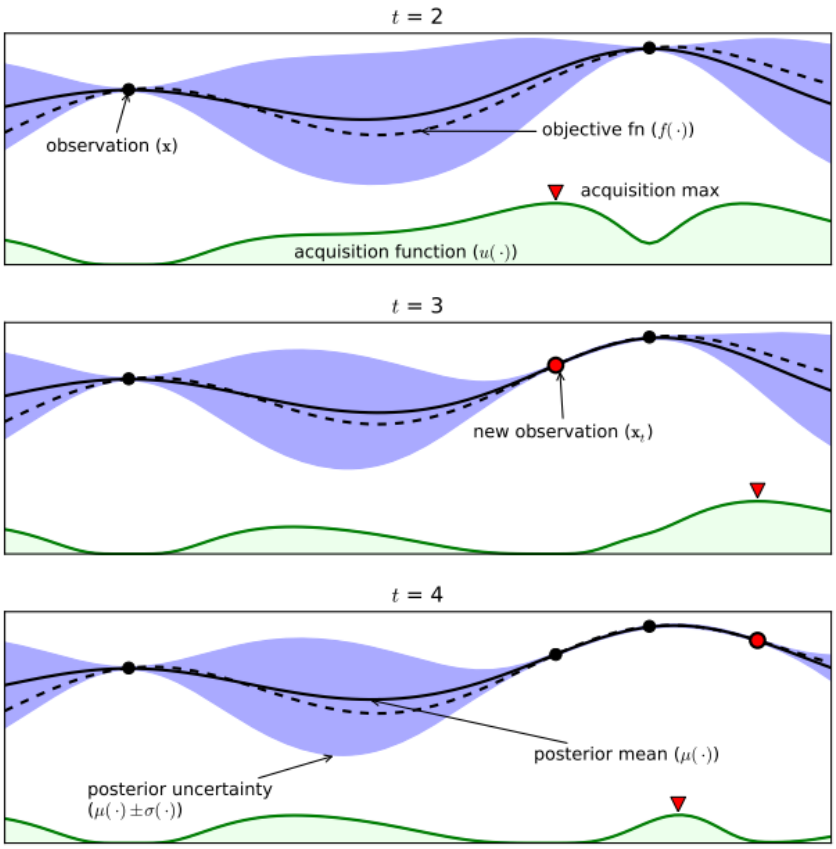

Figure 2.5. Schematic diagram of the iterative process of Bayesian optimisation [50]. In this example, there is only one design variable to be optimised.

Unlike the aforementioned derivative-free algorithms, the Bayesian optimisation algorithm is not a nature-inspired heuristic algorithm. After calculating the objective function values of a set of initial sampling points, a Gaussian process regression model is established based on the sampling points and their corresponding objective function values [50]. The next sampling point is then calculated through the acquisition function and the previous process is repeated. Figure 2.5 illustrates the iterative process of using Bayesian optimisation to solve an optimisation problem with only one design variable. As an advanced algorithm, Bayesian optimisation has been widely applied in the field of artificial intelligence [51, 52].

This section has summarised typical solution algorithms for optimisation problems. It is worth noting that although derivative-free algorithms can also be used to solve optimisation problems when gradient information is available, their computational efficiency is usually not as ideal as gradient-based optimisation algorithms in such cases.

2.4.2 Algorithms for Solving Optimal Control Problems

As can be seen from Section 2.2, the predictive problem, force sharing problem and tracking problem in human motion can all be formulated as optimal control problems for solution. The general expression of the optimal control problem is shown in Equation (2.2).

$$
\begin{aligned}
&minimise\ J = \int_0^T \phi(\boldsymbol{x}(t), \boldsymbol{u}(t), t)dt \\
&subject\ to\ \dot{\boldsymbol{x}}(t) = \boldsymbol{G}(\boldsymbol{x}(t), \boldsymbol{u}(t), t) \\
&\qquad \boldsymbol{H}_l \leq \boldsymbol{H}\big(\boldsymbol{x}(t), \boldsymbol{u}(t), t, \boldsymbol{x}(0), \boldsymbol{u}(0), \boldsymbol{x}(T), \boldsymbol{u}(T)\big) \leq \boldsymbol{H}_u
\end{aligned} \tag{2.2}
$$

where J is the objective function, ϕ is the integrand function related to the optimisation objective, $\boldsymbol{x}$ is the state vector, $\boldsymbol{u}$ is the control vector, t is the time, T is the motion duration, $\boldsymbol{G}$ is the vector function related to human dynamics, $\boldsymbol{H}$ represents the constraints, $\boldsymbol{H}_l$ represents the lower limit of the constraints, and $\boldsymbol{H}_u$ represents the upper limit of the constraints.

The main methods for solving optimal control problems are introduced in detail below.

Direct collocation methods

From Equation (2.2), it can be seen that the objective function is expressed in integral form, and the dynamic constraint is a differential equation. The direct collocation method can transcribe the dynamic constraint equations into algebraic equations. During the transcription process, the entire motion duration is divided into multiple sub-intervals, and then the continuous state variables and control variables are discretized into several collocation points according to the selected transcription method. Subsequently, the calculation of the objective function can be achieved through numerical integration, and the optimal control problem can be transformed into a nonlinear programming problem for solution. Common transcription methods include the Euler method, trapezoidal method and Hermite-Simpson method [53],

which are introduced one by one below.

The Euler method transforms the dynamic differential equation into the following algebraic equation:

$$\boldsymbol{x}(t_{j+1}) - \boldsymbol{x}(t_j) = (t_{j+1} - t_j)\boldsymbol{G}\big(\boldsymbol{x}(t_j), \boldsymbol{u}(t_j), t_j\big) \tag{2.3}$$

where $\boldsymbol{x}$ is the state vector, $\boldsymbol{u}$ is the control vector, t_j is the left endpoint of the j-th interval, t_{j+1} is the right endpoint of the j-th interval, and $\boldsymbol{G}$ is the vector function related to human dynamics.

The objective function can be calculated using Equation (2.4):

$$J \approx \sum(t_{j+1} - t_j)\, \phi\big(\boldsymbol{x}(t_j), \boldsymbol{u}(t_j), t_j\big) \tag{2.4}$$

The trapezoidal method transforms the dynamic differential equation into the following algebraic equation:

$$\boldsymbol{x}(t_{j+1}) - \boldsymbol{x}(t_j) = \frac{t_{j+1}-t_j}{2}\Big(\boldsymbol{G}\big(\boldsymbol{x}(t_j), \boldsymbol{u}(t_j), t_j\big) + \boldsymbol{G}\big(\boldsymbol{x}(t_{j+1}), \boldsymbol{u}(t_{j+1}), t_{j+1}\big)\Big) \tag{2.5}$$

The objective function can be calculated using Equation (2.6):

$$J \approx \sum \frac{t_{j+1}-t_j}{2}\Big(\phi\big(\boldsymbol{x}(t_j), \boldsymbol{u}(t_j), t_j\big) + \phi\big(\boldsymbol{x}(t_{j+1}), \boldsymbol{u}(t_{j+1}), t_{j+1}\big)\Big) \tag{2.6}$$

The collocation points of the Euler method and the trapezoidal method coincide with the endpoints of the subintervals. In contrast, the collocation points of the Hermite-Simpson method include the endpoints and midpoint of each subinterval,

resulting in high accuracy.

Let $t_{j_{mid}}$ be the midpoint of the j-th interval, that is,

$$t_{j_{mid}} = \frac{1}{2}(t_j + t_{j+1}) \tag{2.7}$$

The Hermite-Simpson method transforms the dynamic differential equation into Equation (2.8) and (2.9):

$$\boldsymbol{x}(t_{j_{mid}}) = \frac{1}{2}\left(\boldsymbol{x}(t_j) + \boldsymbol{x}(t_{j+1})\right) - \frac{t_{j+1}-t_j}{8}\left(\boldsymbol{G}(\boldsymbol{x}(t_{j+1}), \boldsymbol{u}(t_{j+1}), t_{j+1}) - \boldsymbol{G}(\boldsymbol{x}(t_j), \boldsymbol{u}(t_j), t_j)\right) \tag{2.8}$$

$$\begin{aligned}\boldsymbol{x}(t_{j+1}) - \boldsymbol{x}(t_j) = \frac{t_{j+1}-t_j}{6}\big(&\boldsymbol{G}(\boldsymbol{x}(t_j), \boldsymbol{u}(t_j), t_j) + 4\boldsymbol{G}(\boldsymbol{x}(t_{j_{mid}}), \boldsymbol{u}(t_{j_{mid}}), t_{j_{mid}}) \\ &+\boldsymbol{G}(\boldsymbol{x}(t_{j+1}), \boldsymbol{u}(t_{j+1}), t_{j+1})\big)\end{aligned} \tag{2.9}$$

The objective function can be calculated using Equation (2.10):

$$J \approx \sum \frac{t_{j+1}-t_j}{6}\left(\phi(\boldsymbol{x}(t_j), \boldsymbol{u}(t_j), t_j) + 4\phi(\boldsymbol{x}(t_{j_{mid}}), \boldsymbol{u}(t_{j_{mid}}), t_{j_{mid}}) + \phi(\boldsymbol{x}(t_{j+1}), \boldsymbol{u}(t_{j+1}), t_{j+1})\right) \tag{2.10}$$

Opensim Moco [54] is a toolbox for solving optimal control problems of human motion using the direct collocation method. This toolbox includes the MocoInverse tool and the MocoTrack tool, which can be used to solve force sharing problems and tracking problems, respectively. Most importantly, for predictive problems with high flexibility, users can conduct personalised research based on the MocoStudy class.

Direct shooting methods

Direct shooting methods are another type of method to solve the optimal control problem. After giving a set of control variables, the objective function value can be evaluated by performing forward integration on the dynamic differential equation. The single shooting method and multiple shooting method are two specific forms of direct shooting methods [55]. In the single shooting method, the dynamic equations are integrated over the entire motion duration. In the multiple shooting method, integration is performed separately on multiple sub-intervals of the motion duration, which can reduce integration errors compared to the single shooting method. Since the shooting method requires multiple integrations of the dynamic equations, its computational efficiency is lower than that of the direct collocation method [37].

2.5 Current Research Gaps and Proposed Solutions

Through the above comprehensive literature review, the author found that there are several research gaps and limitations in the field of human lower limb movement prediction, which are summarised as follows:

1.Existing predictive simulation research focuses more on the normal walking behaviour of the human body, with less attention paid to other functional movement.

2. The research subjects are usually healthy people, and there are few studies on the movement behaviour of people with limb amputations or limb dysfunctions.

3. The existing bilevel optimisation methods for solving the inverse optimal

control problem of human movement are inefficient.

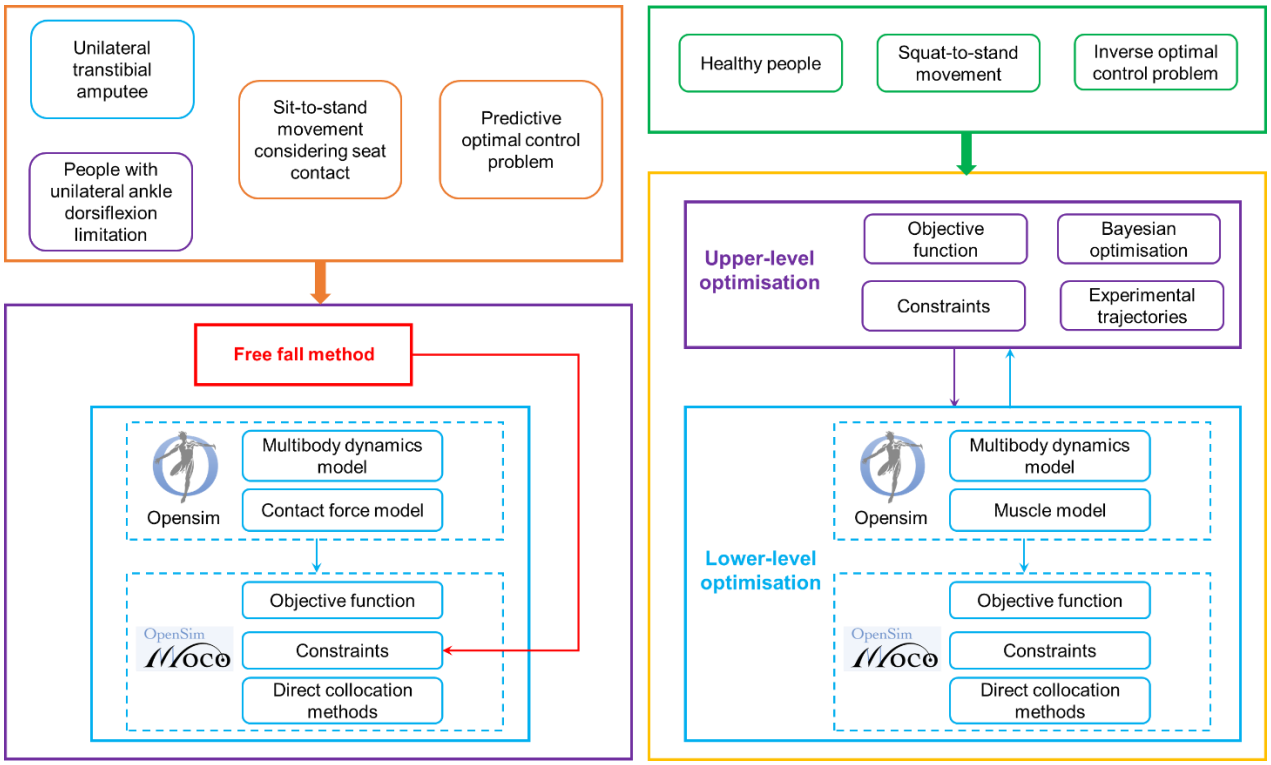

Figure 2.6. Flowchart of the overall research methodology.

The following chapters of this thesis will be devoted to filling the aforementioned research gaps and addressing the relevant limitations in this field. Figure 2.6 shows the overall research methodology of this thesis.

2.6 Conclusion

In this chapter, the author first elaborated on the relevant theories of multi-body dynamics models, then classified the problems and methods of biomechanical simulation in detail, and finally summarised the relevant solution algorithms. It can be

seen that predictive simulation can generate new movements in the absence of experimental data, which is a cutting-edge research direction in the field of human motion biomechanics. In addition, due to its high solution efficiency, the direct collocation method has great potential in solving predictive simulation problems. However, research on predicting human movement is currently in the development stage, and there are still several issues that need to be addressed urgently. The existing research gaps and limitations were summarised based on the above comprehensive review of research progress. In order to fill these research gaps and address relevant limitations, the overall research methodology of this thesis was proposed to guide the research work in subsequent chapters.

Chapter 3. Sit-to-stand Optimal Control Prediction Considering Seat Contact for the Unilateral Transtibial Amputee：a Novel Optimisation Framework Based on Direct Collocation

The content of this chapter is intended to be submitted to *Nature* or *Science Robotics* at an appropriate time in the future. (Authors: Weida Wang, Ziyun Ding, Anthony Bull and Duncan Shepherd.)

3.1 Introduction

As one of the high-frequency activities in daily life [56, 57], sit-to-stand is closely related to an individual's quality of life. Lower limb injuries, especially amputation, can increase the difficulty for patients to complete sit-to-stand transition. Furthermore, it causes serious harm to human body's physical and mental health. Therefore, there is an urgent need to explore the biomechanical mechanisms of sit-to-stand motion for lower limb amputees, which is beneficial to the development of clinical medicine and rehabilitation treatment.

Experimental measurement is a common method for studying the sit-to-stand behaviour of patients with lower limb amputation. [58] is the first experimental study to analyse the asymmetry of weight distribution on both lower limbs of unilateral transtibial amputees, with and without the assistance of arm during the motion. In [59], it was found that patients with unilateral transtibial amputation not only exhibit

weight-bearing asymmetry, but also exhibit significant differences in parameters such as sway velocity and rising index compared to healthy subjects. Research methods based on experimental measurements can provide useful insights, however, they also have obvious limitations. For example, patients are at risk of being injured again during the experiment. In addition, conducting experiments is time-consuming, labour-intensive and costly.

Predictive simulations based on optimisation theory can perform calculations completely separated from experimental data, thus having significant advantages when relevant experimental data are lacking or experiments are difficult to carry out. Based on a planar human body model with three degrees of freedom, Pandy *et al.* [26] took the lead in using optimal control theory to predict the sit-to-stand motion of healthy people. In [27], using a human body model similar to [26], the sit-to-stand movement of intact people with muscle weakness and external assistance was successfully predicted by single shooting method. Existing studies provide a good foundation for predicting the sit-to-stand transition for intact individuals, however, predictive simulation studies on lower limb amputees are extremely rare. Patients with lower limb amputations have asymmetries in their bodies, which undoubtedly brings greater difficulty to simulation calculations. As the only predictive simulation study on the sit-to-stand motion of patients with lower limb amputation in the current literature, the movement behaviour of transfemoral amputees was successfully synthesised [60]. However, the movement phase where the buttocks were in contact

with the seat was not considered in their study. In summary, there are significant challenges in predicting the entire course of sit-to-stand motion (i.e. considering butt contact) for lower limb amputees through dynamic optimisation methods.

To the best of our knowledge, this is the first simulation study to predict entire course of sit-to-stand transition in patients with lower limb amputations. A human body model representing a unilateral transtibial amputee, combined with the smooth Hunt-Crossley force model, can successfully simulate the contact force interaction between the human body and external environment. A novel “free fall method” was proposed to determine the initial static sitting and final static standing postures of the model. Subsequently, the formulated optimal control problem was solved by the direct collocation method to achieve the prediction of transition from sitting to standing. After validated by experimental data, the proposed simulation framework was further used to study the effect of changing the prosthetic stiffness on motion. This study fills the research gap in predicting sit-to-stand motion for unilateral transtibial amputees and deepens the understanding of the movement mechanism. It has great potential to accelerate the design of prostheses and rehabilitation training programs for lower limb amputees.

3.2 Methods

We established a simulation framework to predict the sit-to-stand movement

behaviour of the unilateral transtibial amputee considering seat contact, as shown in Figure 3.1. The human body postures at the initial and final time points need to be determined first using the proposed “free fall method”. The prediction of sit-to-stand motion can then be achieved by solving the optimal control problem. To evaluate the effectiveness of this simulation framework, we compared the simulation at a representative prosthetic stiffness (referred to “nominal simulation”) with experimental results. Finally, the effect of changes in the prosthetic stiffness on dynamic performance was explored.

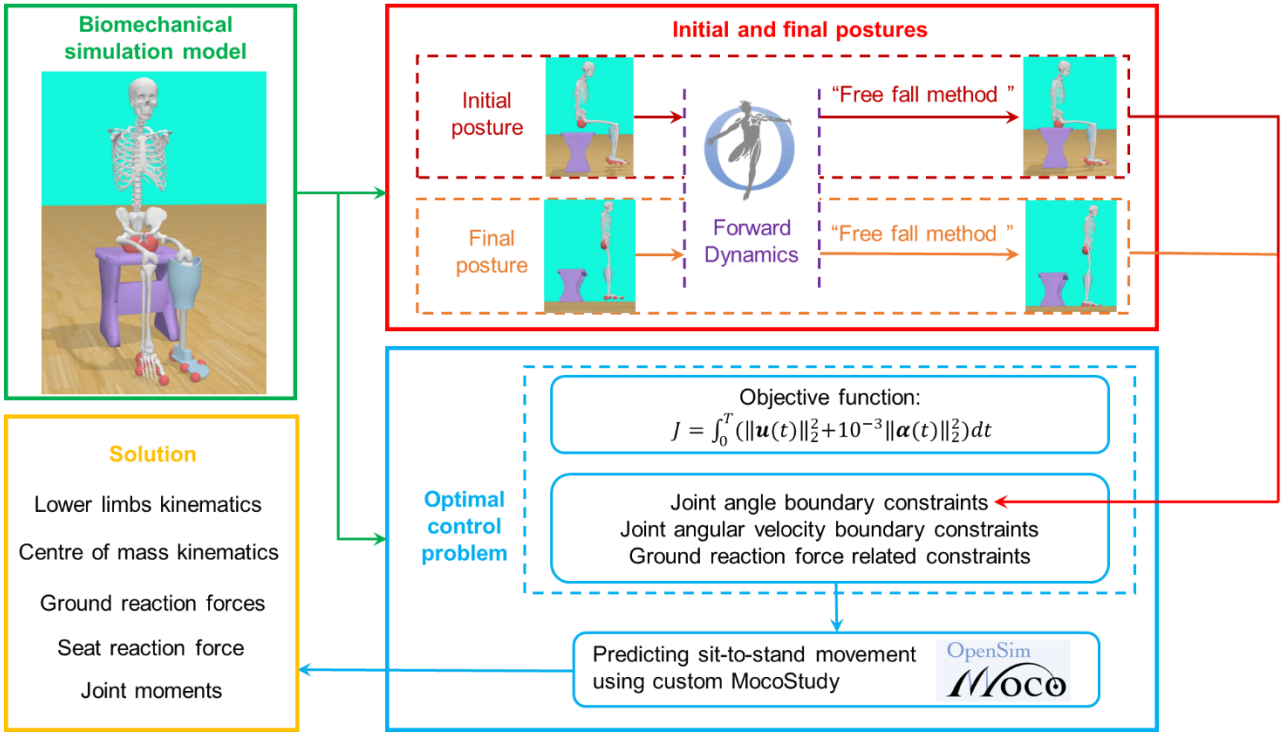

Figure 3.1. Flowchart of the simulation framework for predicting sit-to-stand movement in the unilateral transtibial amputee. The “free fall method” is described in section 3.2.2. The specific meanings of all symbols in the figure are detailed in section 3.2.3.

3.2.1 Biomechanical Simulation Model

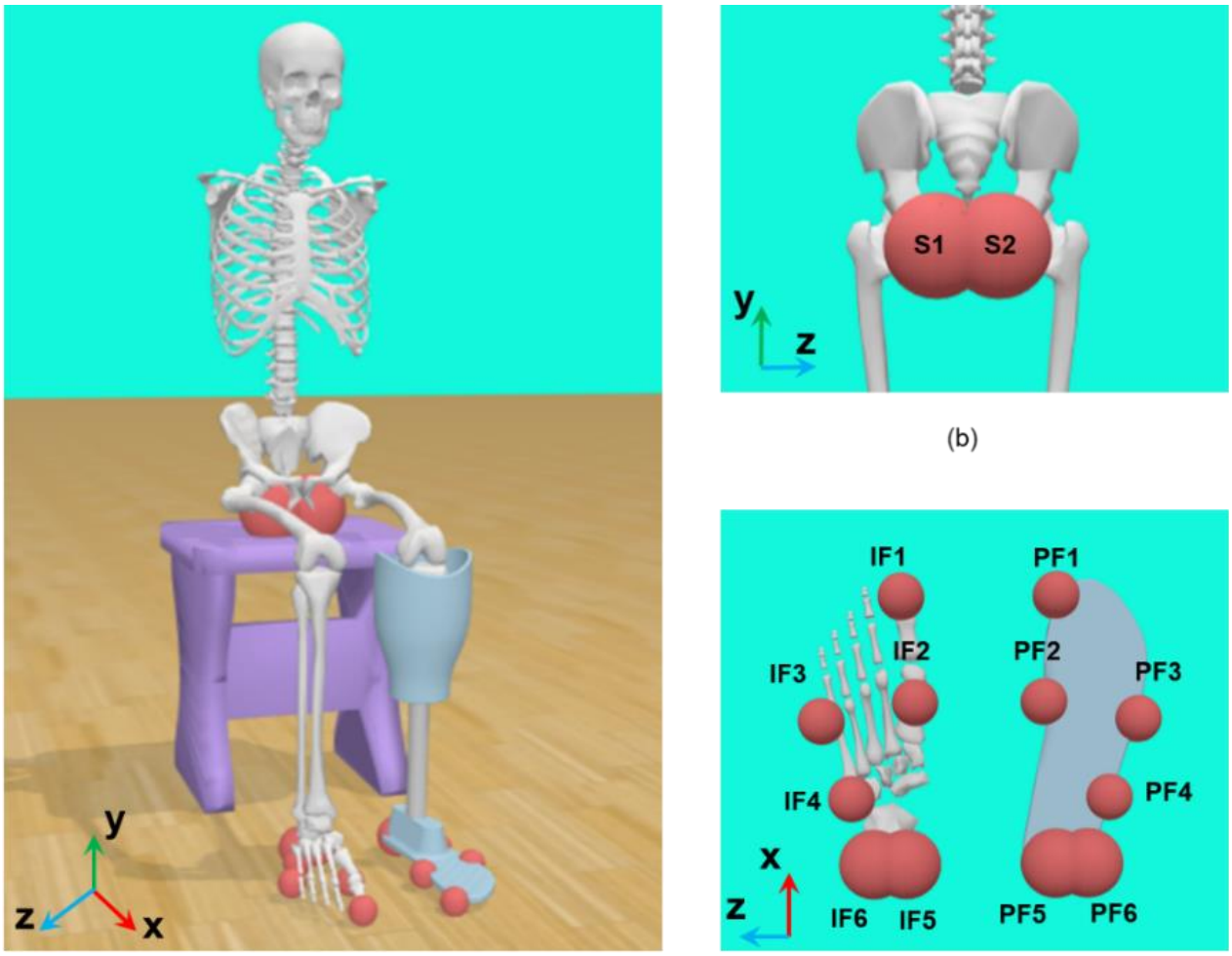

Figure 3.2. The biomechanical simulation model of the unilateral transtibial amputee established in OpenSim (the coordinate axes in the figure are only used to indicate directions rather than specific positions). (a) is an overall view. (b) is a partial view of the human buttocks, on which two contact spheres S1 and S2 were placed. (c) is a partial view of the soles of both feet, with six contact spheres placed on each foot. The contact spheres on the prosthetic foot were PF1-PF6, and the contact spheres on the intact foot were IF1-IF6.

The human body model used in this study was modified based on a generic OpenSim model [61] representing a patient with the left transtibial amputation. This

planar human model (as shown in Figure 3.2) consists of nine segments, which are: torso, pelvis, left and right femur, left residual tibia, prosthetic socket-pylon combination, right intact tibia, prosthetic foot, and right intact foot. These segments were interconnected by seven single degree of freedom (DOF) joints (lumbar joint, both hip joints, both knee joints and both ankle joints). We slightly adjusted the orientations of the joint frames to ensure that all segments move within the sagittal plane. Additionally, a three DOFs (two translations and one rotation) joint was constructed between the ground and the pelvis, allowing the human model to move freely.

Except for the ground-pelvis joint and the prosthetic ankle joint, each other joint was driven by an active torque actuator. For the passive prosthesis, the ankle joint was driven by a linear spring-damper torque actuator [62]. The torque generated by this passive actuator can be calculated using Equation (3.1).

$$M_p = -k_p \theta_p - b_p \omega_p \tag{3.1}$$

where M_p is the passive torque of the prosthetic ankle joint; k_p is the stiffness of the prosthesis, which was taken as 400N·m/rad [63] in the nominal simulation; b_p is the coefficient of viscous damping, which was taken as 0.5 N·m·s/rad in all simulations; θ_p is the angle of the prosthetic ankle joint; ω_p is the angular velocity of the prosthetic ankle joint.

Due to its advantage in gradient-based optimisation, the smooth Hunt-Crossley

force model [18] was used to generate the interaction forces between the human body and the external environment. We added six contact spheres on each foot to simulate foot-ground contact. In addition, a total of two contact spheres were added on the left and right ischial tuberosities to simulate buttocks-seat contact. In order to simulate the contact forces reasonably, the locations and sizes of the contact spheres were set based on the possible contact area between the human body and the external environment during movement. The specific locations of all contact spheres are illustrated in the Figure 3.2 (b) and (c). The mechanical parameters of the contact spheres were chosen based on suggestions from Antoine [64].

3.2.2 Initial and Final Postures

At the beginning and end of the motion, the human body is in the state of static balance. In other words, at these two time points, resultant force and resultant moment of the external forces exerted on the human body are both zero. The external forces on the human body were composed of gravity and contact forces, with gravity being constant. However, the normal component of the contact force calculated through the smooth Hunt-Crossley force model is very sensitive to how deeply the contact sphere penetrates the corresponding plane. Therefore, we need to determine the postures of the human body model at the initial and final time points, so that the contact forces exerted by the environment are balanced with gravity. The angles of human physiological joints are commonly set based on experience. For the

ground-pelvis joint, the horizontal translation coordinate has no effect on the balance of the model. However, slight changes in the remaining coordinates of the ground-pelvis joint can alter the depth of each contact sphere penetrating into the corresponding plane, thereby significantly affecting the force situation, making the accurate determination of equilibrium posture challenging. To overcome this challenge, we proposed a novel "free fall method", whose overall implementation process is shown in Figure 3.3. The specific details of the proposed method are described in detail below.

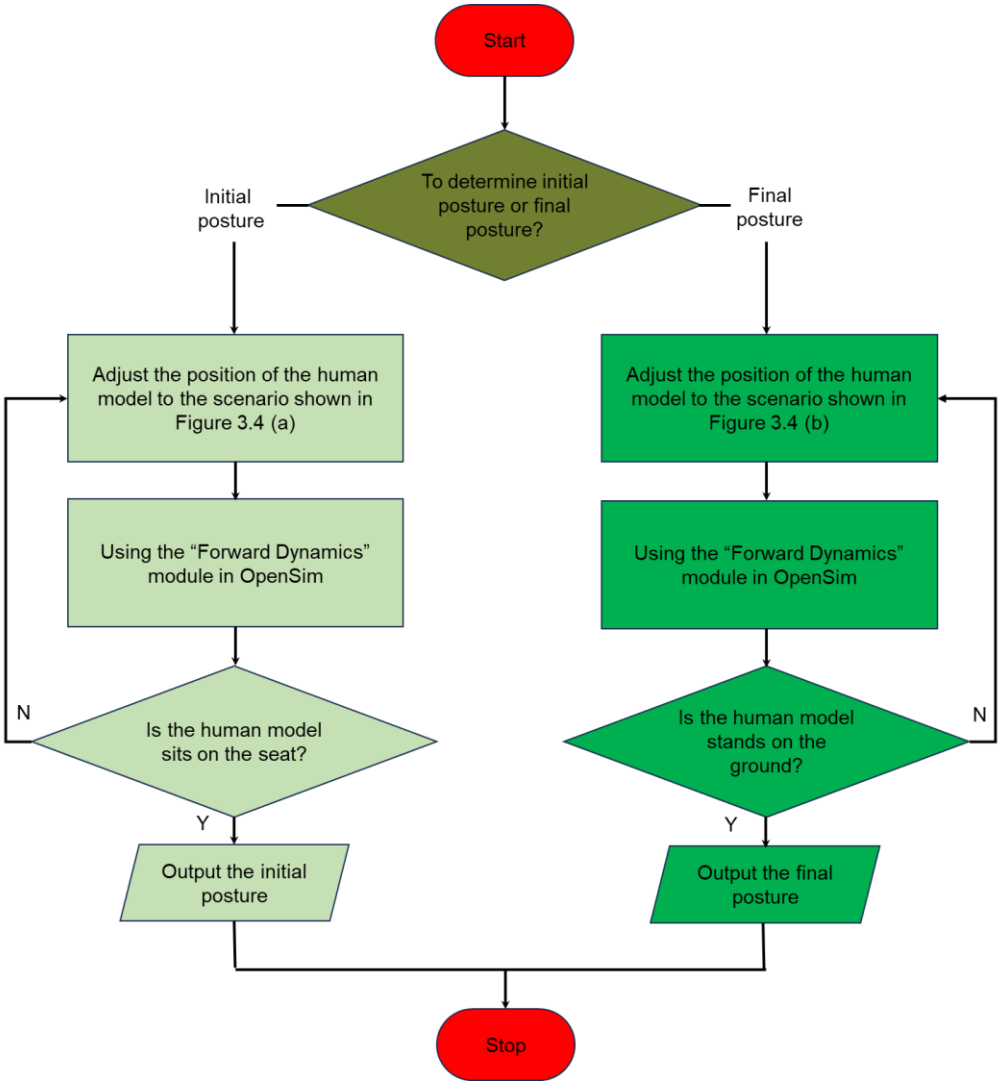

Figure 3.3. Flowchart of the “free fall method”.

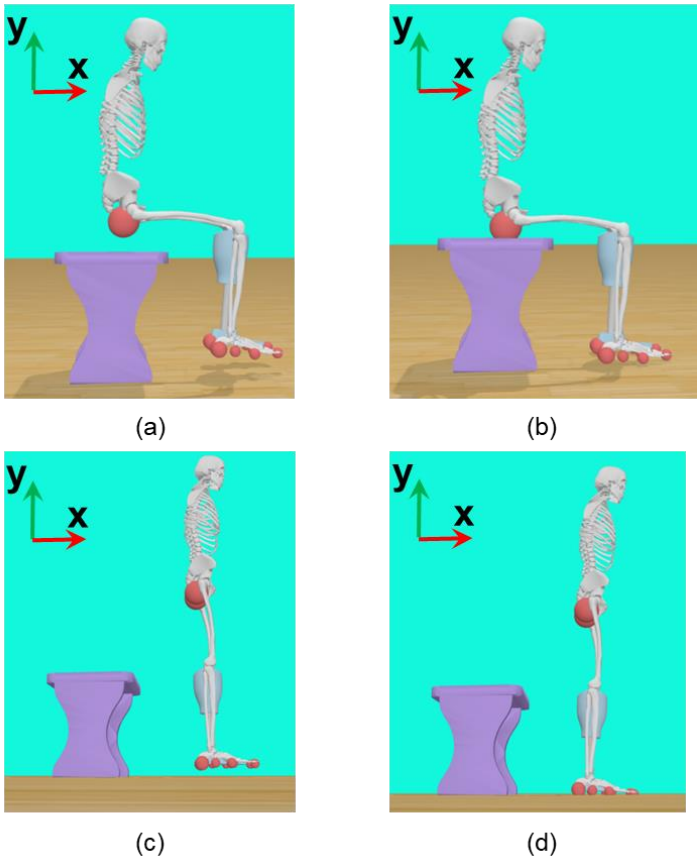

Figure 3.4. The schematic diagram of using the “free fall method” to determine the initial and final postures, which can be implemented through the "Forward Dynamics" tool in OpenSim (the coordinate axes in the figure are only used to indicate directions rather than specific positions). (a) is the sitting posture before the "free fall". (b) is the static sitting posture after the “free fall”. (c) is the standing posture before the "free fall". (d) is the static standing posture after the “free fall”.

At the initial time point of the movement, the human body was in the stationary sitting position, in contact with both the seat and the ground. We empirically specified the angles of the lumbar joint, both hip joints, and both knee joints. The specific values were listed in Table 3.1. These joints were then locked to maintain their angles unchanged. We adjusted the rotation coordinate and vertical translation coordinate of the ground-pelvis joint so that the contact spheres on the buttocks and feet were

respectively separated from the seat and the ground by a certain distance, as shown in Figure 3.4 (a). The distance between the centre of the contact sphere on the buttocks and the seat should be greater than the radius of the sphere, and the distance between the centre of the contact sphere on the feet and the ground should be greater than the radius of the sphere. The “Forward Dynamics” tool implemented in OpenSim [1–3] was used to perform forward integration in time from this posture, so that the model free-falling under the action of gravity until it reached the static sitting posture in Figure 3.4 (b). In this way, the angles of both ankle joints, as well as the rotation and vertical translation coordinates of the ground-pelvis joint, can be uniquely determined (see Table 3.1).

At the end of the motion, the human body was in the stationary standing position, only in contact with the ground. After specifying the angles of the lumbar joint, both hip joints, both knee joints, and right ankle joint, we locked these joints. Subsequently, we adjusted the remaining DOFs in the model to maintain a certain distance between the ground and the contact spheres on feet (see Figure 3.4 (c)). The distance between the centre of the contact sphere on the feet and the ground should be greater than the radius of the sphere. Similar to the above, the “Forward Dynamics” tool was used to simulate the model's free fall motion. After landing, the model underwent an inverted pendulum-like motion with gradually decreasing amplitude, and finally reached the static standing posture illustrated in Figure 3.4 (d). The joint coordinate values under the initial and final postures in the nominal simulation were

summarised in Table 3.1.

Table 3.1: Generalised coordinate values under the initial and final postures in the nominal simulation

Generalised coordinate	Value in the initial posture	Value in the final posture
Hip flexion in amputated side	60°	0°
Hip flexion in intact side	60°	0°
Knee flexion in amputated side	85°	0°
Knee flexion in intact side	85°	0°
Ankle dorsiflexion in amputated side	0.74°*	1.31°*
Ankle dorsiflexion in intact side	1.93°*	0°
Lumbar flexion	35°	10°
Vertical translation of the ground-pelvis joint	0.63m*	0.95m*
Rotation of the ground-pelvis joint	21.39°*	-3.55°*

* indicates coordinate values determined by the “free fall method”.

3.2.3 Solution of the Predictive Optimal Control Problem

We used the optimal control theory to achieve prediction of the sit-to-stand motion. The optimal control problem commonly consists of an objective function and

several constraints. The objective function that needs to be minimised is defined in Equation (3.2):

$$J = \int_0^T \|\boldsymbol{u}(t)\|_2^2 \, dt + 10^{-3} \int_0^T \|\boldsymbol{\alpha}(t)\|_2^2 \, dt \tag{3.2}$$

where J represents the objective function of the optimal control problem, $\boldsymbol{u}$ is the control vector of active torque actuators, $\boldsymbol{\alpha}$ is the vector of generalised accelerations, t is the time variable, and T is the duration of the sit-to-stand motion.

The objective function J consists of two specific goals. The first goal penalises the integral of the squared L2 norm of $\boldsymbol{u}$ over time, aiming to reduce human fatigue (similar to [65]). The second goal penalises the integral of the squared L2 norm of $\boldsymbol{\alpha}$ over time, which is beneficial to improving the smoothness of joint motion [64, 66].

We defined several constraints to reflect the features of the sit-to-stand movement: 1) The joint generalised coordinate values at the initial and final time points were selected according to the Table 3.1; 2) all generalised velocities at the initial and final time points were set to zero; 3) the normal forces exerted by the ground on the contact spheres IF1, IF5, PF1 and PF5 were constrained within [3N, 500N].

To ensure high computational efficiency, we employed the direct collocation method to solve the above optimal control problem. The computational solution was implemented in OpenSim Moco [54] using the Hermite-Simpson method [53, 55] as the transcription scheme.

3.2.4 Validation of the Nominal Simulation

To ensure that the proposed simulation framework can effectively predict the behavioural characteristics of sit-to-stand motion, we compared the nominal simulation results with experimental data. The experimental data used for comparison came from an experimental study [67] on sit-to-stand motion of unilateral transtibial amputees. According to the needs of this study, we reprocessed the original experimental measurement data of five subjects, including motion capture data, ground reaction force data of each foot, and seat reaction force data. The “Inverse Kinematics” tool in OpenSim [1–3] was employed to complete the computational solution of joint kinematics. Subsequently, the joint kinematics results and force data were filtered by a fourth-order zero-lag Butterworth filter, followed by time normalisation to 0-100%. For the sit-to-stand movement, we were mainly interested in the changing trends of the lower limb joint angles, vertical components of ground reaction forces and seat reaction force. Therefore, the nominal simulation results of these mechanical variables were compared with the corresponding processed experimental data.

3.2.5 Predictive Simulations under Different Prosthetic Stiffness

We select prosthetic stiffness as a representative to explore the effect of changes in prosthetic parameter on the patient’s dynamic behaviour. The prosthetic

stiffness k_p in the human body model was adjusted to 600 N·m/rad, 800 N·m/rad, and 1000 N·m/rad in sequence. Subsequently, the motion was predicted using the above methods, and the dynamic calculation results under different prosthetic stiffness were compared with each other.

3.3 Results

3.3.1 Predictive Simulation Results under Nominal Prosthetic Stiffness

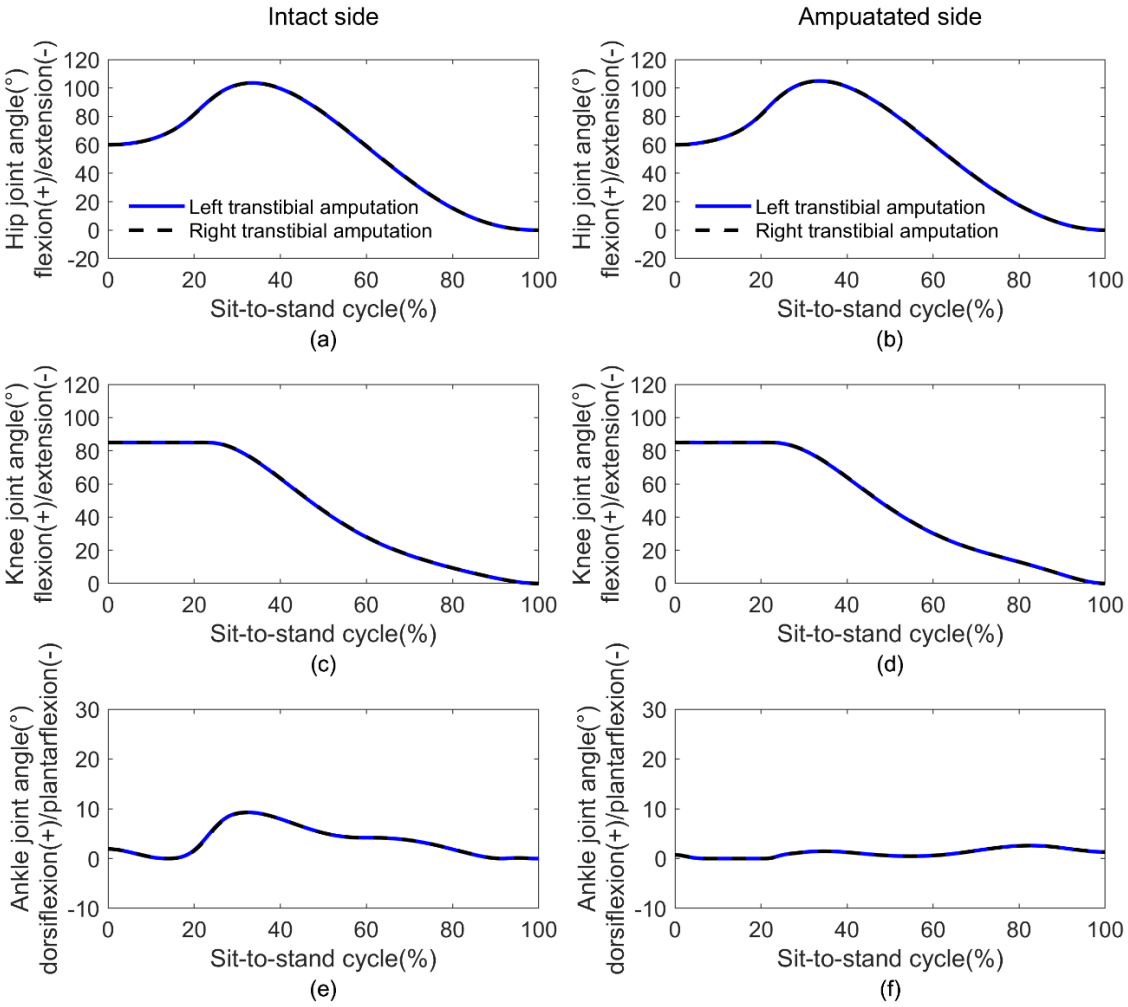

Figure 3.5. Lower limb joint angles during sit-to-stand motion. The blue lines illustrate the results predicted using the left transtibial amputee model, the black lines

represent results predicted using the right transtibial amputee model. (a) Hip joint angles in intact side. (b) Hip joint angles in amputated side. (c) Knee joint angles in intact side. (d) Knee joint angles in amputated side. (e) Ankle joint angles in intact side. (f) Ankle joint angles in amputated side.

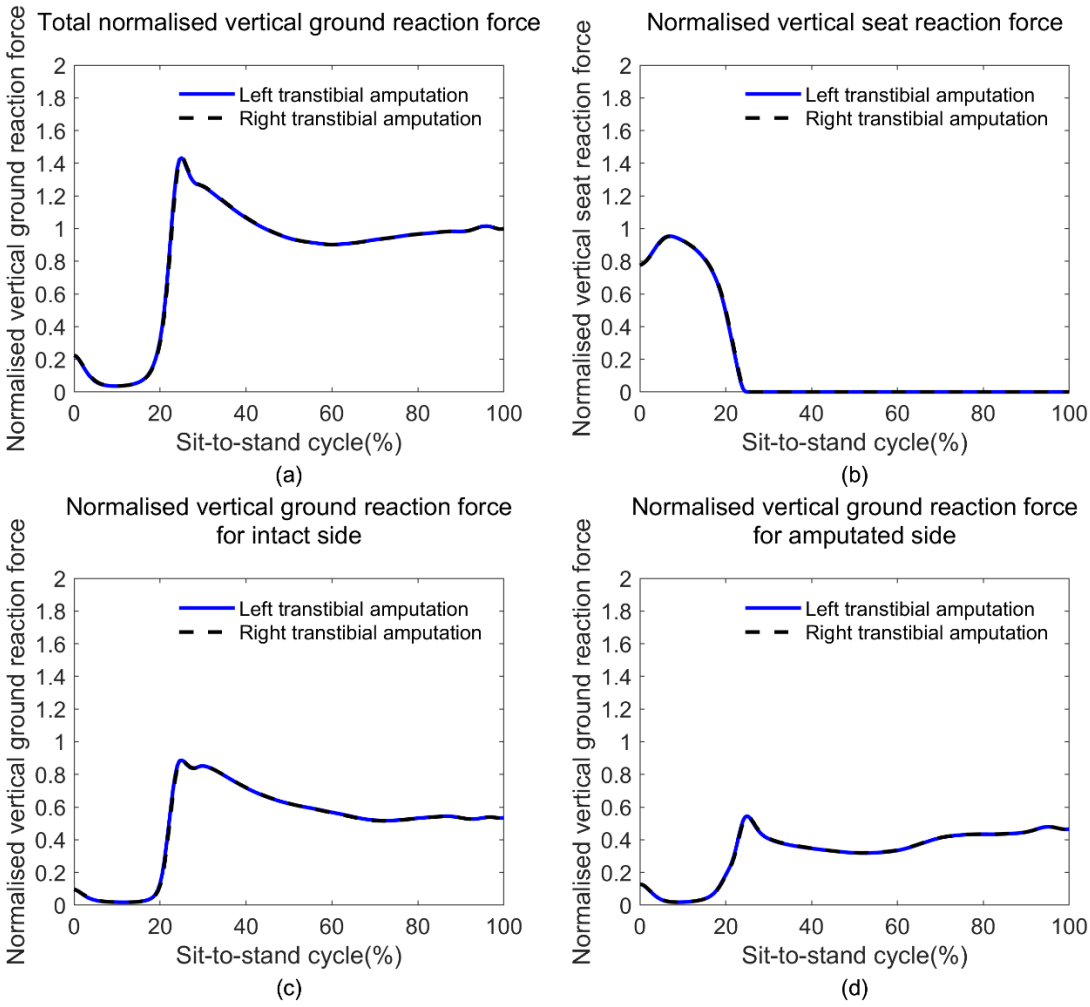

Figure 3.6. The contact forces between the human body and the external environment during sit-to-stand motion. The blue lines illustrate the results predicted using the left transtibial amputee model, the black lines represent results predicted using the right transtibial amputee model. (a) Total vertical ground reaction forces normalised by bodyweight. (b) Vertical seat reaction forces normalised by bodyweight. (c) Vertical ground reaction forces normalised by bodyweight for intact side. (d) Vertical ground reaction forces normalised by bodyweight for amputated side.

To test the robustness of the simulation framework and investigate whether the choice of amputation side in the human model has an effect on the simulation results,

a right transtibial amputee model was also used for predicting sit-to-stand motion. The results of the kinematics and contact forces predicted using the left and right transtibial amputee models are almost identical (Figure 3.5 and 3.6), indicating that the choice of amputation side in the model has no effect on the results, and also verifying the robustness of the simulation framework.

In general, the predicted lower limb joint angles were in good agreement with the experimental data. The root mean square errors and mean absolute errors of all joint angles were within 2.5 standard deviation (SD). Except for the prosthetic ankle joint, the Pearson correlation coefficients of the other lower limb joint angles were all greater than 0.87 (Table 3.2). During the movement, the angles of the hip and knee joints on both sides were symmetrical (Figure 3.7). As the movement progressed, the hip joint angles first increased and then decreased [Figure 3.7 (a) and (b)], while the knee joint angles first remained at a certain level and then decreased [Figure 3.7 (c) and (d)]. The ankle joints on both sides showed different motion patterns: the angle of the amputated side fluctuated slightly near the initial point, in contrast, the intact side had a larger range of motion and an obvious peak [Figure 3.7 (e) and (f)].

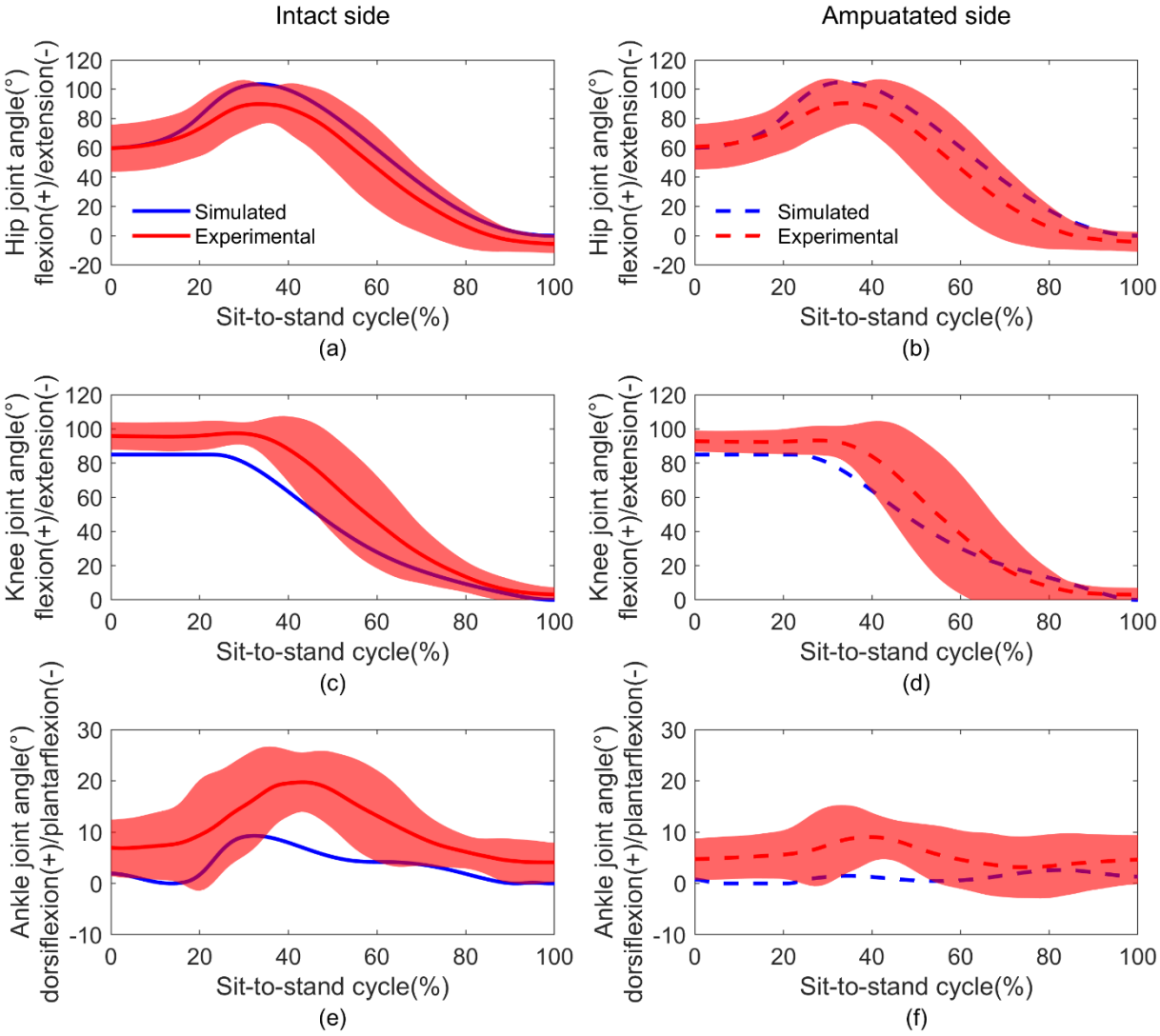

Figure 3.7. Lower limb joint angles during sit-to-stand motion. The blue lines illustrate the results from the nominal predictive simulation, the red lines and shaded regions represent the mean and two standard deviations of the experimental data. Solid lines represent intact legs and dashed lines represent amputated legs. (a) Hip joint angles in intact side. (b) Hip joint angles in amputated side. (c) Knee joint angles in intact side. (d) Knee joint angles in amputated side. (e) Ankle joint angles in intact side. (f) Ankle joint angles in amputated side.

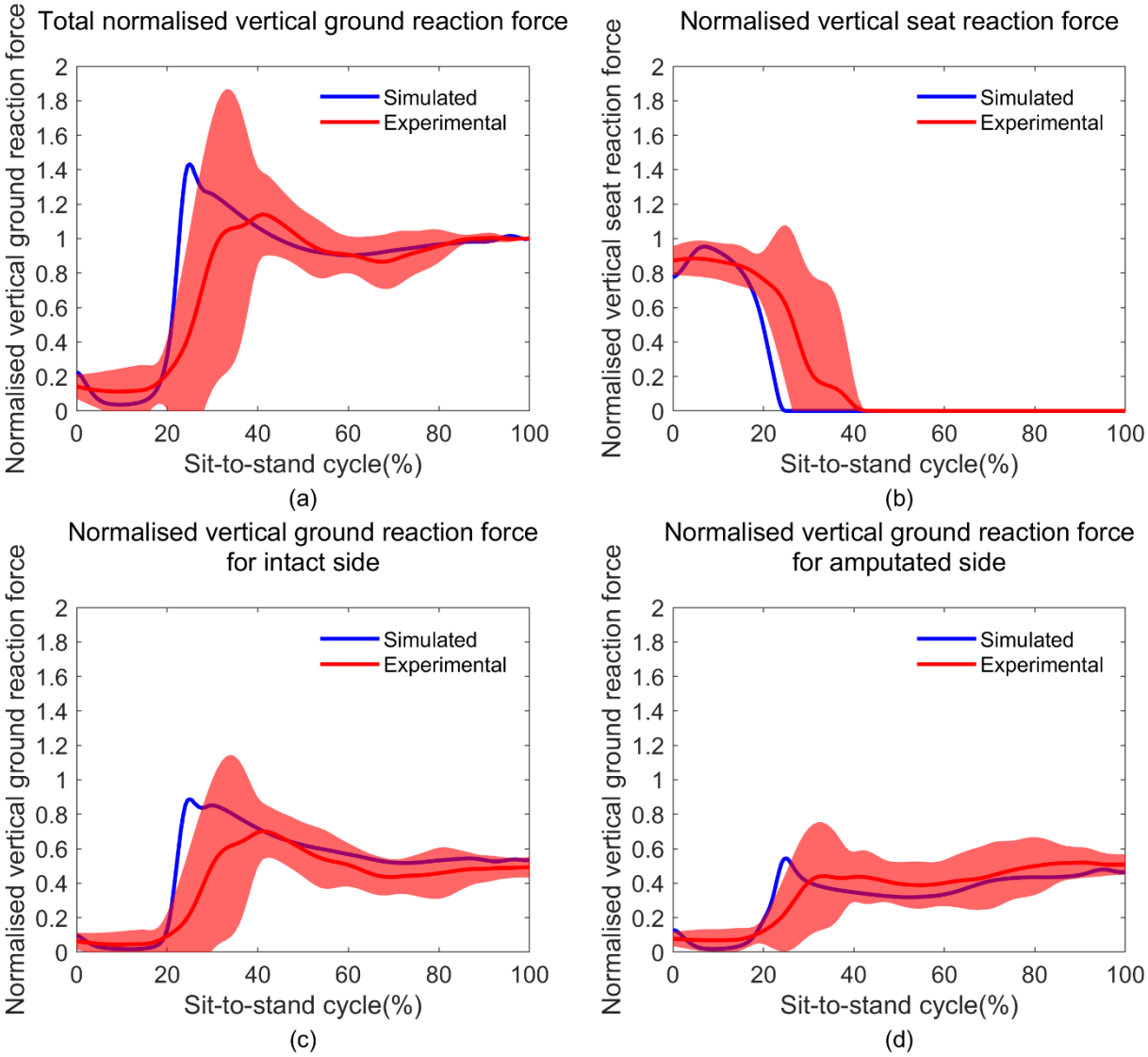

Figure 3.8. The contact forces between the human body and the external environment during sit-to-stand motion. The blue lines illustrate the results from the nominal predictive simulation, the red lines and shaded regions represent the mean and two standard deviations of the experimental data. (a) Total vertical ground reaction forces normalised by bodyweight. (b) Vertical seat reaction forces normalised by bodyweight. (c) Vertical ground reaction forces normalised by bodyweight for intact side. (d) Vertical ground reaction forces normalised by bodyweight for amputated side.

The nominal predictive simulation can effectively capture the main characteristics of the contact forces between the human body and the external environment. The root mean square errors and mean absolute errors between the

predicted vertical reaction forces and the experimental data were all within 1.3 SD, and all Pearson correlation coefficients were greater than 0.82 (Table 3.3). Near the moment when the buttocks left from the seat, the vertical ground reaction force borne by both legs increased sharply, with the intact leg reached a larger peak [Figure 3.8 (c) and (d)]. With a sharp increase in the total vertical ground reaction force, the seat reaction force declined rapidly to zero, marking the complete detachment of the human body from the seat [Figure 3.8 (a) and (b)].

Table 3.2: Root Mean Square Errors, Mean Absolute Errors and Pearson Correlation Coefficients of Joint Angles in Lower Limbs between Experimental Data and Nominal Simulation

		Hip	Knee	Ankle
Root mean square error (SD)	Intact side	1.2004	2.3038	2.3649
	Amputated side	1.2234	1.7165	1.9657
Mean absolute error (SD)	Intact side	1.0790	2.0175	2.2356
	Amputated side	1.0923	1.4676	1.7127
Pearson correlation coefficient	Intact side	0.9929	0.9835	0.8790
	Amputated side	0.9884	0.9862	-0.3116

The unit of the root mean square error is standard deviation (SD).

Table 3.3: Root Mean Square Errors, Mean Absolute Errors and Pearson Correlation Coefficients of Ground Reaction Forces and Seat Reaction Force between Experimental Data and Nominal Simulation

	Total GRFv	GRFv in intact side	GRFv in amputated side	SRFv
Root mean square error (SD)	1.1347	1.2857	1.2253	1.1107
Mean absolute error (SD)	0.8536	1.0587	1.0814	0.7545
Pearson correlation coefficient	0.8392	0.8238	0.8719	0.9067

GRFv represents the vertical ground reaction force normalised by bodyweight. SRFv represents the vertical seat reaction force normalised by bodyweight. The unit of the root mean square error is standard deviation (SD).

During the sit-to-stand motion, the coordinate value of the centre of mass in the anterior-posterior direction continued to increase [Figure 3.9 (a)], which means that the horizontal velocity was always positive [Figure 3.9 (d)]. In contrast, the coordinate value of the centre of mass in the superior-inferior direction mainly showed a trend of first decreasing and then increasing [Figure 3.9 (b)], which was reflected in the appearance of two peaks in the vertical velocity, one positive and one negative

[Figure 3.9 (d)].

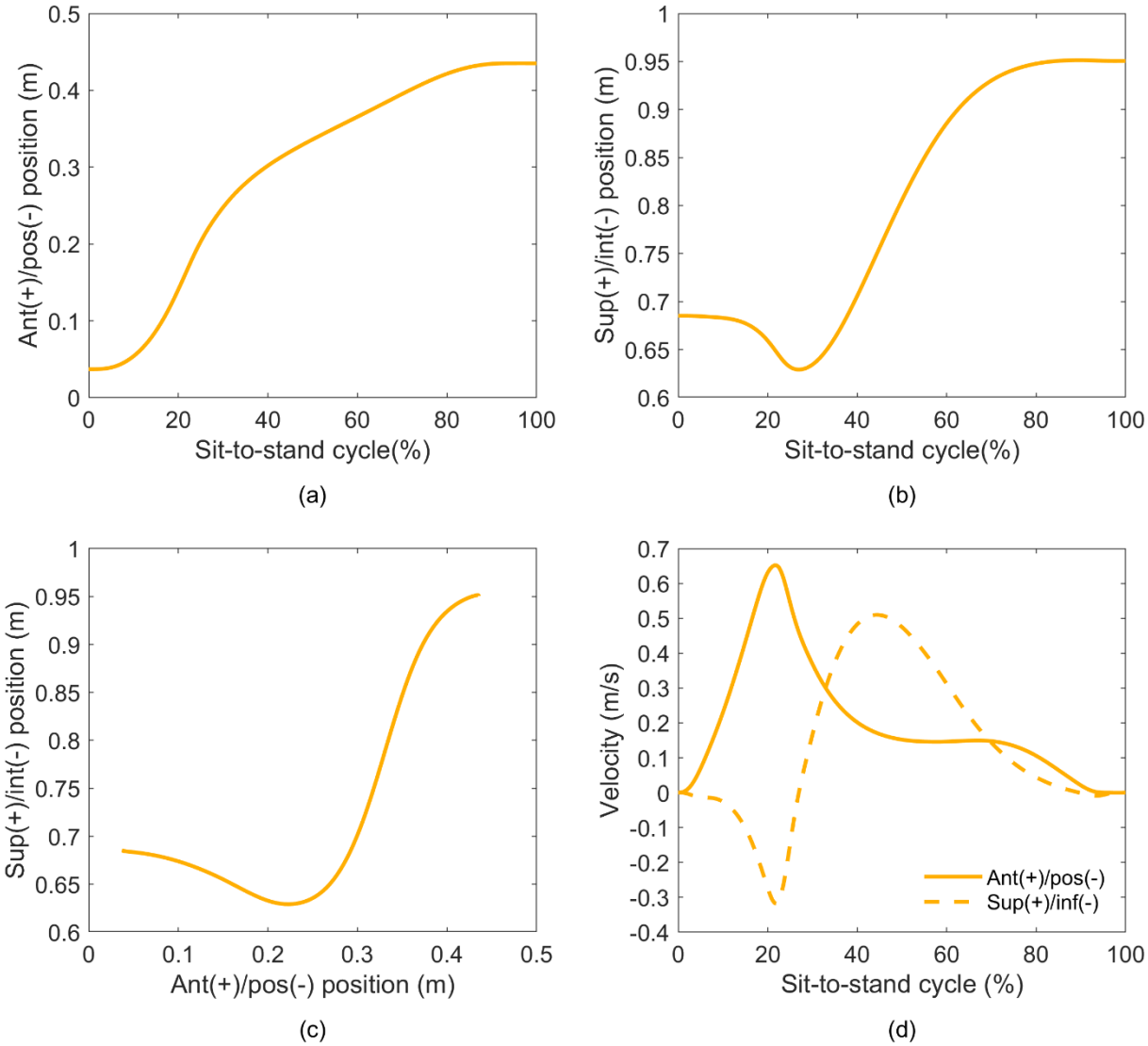

Figure 3.9. Kinematics of the centre of mass during sit-to-stand motion. The positions and velocities of the centre of mass in the Anterior (Ant)/posterior (pos) direction and the Superior (Sup)/Inferior (Inf) direction were obtained through the nominal predictive simulation. (a) The position of the centre of mass in the Ant/pos direction. (b) The position of the centre of mass in the Sup/Inf direction. (c) The motion curve of the centre of mass in the sagittal plane. (d) The velocity of the centre of mass in the Ant/pos (solid line) and Sup/Inf (dashed line) directions.

3.3.2 Effects of Varying Prosthetic Stiffness on Patients' Dynamic Behaviour

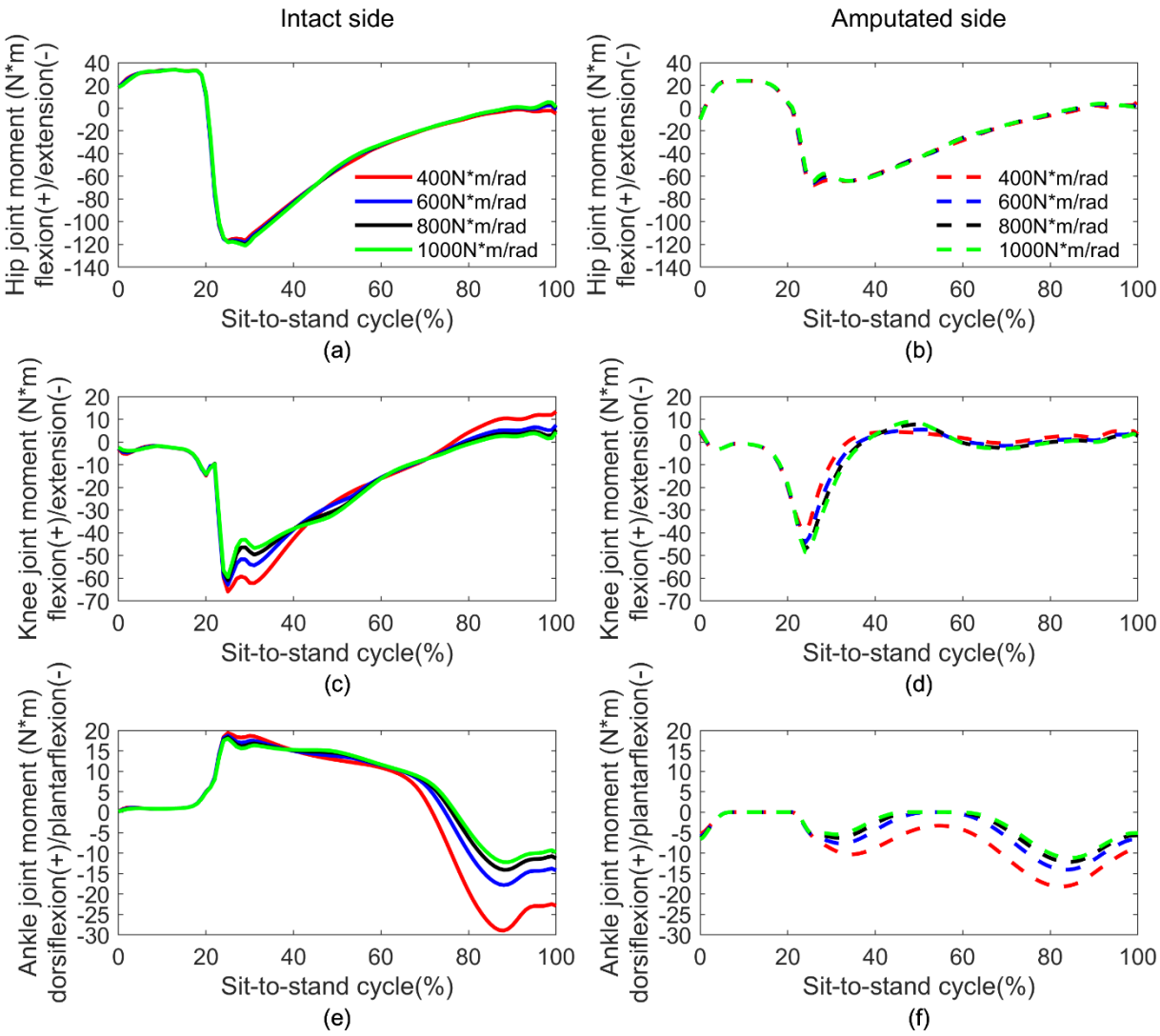

Figure 3.10. Joint moments of the lower limb at different prosthetic stiffness. The red lines, blue lines, black lines, and green lines represent the situation when the prosthetic stiffness is 400 N*m/rad, 600 N*m/rad, 800 N*m/rad, and 1000 N*m/rad respectively. Solid lines represent intact legs (left column), dashed lines represent amputated legs (right column). (a) Hip joint moments of the intact leg. (b) Hip joint moments of the amputated leg. (c) Knee joint moments of the intact leg. (d) Knee joint moments of the amputated leg. (e) Ankle joint moments of the intact leg. (f) Ankle joint moments of the amputated leg.

Table 3.4: Peak Moments of Lower Limb Joints under Different Prosthetic Stiffness

Prosthetic stiffness (N*m/rad)	Peak hip extension moment(N*m)		Peak knee extension moment(N*m)		Peak ankle plantarflexion moment(N*m)	
	Intact side	Amputated side	Intact side	Amputated side	Intact side	Amputated side
400	116.75	67.73	65.85	39.57	28.94	18.17
600	118.52	65.91	62.84	44.34	17.82	14.06
	(+1.52%)	(-2.69%)	(-4.57%)	(+12.05%)	(-38.42%)	(-22.62%)
800	120.09	65.09	60.83	47.05	14.10	12.14
	(+2.86%)	(-3.90%)	(-7.62%)	(+18.90%)	(-51.28%)	(-33.19%)
1000	121.08	64.59	59.46	48.48	12.22	11.19
	(+3.71%)	(-4.64%)	(-9.70%)	(+22.52%)	(-57.77%)	(-38.41%)

The values in the parentheses represent the growth rate of the current peak joint moment relative to the peak moment of the same joint in the nominal simulation.

There are obvious peaks in the extension moments of the hip and knee joints on both sides (Figure 3.10). As the prosthetic stiffness gradually increased from 400 to 1000 in increments of 200, the peak moments of the hip, knee and ankle joints on the both sides showed different change patterns (Table 3.4 and Figure 3.10). For the peak extension moments of the hip joints, the values increased on the intact side and decreased on the amputated side. In contrast, the peak knee extension moment decreased on the intact side and increased on the amputated side. However, the peak plantarflexion moment of the ankle joints decreased on both sides. Among all

the peak joint moments in the lower limbs, the ankle joints had the largest percentage change, with -57.77% on the intact side and -38.41% on the amputated side; while the hip joints had the smallest change, with +3.71% on the intact side and -4.64% on the amputated side.

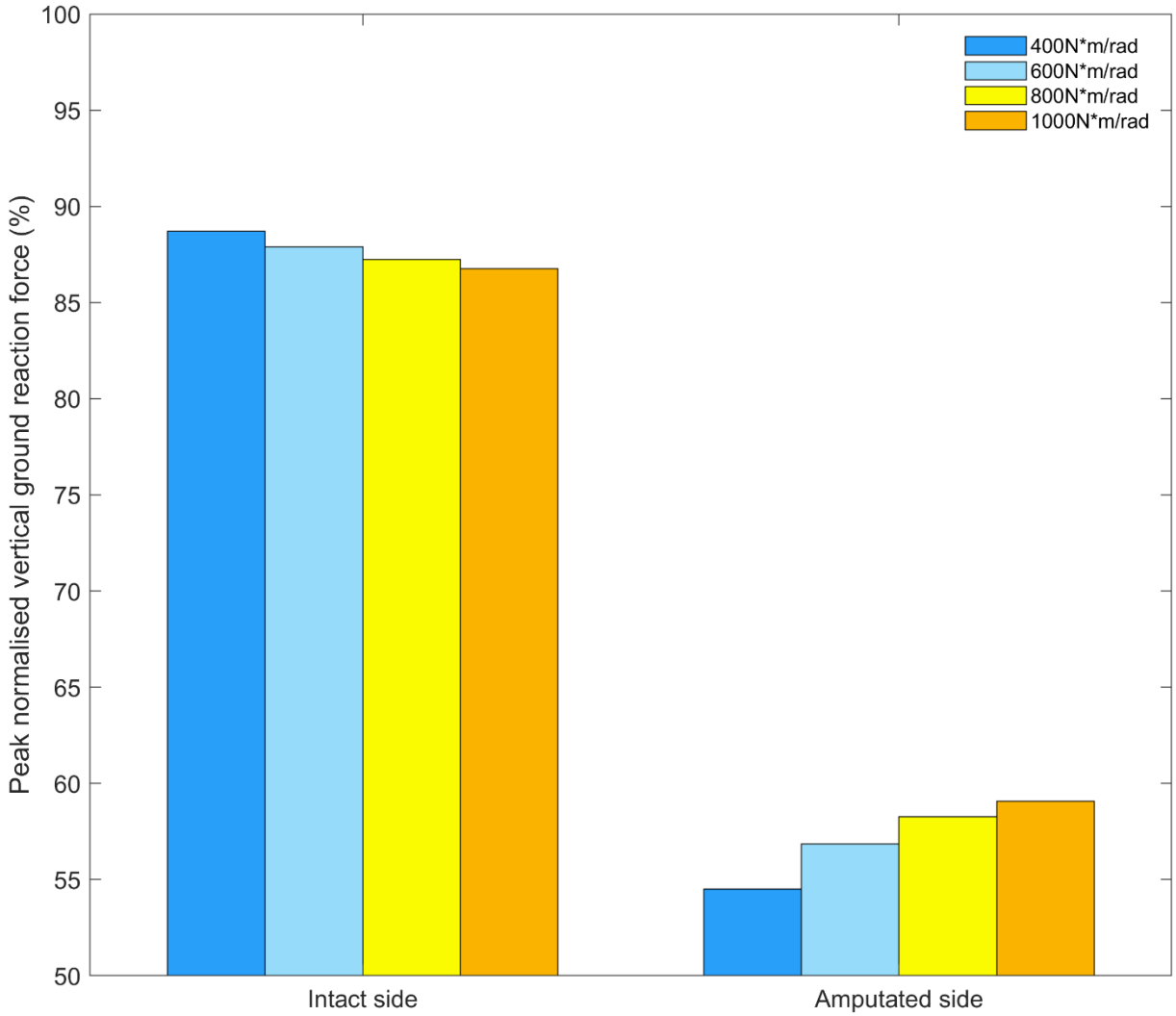

Figure 3.11. Normalised peak vertical ground reaction forces of both lower limbs under different prosthetic stiffness. Peak vertical ground reaction forces were normalised by bodyweight.

In predictive simulations under different prosthetic stiffness conditions, the

normalised peak vertical ground reaction force loaded by the intact leg was always higher than that of the amputated leg (Figure 3.11). As the prosthetic stiffness increased, the normalised peak vertical ground reaction force borne by the intact leg gradually decreased from 88.69% to 86.77%, while that borne by the amputated leg gradually rose from 54.49% to 59.08%.

3.4 Discussion

In this study, we proposed a novel simulation framework that can predict the sit-to-stand behaviour of the unilateral transtibial amputee considering seat contact. The effectiveness of the simulation framework was validated by the experimental data. Using this simulation framework, we further analysed the effect of changes in prosthetic stiffness on the dynamic behaviour of lower limbs.

Combining the lower limbs on both sides and establishing an immobile joint between the feet and ground is a common method for predicting sit-to-stand movements in intact people [26, 27]. However, this method assumes perfect symmetry on both sides of the human body and is not suitable for studying the movement of unilateral amputees. Therefore, a floating base human body model was adopted in this study, and the contact forces between the human body and the external environment were simulated through the smooth Hunt-Crossley force model. We first proposed the “free fall method” to determine the initial and final postures of the human body model, and then completed the nominal predictive simulation

through the efficient direct collocation method. Joint angles in the lower limbs and contact forces obtained through nominal simulation exhibited similar patterns to experimental data, enhancing our confidence in the proposed simulation framework. The physical asymmetry of the body can lead to asymmetry in kinematics and kinetics. The ankle joint on the intact side had a larger range of motion than the amputated side [Figure 3.7 (e) and (f)], which is due to the resistance effect of the passive moment provided by the prosthesis [as shown in Equation (3.1)]. In addition, compared with the amputated leg, the intact leg bore a greater peak vertical ground reaction force [Figure 3.8 (c) and (d)], which is consistent with previous experimental studies [58, 59]. However, there are certain numerical differences between the results predicted through nominal simulation and experimental data, which may be caused by various reasons. For example, the motion of the human body model is limited to the sagittal plane, and the degrees of freedom of the prosthesis have been greatly simplified. In addition, amputation has strong subject specificity, which can also contribute to these differences.

At the initial and final point of the transition from sitting to standing, the projections of the centre of mass velocity in the anterior-posterior direction and the superior-inferior direction are both zero [Figure 3.9 (d)], which well reflects the static state of the human body. At the beginning of the movement, the human trunk first flexed forward to prepare for leaving the seat, which was reflected in the forward and downward movement of the centre of mass, causing the centre of mass velocity to

peak in the anterior direction and downward direction respectively. After leaving the seat, the motion of the centre of mass was mainly reflected as an upward lift [Figure 3.9 (c)], resulting in a peak in the upward velocity of the centre of mass.

Knee osteoarthritis is more prevalent in patients with lower limb amputation [68], which may be attributed to higher knee joint contact force [69]. Although there are no muscles in our human body model and the specific magnitude of the knee joint contact forces cannot be directly calculated, our results can indirectly support this opinion. Joint contact force is determined by the intersegmental reaction forces and muscle forces [70]. A smaller peak vertical ground reaction force on the amputated leg [Figure 3.8 (d) and 3.11] will result in a smaller axial intersegmental force. In addition, the smaller peak extension moment of knee joint in the amputated leg [Figure 3.10 (d) and Table 3.4] suggests smaller peak contraction forces in the knee extensor muscle group (i.e. quadriceps femoris). Compared to the intact side, the amputated side has a smaller knee joint contact force, which is the comprehensive result of the above effects.

Changing the prosthetic stiffness affected the peak moments of the lower limb joints on both sides (Figure 3.10 and Table 3.4). Overall, the ankle joints were most affected, followed by the knee joints, and the hip joints were least affected. This indicates that the further the joint is from the prosthesis, the less its peak extension moment is affected by changes in prosthetic stiffness. In addition, although the amputation occurred on one side, the peak moments of the joints in the intact leg

also changed, indicating that changes in the prosthetic stiffness not only affect the amputated side, but also affect the force state of the joints on the intact side. Increasing the prosthetic stiffness can reduce the peak knee extension moment and vertical ground reaction force on the intact side (Table 3.4 and Figure 3.11), which may help alleviate the knee joint contact force within the intact leg. However, this change will in turn increase the peak vertical ground reaction force and knee extension moment on the amputated side, and the percentage increase on this side is much greater than the percentage decrease on the intact side. As a result, the knee joint contact within the amputated leg may become worsened. Therefore, when adjusting the prosthetic stiffness, it is necessary to consider the actual physical condition of the patient and balance the effect on the bilateral knee joint contact forces.

The work in this chapter needs to be implemented through two softwares, namely OpenSim and MATLAB. Therefore, the configuration of the computer used should meet the basic requirements for running OpenSim and MATLAB. For example, a computer with an Intel core i7 processor and 16GB random-access memory (RAM) was used to complete the simulation studies in this chapter. Since this is the first study to predict sit-to-stand movement considering seat contact in the unilateral transtibial amputee, there are almost no relevant literature available for reference. Therefore, several challenges were encountered during the research process, such as difficulty in convergence of the optimisation process and unrealistic motion

obtained from calculations. After thousands of failures and attempts at various innovative methods, success finally arrived. This chapter involves various theories, such as optimal control theory, direct collocation method, multi-body dynamics, contact mechanics, etc. In addition, it also involves the application of various technologies, such as the usage of OpenSim and how to call the OpenSim API through MATLAB programming.

The proposed simulation framework can effectively predict the sit-to-stand behaviour of the unilateral transtibial amputee. In future studies, muscle-driven predictive simulation of sit-to-stand movement for the unilateral transtibial amputee can be performed to extend the proposed simulation framework. The simulation framework proposed in this study can provide new inspiration for prosthetic design and theoretical guidance for developing rehabilitation treatment plans.

3.5 Conclusion

This study is the first to predict the sit-to-stand motion of the unilateral transtibial amputee considering seat contact. We proposed a novel “free fall method” to solve the problem of difficulty in solving the initial and final equilibrium postures of human models. The effect of the change in prosthetic stiffness on the dynamic behaviour was studied using the proposed simulation framework. This chapter provides a new approach to study the sit-to-stand motion behaviour of patients with unilateral transtibial amputation, which can promote the development of prosthesis design,

rehabilitation training and other fields.

Chapter 4. Predictive Simulation of Sit-to-stand Movement for People with Ankle Movement Impairments Using Optimal Control

The content of this chapter is intended to be submitted to *IEEE Robotics and Automation Letters* at an appropriate time in the future. (Authors: Weida Wang, Ziyun Ding.)

4.1 Introduction

The health of the lower limbs determines a person's mobility. As the distal joints of the body, the ankle joints bear most of the weight and play a crucial role in lower limb movements. However, since the ankle joints directly bear the impact of the ground reaction forces, they are easily injured during sports or accidents, resulting in serious damage to their structure and function.

Limited range of motion is a common symptom after ankle trauma and surgery [71]. This symptom may be caused by factors such as ligament adhesion and changes in bone structure. As one of the important degrees of freedom in the ankle joint, the range of dorsiflexion is the focus of clinical attention. The knee-to-wall test is commonly used to assess the range of motion of ankle dorsiflexion [72]. When the knee touches the wall and the foot remains in full contact with the ground, the greater the maximum distance (d_n) that can be achieved between the big toe and the wall, the larger the range of ankle dorsiflexion (Figure 4.1). When the range of ankle

dorsiflexion is limited, it may alter a person's normal movement pattern and cause a decrease in mobility. The sit-to-stand movement requires high functional capacity of the lower limbs and is also a prelude to other daily life activities. Therefore, exploring the effect of restricted ankle dorsiflexion on the sit-to-stand movement has important clinical and academic significance.

Traditional simulation research in the field of biomechanics typically requires experimental data as input, which greatly limits the scope of research that can be conducted. Fortunately, predictive simulations based on optimal control theory do not rely on experimental data, making it more convenient to explore the causal relationship between different physical conditions and changes in motion behaviour. However, there are currently very few predictive studies on sit-to-stand motion for patients with lower limb dysfunction. Based on the predictive simulation method, Kumar *et al.* [27] studied the effect of decreased lower limb muscle strength on sit-to-stand movement. In Chapter 3, the author established a predictive model for sit-to-stand motion in unilateral lower limb amputees. Based on this model, the influence of varying prosthetic stiffness on dynamic behaviours was then explored. To my best knowledge, there is currently no predictive simulation study on the sit-to-stand movement of people with ankle dorsiflexion restriction.

The author accidentally missed several steps while going down the stairs, causing a unilateral ankle sprain. After the injury, the ankle joint showed symptoms such as limited range of motion and pain, which troubled me for a long time. Based

on my own injury experience and inspiration gained from it, this chapter delves into the potential negative effects of ankle joint injuries in the human body. This study focuses on people with unilateral ankle dorsiflexion limitation and investigates their sit-to-stand behaviour through predictive simulation. The multi-body dynamics model was established in OpenSim. The predictive problem can be formulated as the optimal control problem, which can be solved through the direct collocation method. The established simulation framework was then used to study the effects of different levels of ankle dorsiflexion limitation on the individual's sit-to-stand movement behaviour. This study can be conducted without experimental data, providing a new pathway for studying the effect of unilateral ankle dorsiflexion limitation on human movement behaviour. In addition, it can also provide valuable insights for clinical treatment and rehabilitation training.

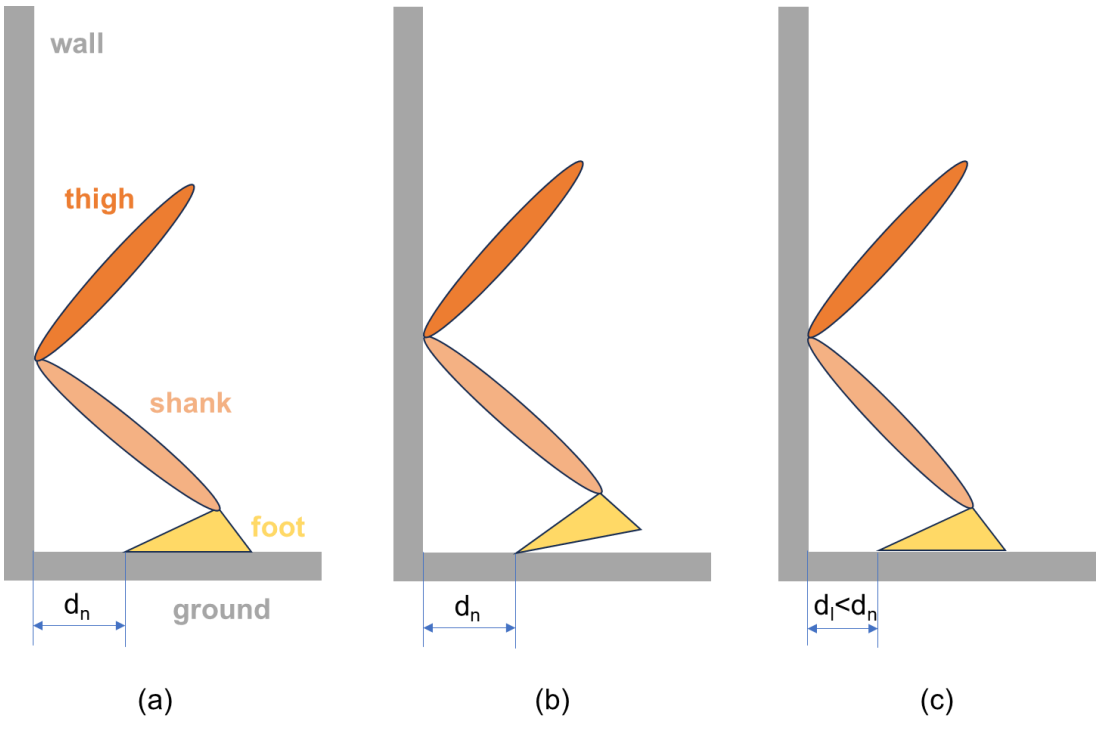

Figure 4.1. Schematic diagram of the knee-to-wall test. (a) represents the situation

where the range of ankle dorsiflexion is not restricted, and d_n is the maximum distance that can be reached between the big toe and the wall. (b) represents the situation where the range of ankle dorsiflexion is restricted. When the distance between the big toe and the wall remains d_n, the patient's heel will lift. (c) represents another situation where the range of ankle dorsiflexion is restricted. To achieve full contact between the foot and the ground, the distance between the big toe and the wall, d_l, will be less than d_n.

4.2 Methods

This chapter and the Chapter 3 both conduct predictive research on the sit-to-stand movement, with the main difference being the research subjects. In the Chapter 3, a simulation framework for predicting sit-to-stand behaviour in unilateral transtibial amputees was established, and its effectiveness was verified through experimental data. Therefore, the relevant simulation methods developed in Chapter 3 can be adopted for the research in this chapter. The following will highlight the unique features of this chapter's research, and content similar to that in Chapter 3 will be briefly described.

4.2.1 Biomechanical Simulation Model

The author developed a planar human body model in OpenSim [1–3] based on the full body model [73], as shown in Figure 4.2. The motion of all joints in the model was restricted to the sagittal plane. Each lower limb contains a hip, knee, and ankle joint, each of which has only one rotational degree of freedom. In addition, the lower limbs on both sides have the same mass properties. The torso is connected to the pelvis through a lumbar joint with a rotational degree of freedom. The ground-pelvis

joint formed between the pelvis and the ground has one rotational degree of freedom and two translational degrees of freedom. Except for the degrees of freedom of the ground-pelvis joint, each other degree of freedom in the model is driven by a torque actuator. The topological structure and driving method of the human model are shown in Figure 4.3.

The author used a smooth Hunt-Crossley force model [18] to simulate foot-ground contact and buttocks-seat contact. The contact spheres were placed in a similar manner to Chapter 3, with six contact spheres placed on each foot and two on the pelvis. The positions of the contact spheres are shown in Figure 4.2. The mechanical parameters of the contact spheres were chosen based on suggestions from Antoine [64].

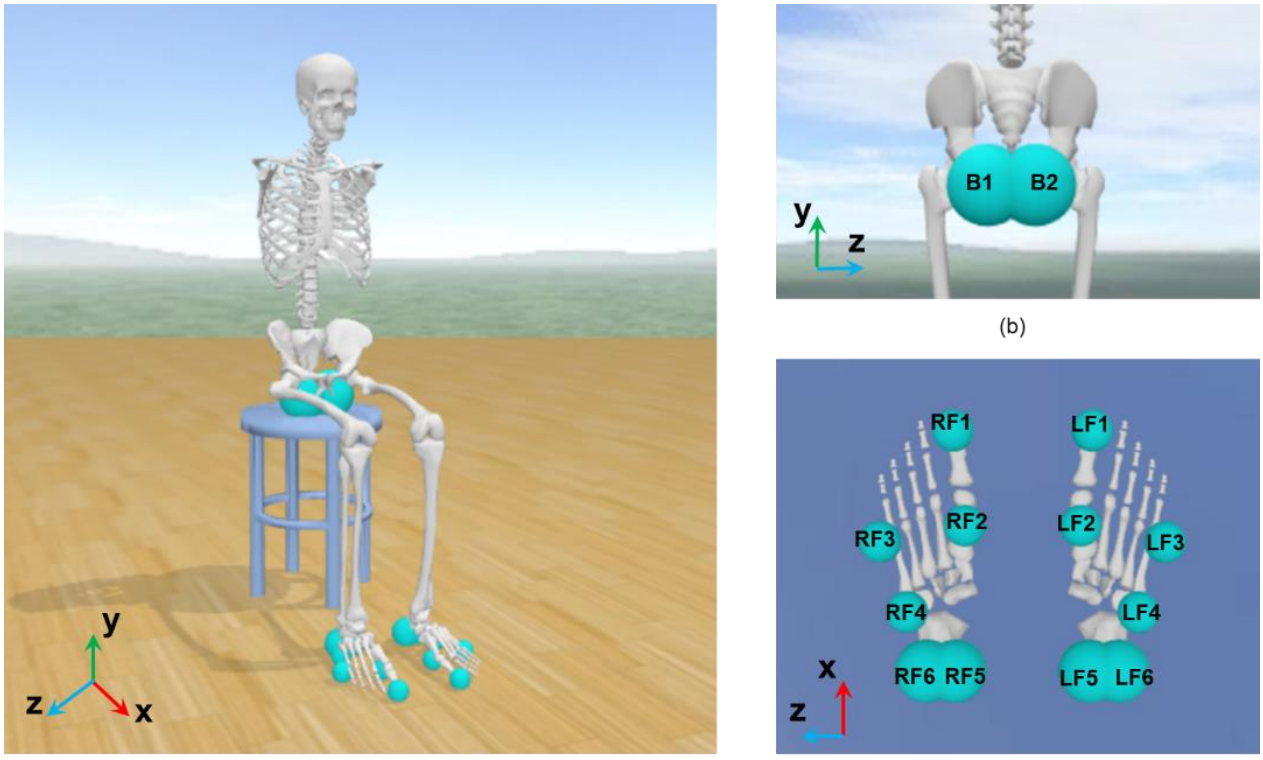

(a) (b) (c)

Figure 4.2. The biomechanical simulation model developed in OpenSim (the

coordinate axes in the figure are only used to indicate directions rather than specific positions). (a) is an overall view. (b) is a partial view of the human buttocks, on which two contact spheres B1 and B2 were placed. (c) is a partial view of the soles of both feet, with six contact spheres placed on each foot. The contact spheres on the left foot were LF1-LF6, and the contact spheres on the right foot were RF1-RF6.

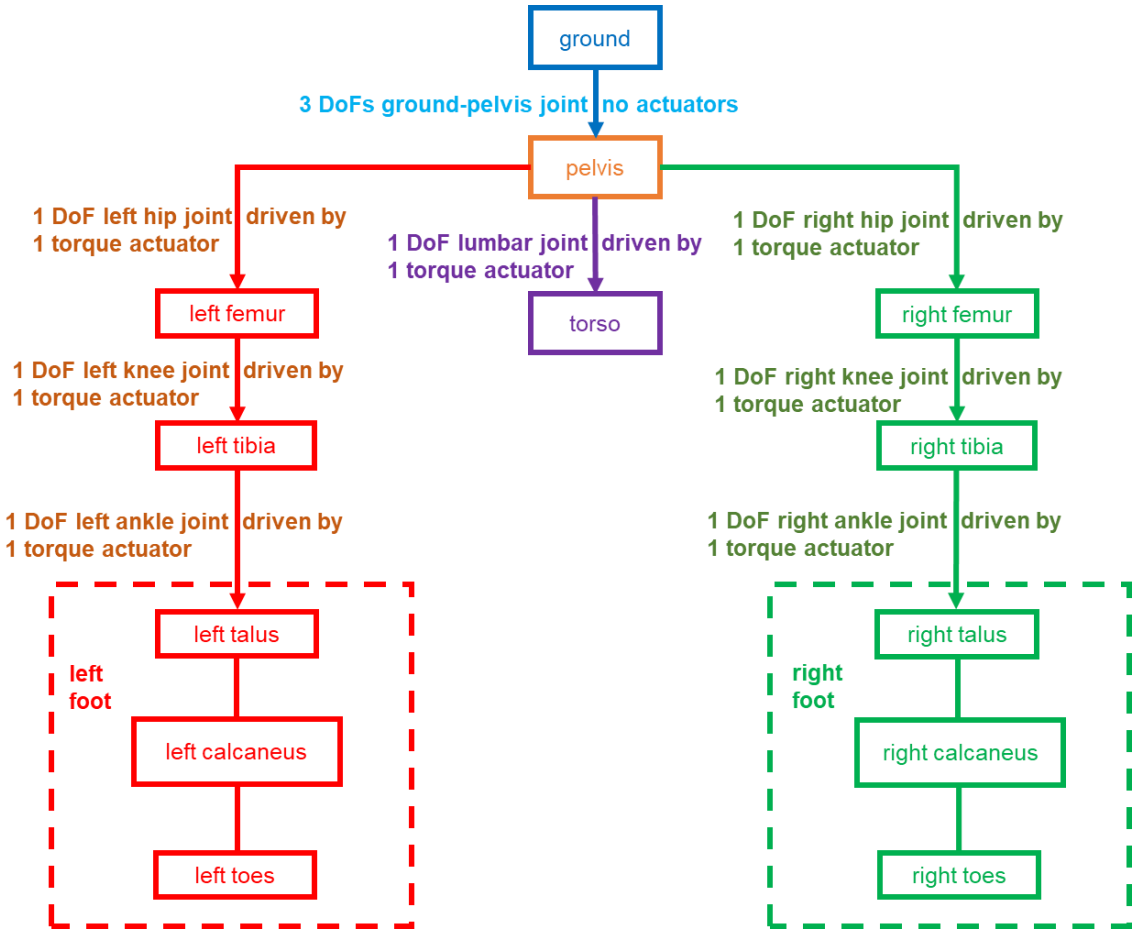

Figure 4.3. The topological structure and driving method of the human body model. The left leg has three degrees of freedom, each driven by one torque actuator. The topology of the right leg is the same as the left leg. There is one degree of freedom (DOF) between the pelvis and torso, driven by a torque actuator. There are three degrees of freedom between the ground and the pelvis, which are not driven by any actuators.

4.2.2 Solution of the Predictive Optimal Control Problem

The initial and final postures of the human model need to be fully determined

first. The generalised coordinate values of the hip, knee, and lumbar joints at the initial moment of the movement and the generalised coordinate values of the hip, knee, ankle, and lumbar joints at the end of the movement were first specified. The other undetermined generalised coordinate values at the initial and final moments were then solved using the "free fall method" proposed in the Chapter 3. The initial and final postures of the human model are finally summarised in Table 4.1.

Table 4.1: Generalised coordinate values of the human model in the initial and final postures

Generalised coordinate	Value in the initial posture	Value in the final posture
Hip flexion in affected side	60°	0°
Hip flexion in unaffected side	60°	0°
Knee flexion in affected side	85°	0°
Knee flexion in unaffected side	85°	0°
Ankle dorsiflexion in affected side	2.32°*	0°
Ankle dorsiflexion in unaffected side	2.32°*	0°
Lumbar flexion	35°	10°
Vertical translation of the ground-pelvis joint	0.63m*	0.95m*
Rotation of the ground-pelvis joint	21.15°*	-1.33°*

* indicates coordinate values determined by the “free fall method”.

The predictive problem of the sit-to-stand motion can be formulated as the optimal control problem for solving. The objective function consists of two terms, as shown in Equation (4.1):

$$J_{ld} = \int_0^T \|\boldsymbol{u}_{ld}(t)\|_2^2 \, dt + 10^{-3} \int_0^T \|\boldsymbol{\alpha}_{ld}(t)\|_2^2 \, dt \tag{4.1}$$

where J_{ld} is the objective function of the optimal control problem, $\boldsymbol{u}_{ld}$ is the control vector of torque actuators in the human model, $\boldsymbol{\alpha}_{ld}$ is the vector of joint generalised coordinate accelerations in the human model, t is the time variable, and T is the duration of sit-to-stand motion. Through some pre-simulation explorations, the second term of the objective function was multiplied by a scaling factor of 10^{-3} to facilitate convergence.

The generalised coordinate values of the model at the initial and final moments were constrained to the corresponding values in Table 4.1. In addition, the range of left ankle dorsiflexion in the model was assumed to be limited, with maximum dorsiflexion angles restricted to 15°, 10°, and 5° to represent mild, moderate, and severe limitations of left ankle dorsiflexion, respectively. The constraints on the generalised coordinate velocities and the vertical ground reaction forces are the same as those in Chapter 3. The author employed OpenSim Moco [54] to solve the formulated optimal control problem using the Hermite-Simpson method [53, 55].

4.3 Results

At the same level of ankle dorsiflexion limitation, the hip and knee joint angles on the affected side are symmetrical with those on the unaffected side during the motion. In contrast, there was an obvious asymmetry in the ankle joint angles on both sides, and the dorsiflexion angle of the affected ankle joint reached the corresponding upper limit in all three cases (Figure 4.4). In addition, the peak vertical ground reaction forces and peak knee extension moments on the affected side were greater than those on the unaffected side (Figure 4.5 and 4.6).

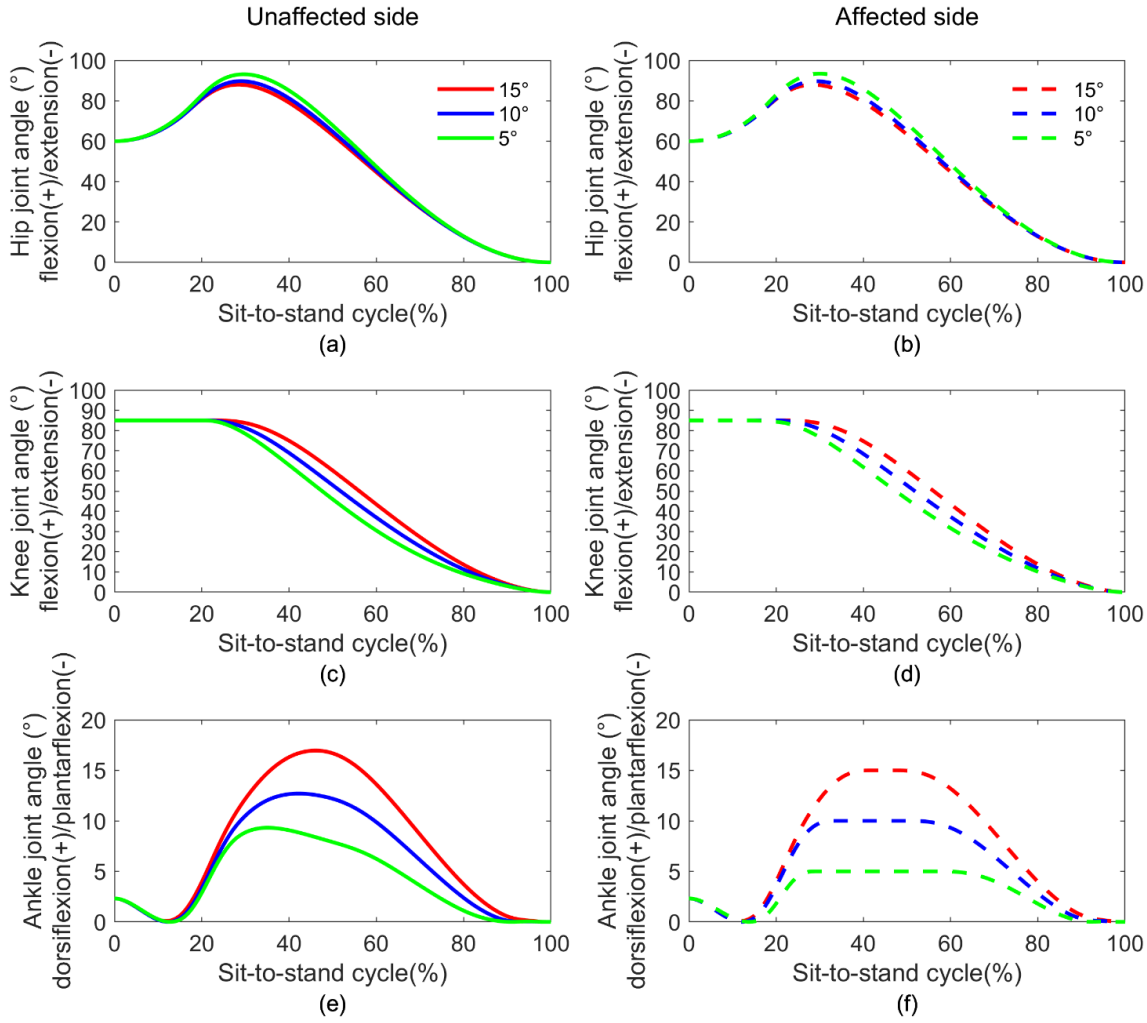

Figure 4.4. The angles of the lower limb joints on both sides at different levels of

ankle dorsiflexion limitation. The solid line represents the unaffected side, and the dashed line represents the affected side. The red, blue, and green lines represent the upper limit of ankle dorsiflexion angle on the affected side at 15°, 10°, and 5°, respectively.

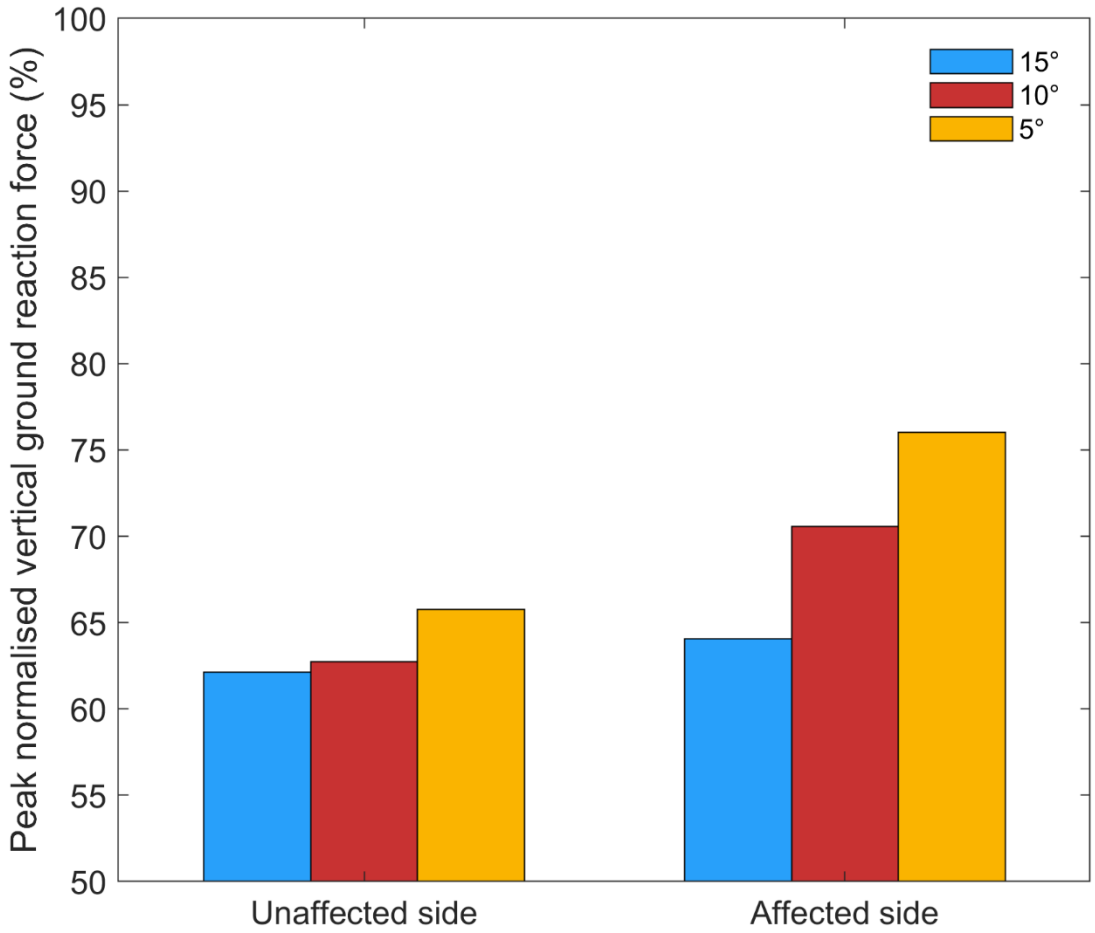

Figure 4.5. Normalised peak vertical ground reaction forces on both lower limbs at different levels of ankle dorsiflexion limitation. Body weight was used to normalise the vertical ground reaction forces.

As the limitation of unilateral ankle dorsiflexion became more severe, the peak flexion angle of both hip joints increased, while the peak dorsiflexion angle of both ankle joints decreased (Figure 4.4). The peak vertical ground reaction forces on both sides showed an upward trend, and the increase in the affected side was more

obvious (Figure 4.5). In addition, the peak extension moment of the affected knee joint went up with the increase of the restricted level (Figure 4.6).

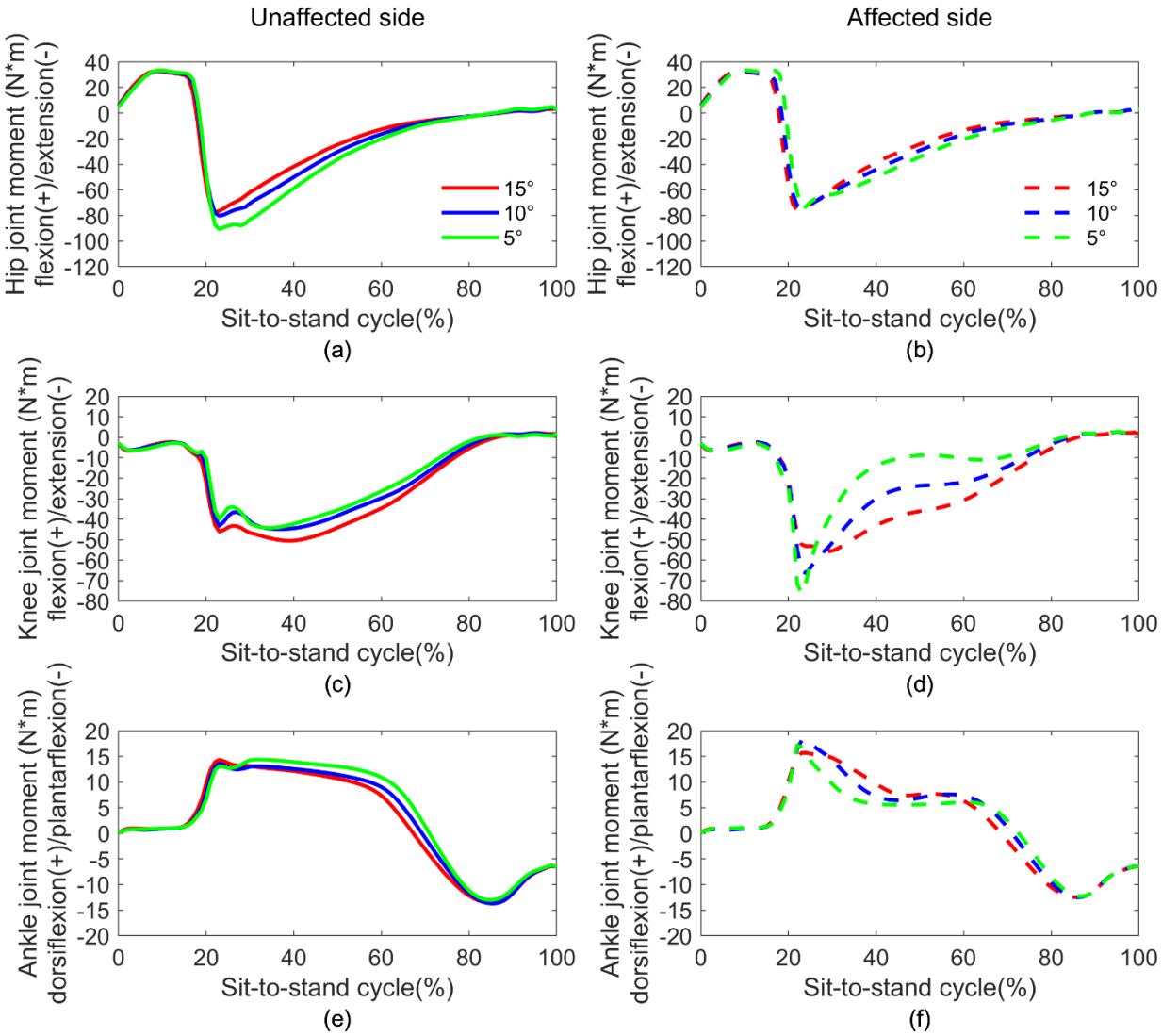

Figure 4.6. Joint moments in both lower limbs at different levels of ankle dorsiflexion limitation. The solid line represents the unaffected side, and the dashed line represents the affected side. The red, blue, and green lines represent the upper limit of ankle dorsiflexion angle on the affected side at 15°, 10°, and 5°, respectively.

4.4 Discussion

In this study, the author established a simulation framework for predicting the sit-

to-stand motion of people with unilateral dorsiflexion limitation. With the help of an efficient direct collocation method, the motion performance of patients at different levels of ankle dorsiflexion limitation was successfully obtained.

The ankle joint angles on both sides at the initial moment determined by the “free fall method” were within the range of the most severe dorsiflexion limitation (<5°), and the ankle dorsiflexion angles on both sides were exactly the same (Table 4.1). In contrast, both ankle joint angles of the unilateral transtibial amputee were not completely equal at the initial moment (Table 3.1). This may be mainly caused by two reasons: 1) The mass and inertia properties of both lower limbs below the knee joints in the unilateral transtibial amputee are asymmetric. In contrast, although the patients studied in this chapter have restricted ankle dorsiflexion angle on one side, their left and right lower limbs have the same mass properties. 2) The prosthetic foot of the unilateral transtibial amputee can generate passive torque, while there is no passive torque in the intact foot, which can also lead to asymmetry in both ankle joint angles. However, there is no passive torque present in both ankles of people with unilateral ankle dorsiflexion restriction.

During the sit-to-stand movement, the dorsiflexion angle of the affected ankle joint rose to the upper limit and then remain there, forming a "plateau" (Figure 4.4). In contrast, the dorsiflexion angle of the unaffected ankle joint immediately decreased after reaching a higher peak, due to the greater flexibility of the unaffected ankle compared to the affected ankle.

The increase in the level of ankle dorsiflexion limitation undoubtedly leads to a decrease in the peak dorsiflexion angle of the affected ankle joint. Interestingly, the peak angle of the unaffected ankle also showed a downward trend (Figure 4.4). This phenomenon is beneficial for promoting symmetrical movements of the lower limbs on both sides. Because the dorsiflexion angle of the affected ankle is limited, multiple other lower limb joints (more than one) adjusted their respective movement patterns and performed corresponding biomechanical compensation. As the restricted level increased, near the moment when the buttocks left the seat, the hip joints on both sides underwent greater flexion while the knee joint flexion angle decreased. These alternative movement patterns may be attributed to the patient's need to maintain stability during sit-to-stand movements. Restricted ankle dorsiflexion is not conducive to the forward movement of the centre of mass, while the alternative movement patterns adopted by the hip and knee joints can promote the centre of mass to move towards the base of support, which can offset the adverse effects of restricted ankle dorsiflexion on stability.

If the human body is regarded as a whole system for dynamic analysis, the upward lift of the centre of mass during the sit-to-stand motion is closely related to the vertical ground reaction forces. The ground reaction forces originate from the two feet pushing down against the ground. In all three cases of unilateral ankle dorsiflexion limitation, the peak vertical ground reaction force borne by the affected lower limb was greater than that on the unaffected side (Figure 4.5). This is because

the ankle with limited dorsiflexion is stiffer than that on the unaffected side, requiring more effort to push against the ground.

A previous study suggested that deficient knee extensor strength may contribute to failure in the sit-to-stand movement [27], indicating that the health of the knee joints play a crucial role in the successful completion of the sit-to-stand movement. At the same level of ankle dorsiflexion restriction, the peak knee extension moment in the affected side was greater than that in the unaffected side (Figure 4.6). In addition, the affected lower limb also bore a greater peak vertical ground reaction force (Figure 4.5). The combined effect of the above two aspects may lead to a greater joint contact force in the affected knee than that in the unaffected side. Although the knee joint in the affected side was not restricted, the limited dorsiflexion of the adjacent ankle joint increased its load burden. This indicates that each lower limb act as a whole during the movement, therefore the healthy knee joint is affected by the abnormality of the adjacent ankle joint. Moreover, as ankle dorsiflexion became more limited, the peak vertical ground reaction force and the peak knee extension moment in the affected side increased (Figure 4.5 and 4.6), which may lead to the deterioration in the health of the ipsilateral knee joint. This suggests that ankle dorsiflexion limitation should not be underestimated. Instead, we should take it seriously enough to avoid negative effects on other healthy joints. Rehabilitation training such as continuous passive motion (CPM) [74] should be carried out as early as possible to improve the range of motion of the injured ankle joint and minimise its

adverse effects on human health.

This is the first predictive study on sit-to-stand movement of people with unilateral ankle dorsiflexion limitation, and there is no relevant literature or technical route available for reference. To carry out this work, researchers need to have solid theoretical knowledge of biomechanics and be able to apply these pieces of theoretical knowledge in a comprehensive manner. In this chapter, the author was inspired by his own personal experience of ankle injury and flexibly applied the knowledge he learned to the research work, using the original "free fall method" for predictive simulation. After numerous attempts and overcoming many difficulties, this study was finally successfully completed. The difficulty and complexity of the specific calculation process are no less than those of the work in Chapter 3.

In this chapter, the predictive simulation of sit-to-stand motion for people with unilateral ankle dorsiflexion limitation was successfully completed. To alleviate the convergence difficulty of the optimal control problem, the author employed a torque driven multi-body dynamics model. The effect of different dorsiflexion restriction levels on human motion behaviour can be obtained, however, the dynamic behaviour of the muscles cannot be predicted. In future studies, the proposed simulation framework can be extended to predict muscle-driven sit-to-stand motion for people with unilateral ankle dorsiflexion limitation. In addition, we can also explore the effect of unilateral ankle dorsiflexion limitation on other daily life activities such as walking.

4.5 Conclusion

In this chapter, the author proposed a simulation framework to achieve successful prediction of sit-to-stand movement in people with unilateral ankle dorsiflexion limitation. Based on this simulation framework, the author further explored the effects of different levels of ankle dorsiflexion limitation on the patient's motion behaviour when experimental data were not available. This framework opens the door to studying pathological movement behaviours of humans after ankle injuries without experimental data, which is beneficial to the development of clinical treatment and rehabilitation training.

Chapter 5. Muscle-Driven Simulation of the Transition from Squatting to Standing Using Inverse Optimal Control

The content of this chapter has been submitted to *IEEE Transactions on Biomedical Engineering*. The current status is *Under review*. (Authors: Weida Wang, Jiayu Hu, Biwei Tang, Duncan Shepherd and Ziyun Ding.)

5.1 Introduction

The transition from squatting to standing is a fundamental movement in our daily lives. It not only facilitates the capacity for independent living but also plays an important role in maintaining balance and stability. This movement is frequently incorporated into rehabilitation for postoperative patients to enhance muscular strength and endurance [75]. Furthermore, the investigation of the movement is not only beneficial for designing assistive devices, such as lower limb exoskeletons to reduce muscle effort [76] and energy consumption [77], but also helps test the movement capabilities of humanoid robots [66, 78]. Therefore, a deep understanding of the behavioural characteristics and underlying mechanisms of this movement can contribute to achieving real human-machine interaction from the biomechanical perspective, thereby ensuring effectiveness and promoting efficiency.

The behavioural characteristics during the transition from squatting to standing are intricately related to the motor control of nervous system and the coordination of

skeletal muscles. The integration of musculoskeletal modelling with in-silico simulation provides an effective method to explore motor control and skeletal muscle coordination mechanisms within the neuromusculoskeletal system.

Through dynamic optimisation, also referred to as optimal control, simulations enable the prediction of movement behaviour. This optimisation algorithm, operating within specified constraints, predicts motion by minimising an objective function. This function is formulated by combining multiple performance criteria to accurately reflect the intended motion. Walking gait is the primary focus of the predictive simulation, where: Anderson *et al.* [29] conducted pioneering work on gait prediction in healthy individuals, where the performance criteria took into account the effects of energy expenditure and joint hyperextension; in [31], after linearly weighting the aforementioned performance criteria with two terms that penalise motion instability, a sagittal plane model was used to simulate the human walking behaviour under abnormal ankle plantar flexion muscles; Falisse *et al.* [64] integrated the effects of energy expenditure, movement smoothness and joint hyperextension in the objective function, enabling the prediction of human gait under various healthy and pathological conditions. The performance criteria in the above studies effectively capture gait patterns that align well with experimental measures, enhancing our understanding of the motor control mechanism in human walking. However, the weights of different terms in the objective function are frequently adjusted manually, imposing a substantial burden in terms of time and labour.

The application of inverse optimal control method has been shown to effectively alleviate the burden of adjusting weights while also yielding prediction results with high accuracy [39]. Despite the valuable insights gained from studies focused on motor control mechanisms, there is a scarcity of research on tasks beyond level walking. Recently, a torque-driven model was established to predict human behaviour during manual material handling [79]. Based on this model, the importance of dynamic effort and stability of movement was explored. In [40], a bilevel optimisation method utilising the particle swarm optimisation algorithm and the direct collocation method was proposed to solve the inverse optimal control problem. Then, the proposed method was combined with the torque-driven model to achieve the prediction of joint angles during human lifting movements. The torque-driven models can greatly reduce the convergence difficulty in dynamic optimisation, leading to enhanced computational efficiency. Nevertheless, this driving method, due to the lack of skeletal muscle modelling, fails to address the complexities of muscle force sharing, therefore limiting a profound understanding of how the nervous system coordinates redundant muscles for such movements.

As far as we know, this study, for the first time, integrates the inverse optimal control method with the muscle-driven musculoskeletal dynamics model to simulate the transition from squatting to standing. Different objective function terms representative of multiple performance criteria were modelled to realistically reflect the goal of performing this movement. In addition, the weights among the objective

function terms were automatically determined by solving an inverse optimal control problem, through the use of bilevel optimisation techniques [39, 40, 80]. This enables an inherent understanding of motor control mechanisms within the nervous system and the in-depth analysis of the muscle function and coordination within the neuromusculoskeletal system.

5.2 Methods

5.2.1 Optimal Control

The prediction of human motion can be formulated as an optimal control problem. The core of solving this problem is to predict motion trajectories by minimising a determined objective function under given constraint conditions, without considering any tracking terms. A general mathematical expression is shown in Equation (5.1):

$$\begin{aligned} &\tilde{\boldsymbol{x}}(t) \in argmin\, J = argmin\, \left(\boldsymbol{\omega}^{\mathrm{T}} \cdot \int_0^T \boldsymbol{\lambda}(\boldsymbol{x}(t), \boldsymbol{u}(t), t)dt\right) \\ &subject\ to\ \dot{\boldsymbol{x}}(t) = \boldsymbol{G}(\boldsymbol{x}(t), \boldsymbol{u}(t), t) \\ &\qquad \boldsymbol{H}_l \leq \boldsymbol{H}\big(\boldsymbol{x}(t), \boldsymbol{u}(t), t, \boldsymbol{x}(0), \boldsymbol{u}(0), \boldsymbol{x}(T), \boldsymbol{u}(T)\big) \leq \boldsymbol{H}_u \end{aligned} \tag{5.1}$$

where $\tilde{\boldsymbol{x}}$ is the optimal solution of the state vector, J is the objective function of optimal control problem, $\boldsymbol{\omega}$ is the weight vector, $\boldsymbol{\lambda}$ is the feature vector without any tracking-related component, $\boldsymbol{x}$ is the state vector to be optimised, $\boldsymbol{u}$ is the control vector, t represents time, T is the duration of the motion process, $\boldsymbol{G}$ is the vector function related to the dynamics of the system to be controlled, $\boldsymbol{H}$ represents possible constraints such as path constraints and boundary constraints, $\boldsymbol{H}_l$ and $\boldsymbol{H}_u$ represent

the lower and upper limit of constraints, respectively.

Numerical methods, such as the shooting method and the direct collocation method, are commonly employed to solve optimal control problems. The direct collocation method, when compared to the shooting method, can directly convert the dynamic differential equation constraints into algebraic equation constraints [53, 55]. Therefore, it avoids the laborious forward integration process and leads to greater computational efficiency and accuracy. Commonly used collocation methods include the Euler method, the trapezoidal method and the Hermite–Simpson method, etc. [53].

5.2.2 Inverse Optimal Control

The essence of the inverse optimal control problem is to deduce the optimal control law in human motion from the given trajectories. The known conditions typically consist of trajectories of state variables, while the specific expression of the objective function J in Equation (5.1) is unknown. Therefore, we initially make a priori assumption on the feature vector $\boldsymbol{\lambda}$, and then iteratively adjust the weight vector $\boldsymbol{\omega}$ to minimise the difference between the vector $\tilde{\boldsymbol{x}}$ and the ground truth of state vector $\hat{\boldsymbol{x}}$. The mathematical relationship can be expressed as a constrained continuous optimisation problem in Equation (5.2):

$$\begin{aligned} &minimise\ L(\boldsymbol{\omega}, \hat{\boldsymbol{x}}(t), \tilde{\boldsymbol{x}}(t)) \\ &subject\ to\ \|\boldsymbol{\omega}\|_1 = 1 \\ &\boldsymbol{\omega} \geq \mathbf{0} \end{aligned} \tag{5.2}$$

where L is the objective function that measures the deviation between the optimal state variable $\tilde{\boldsymbol{x}}$ from Equation (5.1) and the ground truth of the state vector $\hat{\boldsymbol{x}}$. The constraints on the weight vector $\boldsymbol{\omega}$ are used to avoid unnecessary optimisation iterations [81].

5.2.3 Nested Bilevel Optimisation

Our study employed the nested bilevel optimisation algorithm [82] to solve the inverse optimal control problem. The approach consists of upper and lower optimisation structures, with the upper level solved using the Bayesian optimisation method [83–85] and the lower level solved using the Hermite–Simpson method. The Bayesian optimisation method, recognised as a highly effective global optimisation algorithm, has successfully tackled hyperparameter automatic tuning problems [52]. Additionally, it is well-suited for addressing black-box optimisation problems involving expensive functions [50]. The Hermite–Simpson method, a typical direct collocation approach, significantly enhances the computational efficiency and accuracy of lower-level optimisation when compared to the shooting method, thereby improving the overall solution efficiency for the inverse optimal control problem. In bilevel optimisation, the lower-level optimisation predicts the motion trajectories by solving a determined optimal control problem and returns the errors between the predicted trajectories and the given trajectories to the upper-level optimisation. Based on the information returned from the lower-level, the upper-level optimisation optimally

adjusted the weight distribution of the lower-level objective function terms. The updated weight distribution is then passed to the lower-level optimisation for a new round of calculation. When the number of iterations i of the bilevel optimisation exceeds the maximum number of iterations N, the calculation will be terminated. The algorithm is described in Algorithm 1.

Algorithm 1: Algorithm for Solving the Inverse Optimal Control Problem

Input: Set of given trajectories $\{\hat{x}_1, \dots, \hat{x}_n\}$;

Objective function for Bayesian optimisation L;

Objective function for Optimal Control Problem J;

Maximum number of iterations N;

Initialise the weight vector population $\{\boldsymbol{\omega}^{(1)}, \dots, \boldsymbol{\omega}^{(m)}\}$ and calculate the corresponding objective function value $\{L^{(1)}, \dots, L^{(m)}\}$;

for $i = 1{:}\,N$ **do**

Update Gaussian process regression model and acquisition function;

Update the weight vector $\boldsymbol{\omega}^{(m+i)}$;

Update the objective function J for the optimal control problem under the given $\boldsymbol{\omega}^{(m+i)}$;

Calculate the optimal trajectory set $\{\tilde{x}_1^{(i)}, \dots, \tilde{x}_n^{(i)}\}$ using the Hermite-Simpson method;

Calculate the objective function value $L^{(m+i)}$;

end

The Bayesian optimisation method was implemented using the Statistics and Machine Learning Toolbox in MATLAB (The MathWorks, Inc, R2023a) with the expected-improvement-plus function and ARD Matern 5/2 function.

5.2.4 General Case of the Inverse Optimal Control Problem

A general inverse optimal control problem with the known solution was first used to test the accuracy and robustness of Algorithm 1. This case is adapted from [86] and is a typical representative of the inverse optimal control problem that exists in nonlinear systems. It was formulated as a composition of equations (5.3) and (5.4) where (5.3) can be regarded as an upper-level optimisation problem and (5.4) can be regarded as a lower-level optimisation problem.

$$\begin{aligned} &\tilde{\boldsymbol{\omega}} = argmin\, L^B(\boldsymbol{\omega}) = argmin(10 \times \sum_{j=1}^{3} \frac{\sqrt{\frac{1}{T_t}\int_0^{T_t}(\tilde{x}_j(t)-\hat{x}_j(t))^2 dt}}{\max(\hat{x}_j(t))-\min(\hat{x}_j(t))}) \\ &subject\ to\ \|\boldsymbol{\omega}\|_1 = 1 \\ &\qquad\qquad \boldsymbol{\omega} \geq \mathbf{0} \end{aligned} \tag{5.3}$$

where $L^B(\boldsymbol{\omega})$ represents the upper-level objective function; $\boldsymbol{\omega}$ is the weight vector to be optimised; $\tilde{\boldsymbol{\omega}}$ is the weight vector obtained by the bilevel optimisation algorithm; T_t is the constant representing the duration and we set T_t to 6 in this case; $\hat{x}_j$ is the ground truth of the *j*th state variable trajectory; $\tilde{x}_j$ is the trajectory of the *j*th state variable obtained by solving Equation (5.4).

$$\begin{aligned} &minimise\ \int_0^{T_t}(\omega_1 x_1^2(t) + \omega_2 x_2^2(t) + \omega_3 x_3^2(t) + \omega_4 u^2(t))dt \\ &subject\ to\ \dot{\boldsymbol{x}}(t) = (\cos(x_3(t)), \sin(x_3(t)), u(t))^{\mathrm{T}} \\ &\qquad\qquad \boldsymbol{x}(0) = (3,2,1)^{\mathrm{T}} \end{aligned} \tag{5.4}$$

where $\omega_1 \sim \omega_4$ are the components of the weight vector $\boldsymbol{\omega}$, $x_1 \sim x_3$ are the components of the state vector $\boldsymbol{x}$, and u is the control variable.

We assessed the robustness of our proposed algorithm by solving this general problem six times, employing different seeds to control the generation of random number sequences. Upon the completion of all tests, the solution was evaluated using Equation (5.5).

$$e_r = \frac{\|\hat{\boldsymbol{\omega}} - \tilde{\boldsymbol{\omega}}\|_2}{\|\hat{\boldsymbol{\omega}}\|_2} \tag{5.5}$$

where $\hat{\boldsymbol{\omega}}$ is the ground truth of the weight vector, and e_r is the relative error between $\hat{\boldsymbol{\omega}}$ and $\tilde{\boldsymbol{\omega}}$.

5.2.5 Application to Simulate the Transition from Squatting to Standing

Based on the above algorithm, we established a computational framework to simulate the transition from squatting to standing, as shown in Figure 5.1.

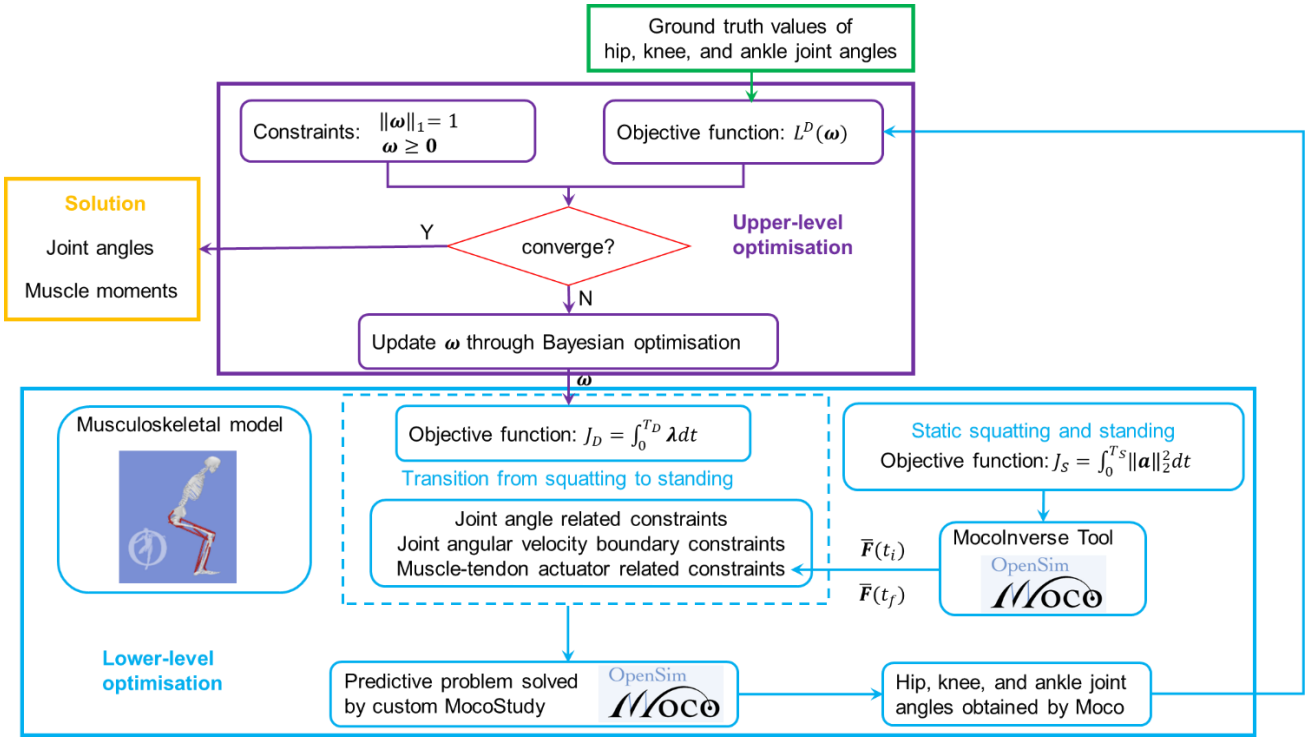

Figure 5.1. The computational framework for simulating the muscle-driven transition from squatting to standing using the inverse optimal control method. The specific meanings of all symbols in the figure are detailed in subsection 3) of section 5.2.5.

1) Experimental data

We obtained ground truth values of lower limb joint angles from the motion capture experiment during the transition from squatting to standing. Six healthy male subjects (age: 27.5 ± 4.6 years, mass: 71.3 ± 4.8 kg, height: 174.2 ± 2.6 cm) participated in this experiment. Data collection was approved by the Ethics Committee of the University of Birmingham. All subjects signed informed consent forms before the data collection. Each subject was required to fold their arms in front of their chest during the movement. At first, the subjects maintained a static squatting posture. In this posture, the feet are placed in a symmetrical position about the sagittal plane, with the toes pointing forward and shoulder width apart. After receiving

verbal instructions, the subjects stood up comfortably and finally maintained a static standing posture. Throughout the whole process, participants were required to keep their feet stationary and their backs straight. Lower limb kinematics data were captured by a motion capture system with a sampling frequency of 100 Hz (Vicon, Oxford, UK). Infrared reflective markers were attached to bony landmarks and clusters. The locations of the bony landmarks were: acromion, the 7th cervical vertebra, anterior superior iliac spine and posterior superior iliac spine, medial and lateral femoral epicondyle, medial and lateral malleolus, calcaneus and 1st, 2nd and 5th metatarsal heads. In addition, clusters with four markers were placed on each thigh and shank. The inverse kinematics method in OpenSim [1–3] was used to calculate the hip, knee, and ankle joint angles, which were subsequently filtered by a 4th-order zero-lag Butterworth filter. We used the cubic spline function to interpolate the processed joint angles, and then numerically differentiated the interpolated curves to obtain the change curves of joint angular velocities over time [79]. The initial point of transition from squatting to standing was defined as the earliest moment when any of the hip, knee, and ankle joints have an angular speed greater than 2°/s, and the final point was the earliest moment when all three joint angular speeds were less than 2°/s. The horizontal axes of the processed joint angle-time curves were subsequently normalised to 0-100% for all subjects. Finally, the average values of the processed joint angles among all subjects [39, 79] were used as ground truth values for subsequent simulation.

2) Musculoskeletal Model

The simulation of the transition from squatting to standing was implemented using a modified musculoskeletal model based on “squatToStand_3dof9musc” in OpenSim 4.4 [31, 73]. The model, as illustrated in Figure 5.2, consists of three degrees of freedom, representing the flexion and extension of the hip, knee, and ankle joints, respectively. In addition, joint frame orientations were fine-tuned to ensure that all joint movements occur in the para-sagittal plane. To represent the symmetrical movement of both lower limbs, the mass and inertia of torso and pelvis were halved. The lower limb was actuated by nine muscle-tendon actuators, namely gluteus maximus, iliopsoas, rectus femoris, vasti, tibialis anterior, soleus, gastrocnemius, biceps femoris short head, and hamstring. The muscle-tendon actuators with compliant tendons were modelled using the De Groote’s muscle model [10]. The width of active-force length curves was adjusted to 1.5 times the original value.

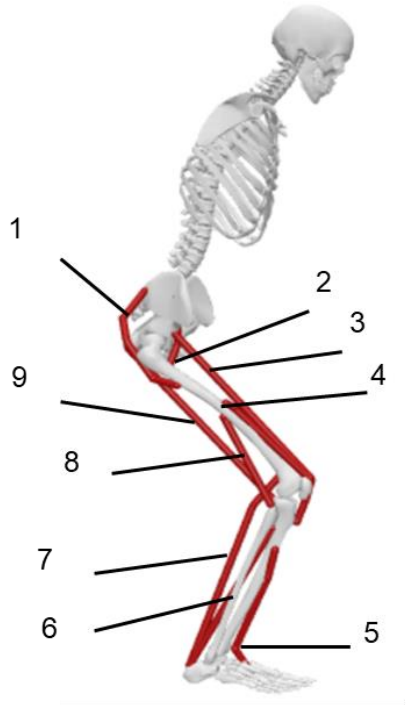

1.gluteus maximus 2. iliopsoas 3. rectus femoris 4. vasti 5. tibialis anterior
6. soleus 7. gastrocnemius 8. biceps femoris short head 9. hamstring

Figure 5.2. Schematic diagram of the musculoskeletal model. This planar model consists of three degrees of freedom, representing the flexion and extension of the hip, knee, and ankle joints, respectively. The lower limb is actuated by nine muscle-tendon actuators, namely gluteus maximus, iliopsoas, rectus femoris, vasti, tibialis anterior, soleus, gastrocnemius, biceps femoris short head, and hamstring.

3) Lower-level Optimisation

The lower-level optimisation was solved using OpenSim Moco 1.2.0 [54], a state-of-the-art tool for solving optimal control problems in biomechanics through the direct collocation method.

The motion trajectory of the transition from squatting to standing was predicted by minimising the objective function as shown in Equation (5.6), where T_D represent the total duration of this process.

Equation (5.6) consists of five objective function terms in the lower-level optimisation. The first term, is a measure of muscle fatigue [65], defined as the sum of muscle activations ($\boldsymbol{a}$) squared. The second term, is the measure of muscle stress [26], defined as the sum of normalised muscle-tendon forces ($\overline{\boldsymbol{F}} = \boldsymbol{F}/\boldsymbol{F_{max}}$) squared. The third term, is a measure of stability during the transition from squatting to standing [39], defined as the difference between the position of the centre of mass ($\boldsymbol{r}_{CoM}$) and the centre of the base of support ($\boldsymbol{r}_{cenBoS}$), followed by the dot product of the difference and the unit vector along the sagittal axis ($\boldsymbol{s}$), squared. In this motion, the base of support is defined as the smallest polygonal area that encompasses the points of contact between the human body and the ground. The fourth term, is the measure of the smoothness in kinematics during the transition from squatting to standing [64, 66], defined as the sum of acceleration of joint coordinates ($\boldsymbol{\alpha}$) squared. The final term is the measure of the smoothness of changes in muscle forces [26], defined as the sum of the derivatives of normalised muscle-tendon force ($\frac{d\overline{\boldsymbol{F}}}{dt}$) squared. Each term is multiplied by corresponding scaling factors to mitigate dimensional differences and enhance the convergence of the optimal control problem [39, 40]. These scaling factors can be easily determined based on experience gained in preliminary simulations.

$$
\begin{aligned}
J_D = \boldsymbol{\omega}^{\mathrm{T}} \cdot \int_0^{T_D} \boldsymbol{\lambda}(\boldsymbol{x}(t), \boldsymbol{u}(t), t)dt \\
= \omega_1 \times \int_0^{T_D} \|\boldsymbol{a}(t)\|_2^2 dt \\
+\omega_2 \times \int_0^{T_D} \|\bar{\boldsymbol{F}}(t)\|_2^2 dt \\
+\omega_3 \times 10^2 \int_0^{T_D} [(\boldsymbol{r}_{CoM}(t) - \boldsymbol{r}_{cenBoS}(t)) \cdot \boldsymbol{s}]^2 dt \\
+\omega_4 \times 10^{-2} \int_0^{T_D} \|\boldsymbol{\alpha}(t)\|_2^2 dt \\
+\omega_5 \times 5 \times 10^{-1} \int_0^{T_D} \left\| \frac{d\bar{\boldsymbol{F}}(t)}{dt} \right\|_2^2 dt
\end{aligned}
\tag{5.6}
$$

The simulations of static squatting and static standing posture were performed to determine the normalised muscle-tendon forces [26]. These were achieved using the MocoInverse tool by minimising the objective function, as shown in Equation (5.7). Subsequently, the normalised muscle-tendon forces in static squatting and static standing were set as constraints for each actuator's normalised muscle-tendon force at the initial point and final point, respectively. Additionally, the following constraints were defined: a) the hip, knee, and ankle joint angles were constrained based on the corresponding ground truth values; b) at the initial point and final point, the joint angular velocities and tendon velocities were set to zero; c) at the initial point, the derivatives of muscle activations with respect to time were set to zero.

$$
J_S = \int_0^{T_S} \|\boldsymbol{a}(t)\|_2^2 \, dt \tag{5.7}
$$

where $\boldsymbol{a}$ is the vector of muscle activations, T_S represents the time required to maintain the static posture.

4) Upper-level Optimisation

The weights of each term in Equation (5.6) were solved so that the predicted kinematics are as close as possible to the ground truth values in the upper-level optimisation, as indicated in Equation (5.8).

$$\begin{aligned} minimise\ L^D(\boldsymbol{\omega}) = 10 \times \Bigg(&\frac{\sqrt{\frac{1}{T_D}\left(\int_0^{T_D}(\theta_{hip}-\theta_{hip}^g)^2 dt\right)}}{\max\left(\theta_{hip}^g\right)-\min\left(\theta_{hip}^g\right)} + \frac{\sqrt{\frac{1}{T_D}\left(\int_0^{T_D}(\theta_{knee}-\theta_{knee}^g)^2 dt\right)}}{\max\left(\theta_{knee}^g\right)-\min\left(\theta_{knee}^g\right)} \\ &+ \frac{\sqrt{\frac{1}{T_D}\left(\int_0^{T_D}(\theta_{ankle}-\theta_{ankle}^g)^2 dt\right)}}{\max\left(\theta_{ankle}^g\right)-\min\left(\theta_{ankle}^g\right)}\Bigg) \\ subject\ to\ &\|\boldsymbol{\omega}\|_1 = 1 \\ &\boldsymbol{\omega} \geq \mathbf{0} \end{aligned} \tag{5.8}$$

where $L^D(\boldsymbol{\omega})$ represents the upper-level objective function; θ_{hip}, θ_{knee} and θ_{ankle} are the hip, knee, and ankle joint angles obtained from the lower-level optimisation, respectively; θ_{hip}^g, θ_{knee}^g and θ_{ankle}^g are the ground truth values of the hip, knee, and ankle joint angles, respectively.

5.3 Results

5.3.1 Results of the General Case

To test the robustness of our proposed bilevel optimisation algorithm, the general case was solved six times, yielding six sets of solutions and errors (Table 5.1). The errors ranged between 0.007717 (Test 3) and 0.042007 (Test 4), with a mean of 0.020433. Despite the worst-performing test (Test 4), the trajectories of the state variables consistently follow the ground truth (Figure 5.3), demonstrating high accuracy in solving the inverse optimal control problem. In all tests, the minimum

value of the upper-level objective function decreased with the number of function evaluations (Figure 5.4), demonstrating satisfactory convergence and robustness of the proposed algorithm.

Table 5.1: Results for six tests of the general case

	Solution $\tilde{\boldsymbol{\omega}}$	Error of solution e_r
Test 1	$(0.100804, 0.199070, 0.303944, 0.396182)^T$	0.010269
Test 2	$(0.102845, 0.193136, 0.309430, 0.394589)^T$	0.024042
Test 3*	$(0.101054, 0.196354, 0.301066, 0.401526)^T$	0.007717
Test 4†	$(0.104373, 0.183616, 0.315216, 0.396795)^T$	0.042007
Test 5	$(0.101781, 0.195838, 0.307217, 0.395164)^T$	0.017885
Test 6	$(0.102257, 0.193416, 0.308098, 0.396229)^T$	0.020676
Mean		0.020433
SD		0.012247
Ground truth $\hat{\boldsymbol{\omega}}$	$(0.1,0.2,0.3,0.4)^T$	

* indicates the test with the lowest error, † indicates the test with the highest error. SD is the standard deviation. To maintain sufficient precision, the weight solutions are retained to six decimal places.

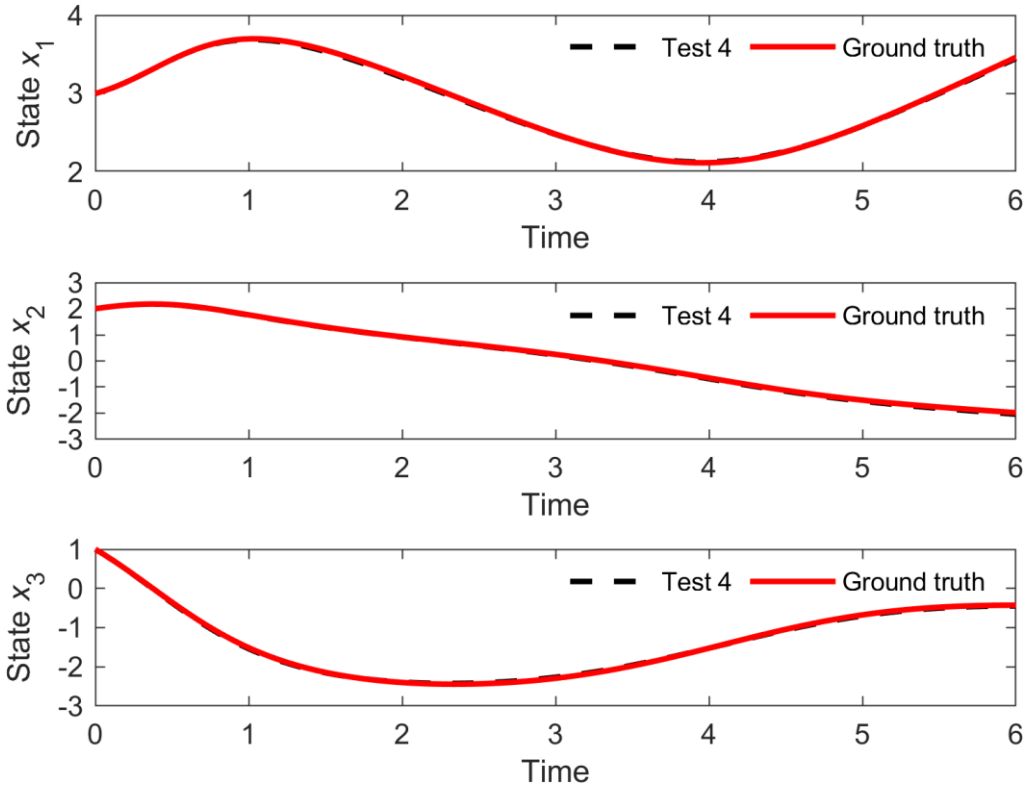

Figure 5.3. The comparison between the state variable trajectories and the ground truth for the Test 4 of the general case.

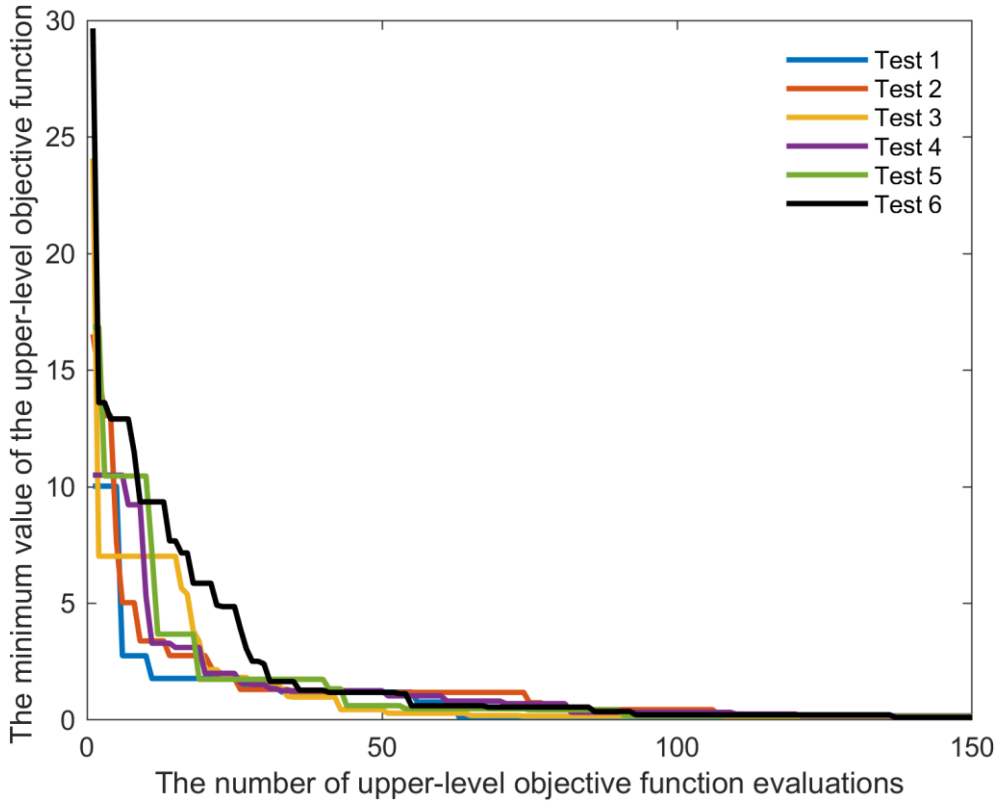

Figure 5.4. The curves of the observed minimum value of the upper-level optimisation

objective function in the six tests versus the number of function evaluations.

5.3.2 Simulation Results of Transition from Squatting to Standing

The predictive lower limb joint angles closely matched the ground truth values during the transition from squatting to standing (Figure 5.5), with root mean square errors (RMSE) of 0.97°, 1.83°, and 0.65° for the hip, knee, and ankle joints, respectively.

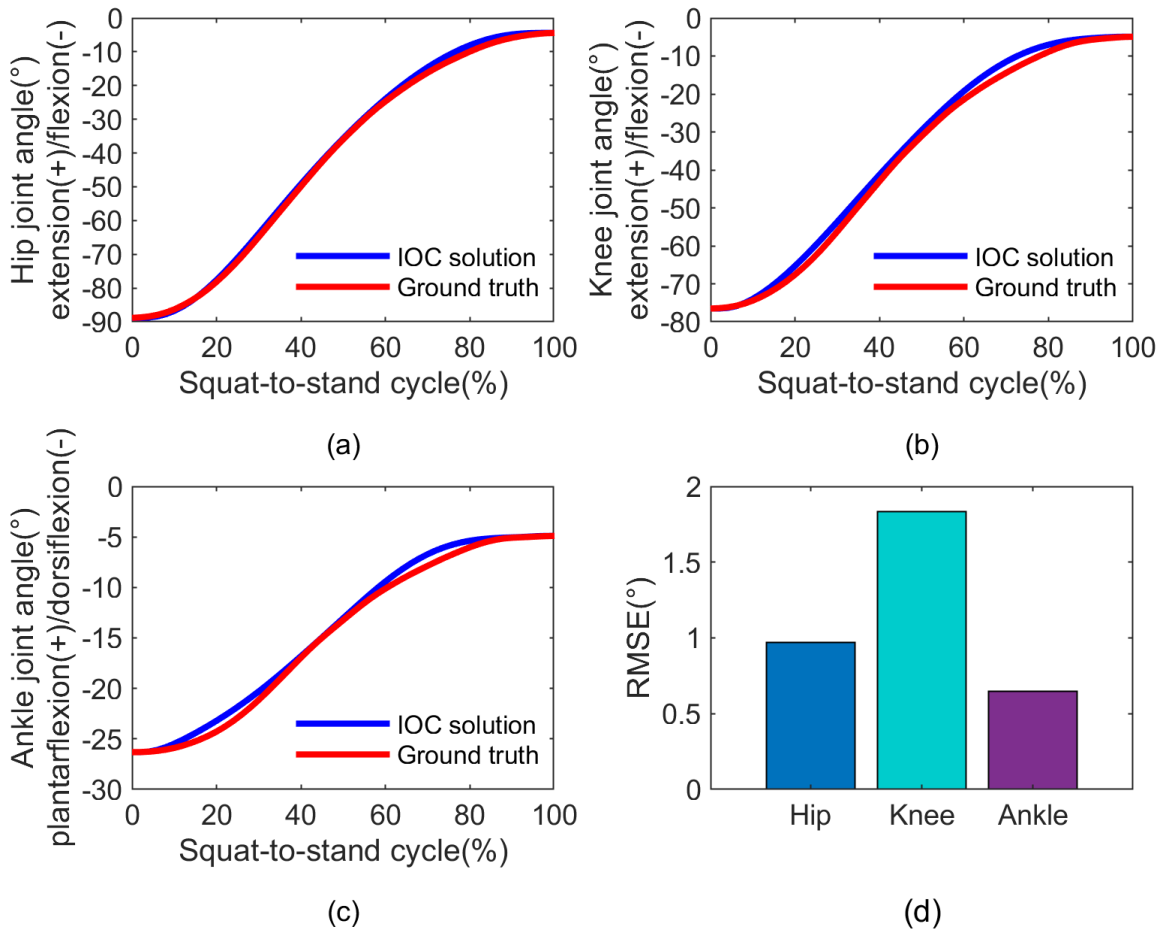

Figure 5.5. Comparison between the ground truth values and solutions of the inverse optimal control (IOC) problem for muscle-driven simulation from squatting to standing. (a) Hip joint angle. (b) Knee joint angle. (c) Ankle joint angle. (d) Root mean square errors (RMSE) of three joint angles.

The joint moments at the hip, knee, and ankle were determined by summing up the moments of individual muscles across the joint (Figure 5.6). At the hip, gluteus maximus and hamstring contributed to the extension moment, with hamstring contributing a greater peak value. Conversely, iliopsoas and rectus femoris opposed this movement by generating the flexion moment.

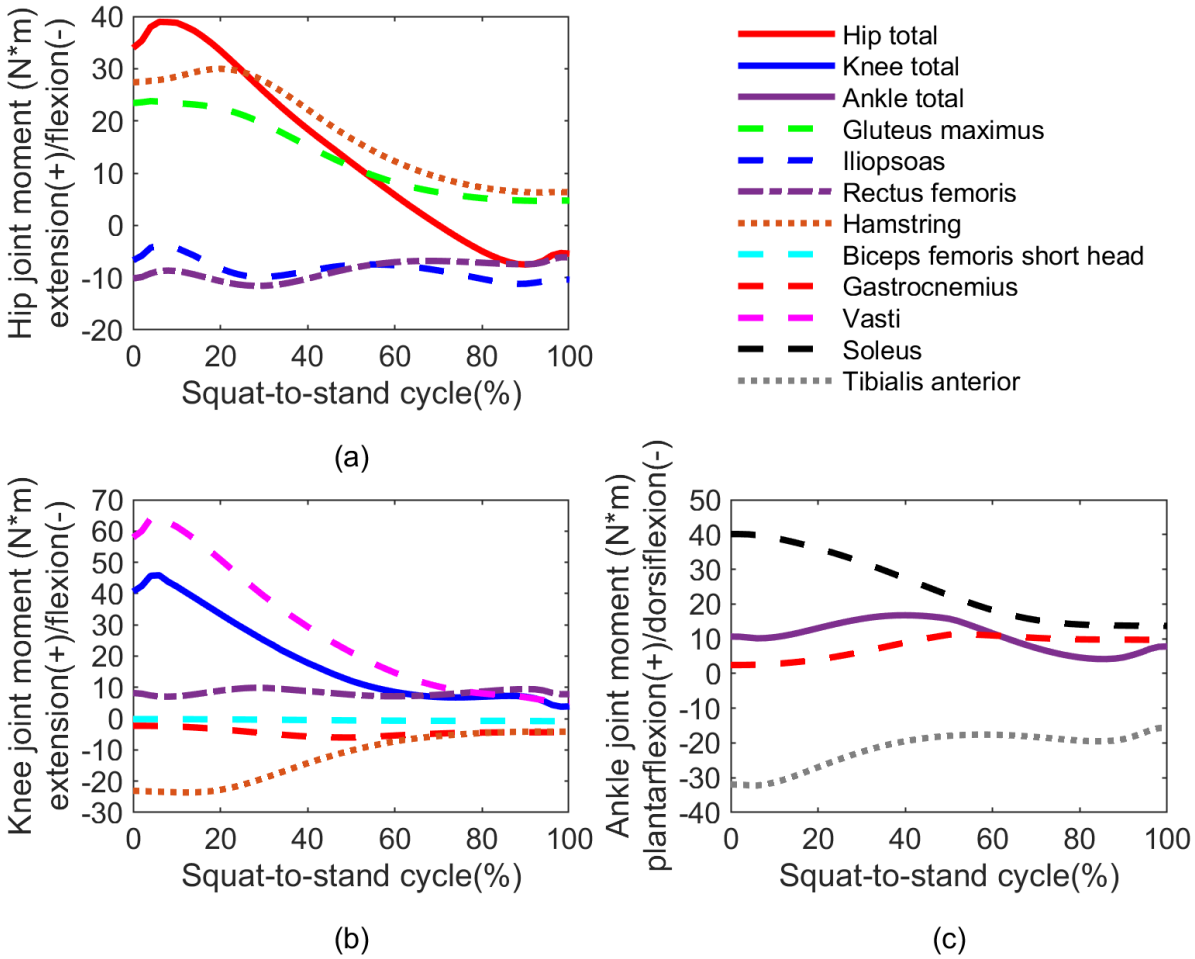

Figure 5.6. The total moments and muscle moments acting on the joints of the lower limb during the transition from squatting to standing. Muscle moment was obtained by multiplying the muscle-tendon force with the corresponding moment arm. (a) Hip joint. (b) Knee joint. (c) Ankle joint.

At the knee, five muscles (vasti, rectus femoris, gastrocnemius, biceps femoris

short head and hamstring) contributed to the knee joint moment: the extension moment was generated by vasti and rectus femoris, while the flexion moment was generated by the other three muscles. The greatest peak extension moment was from vasti and the greatest peak flexion moment was from hamstring.

At the ankle, gastrocnemius and soleus together generated the plantarflexion moment, while the dorsiflexion moment was generated only by tibialis anterior.

5.4 Discussion

In this study, we simulated the muscle-driven human motion of transition from squatting to standing using an inverse optimal control method. The nested bilevel optimisation algorithm was employed to automatically adjust the weights of different objective function terms, thereby completing the simulation process. The results from the bilevel optimisation demonstrated high accuracy, fully verifying the ability of using this algorithm to solve the complex inverse optimal control problem for analysing muscle function and coordination during human motion.

We first examined the feasibility of the nested bilevel optimisation algorithm in solving a general inverse optimal control problem. The high accuracy and robustness evident in the results enhanced our confidence of this algorithm (Table 5.1, Figure 5.3 and 5.4). Furthermore, by integrating the muscle-driven human motion characteristics, we applied this algorithm to simulate the transition from squatting to standing. The errors between the predicted lower limb joint angles and the ground truth values were

small (with an average of 1.15° across three lower limb joints; Figure 5.5). The results demonstrated the feasibility of the optimisation algorithm in addressing a more complex human motion inverse optimal control problem.

In recent years, bilevel optimisations have been used to simulate different types of human motion, with the weights of different objective function terms in the lower level being adjusted by solving the upper-level optimisation problem. Therefore, the evaluation number to solve the lower-level optimisation problem was closely related to the method applied in the upper-level optimisation. In a bilevel optimisation study to simulate human walking, the upper level employed the genetic algorithm, where the population size was 40 and the number of generations was 140 [39]. After solving the lower-level optimisation problem 5600 times (40×140=5600), lower limb motion trajectories that were close to the experimental values were obtained. In a study [40] to simulate human lifting motion, the upper level used the particle swarm optimisation algorithm, which required solving 4000 lower-level optimisation problems (particle swarm optimisation had a population size of 40 and a maximum iteration number of 100) to complete the lifting motion simulation. In contrast, our study applied the Bayesian optimisation method in the upper level and predicted satisfactory joint motion trajectories by solving the lower-level optimisation problem less than 400 times. The improvement in computational efficiency may be related to the fact that Bayesian optimisation is suitable for solving optimisation problems with expensive objective functions [50]. In addition, the range of weights for different objective

function terms was determined based on experience in the aforementioned studies [39, 40]. However, our study narrowed the feasible region of the weights [as shown in Equation (5.2)], which was beneficial to reducing the number of solutions required for the lower-level optimisation problem [81], thereby significantly saving computing resources.

The muscle-driven simulation from squatting to standing exhibited a smooth transition, characterised by synchronous extension of all lower limb joints. This was agreed with the physical experimental measures during the standing up phase of the previous study [79]: the lower limb joint angles showed a consistent change over time with relatively minor fluctuations near the initial and final points of transition.

Experimental measurements are commonly used as a method to obtain ground truth values of motion trajectories [39, 40]. However, it is noteworthy that to fully leverage the potential of inverse optimal control in studying human motor control, motion trajectories can be obtained through methods other than experimental measurements. Specifically, virtual kinematic trajectories can be constructed based on anticipated movement patterns. For instance, in the investigation of motor control among patients exhibiting abnormal kinematic behaviour, pathological kinematic trajectories can be adjusted digitally to simulate expected motion after rehabilitation. Subsequently, changes in motor control laws can be determined through inverse optimal control calculations, offering valuable theoretical insights for designing rehabilitation plans.

Studies utilising torque-driven models [40, 79] are limited to obtain the total moment of each joint, thus unable to reveal the specific contributions of different muscles to these joint moments. While the optimal control method, when integrated with muscle-driven models, can predict the dynamic behaviour of muscles, the manual adjustment of weights for different objective function terms often introduces strong subjectivity, making it challenging to achieve predicted joint kinematics that align closely with experimental data. On the other hand, utilising the inverse optimal control method enables the examination of changes in muscle moments during movement from the perspective of the causal relationship between neural control and motion behaviour, while precisely reproducing joint kinematic trajectories. Although muscle forces can also be calculated by the static optimisation method, the objective function used by this method can only include muscle-related terms, but not multibody dynamics-related terms. As a comparison, our method can include both muscle-related and multibody dynamics-related terms in the objective function, while ensuring the accuracy of the predicted motion. Therefore, our approach holds great potential for advancing future studies by enhancing our understanding of the relationship between motor control, muscle function, and body performance in neurological and orthopaedic conditions, as well as in ageing.

During the squat-to-stand movement, some muscle coordination patterns can be observed: firstly, the hamstring contributes more to hip extension than the gluteus maximus; secondly, in knee extension, vasti plays a more significant role than rectus

femoris; thirdly, as a biarticular muscle, the hamstring plays a major antagonistic role in knee extension.

To further understand the similarities and differences in muscle coordination patterns during different activities of daily living, we compared the results with the most common level walking. During the stance phase of the gait cycle, the hamstring also contributes a greater peak moment to hip flexion than the gluteus maximus [87]. However, during the transition from squatting to standing, the gastrocnemius contributed minor to knee flexion, which is different from the coordination pattern shown in level walking [87].

Since the bilevel optimisation simulation framework requires continuous interaction and iteration between the upper and lower levels, the work in this chapter has higher computational complexity than that in Chapters 3 and 4, resulting in longer solution time. Compared with Chapters 3 and 4, this chapter involves more theoretical knowledge, such as inverse optimal control theory, bilevel optimisation, Bayesian optimisation, muscle model, etc. Therefore, carrying out this research work requires researchers to have a more solid theoretical foundation in biomechanics and to devote more time and effort.

The proposed simulation framework has demonstrated effectiveness in solving the human motion problem of transitioning from squatting to standing. To improve computational efficiency, we used a sagittal musculoskeletal model in the lower-level optimisation. In future studies, in order to more fully explore the physiological

characteristics of human motion, we can extend this simulation framework and use it for predictive studies employing high-fidelity models.

5.5 Conclusion

In this study, we integrated the inverse optimal control method with the muscle-driven musculoskeletal dynamics model to simulate the transition from squatting to standing. We proposed the nested bilevel optimisation algorithm to automatically adjust the weights of different objective function terms. This enables an effective solution to the complex muscle coordination problem during human motion. Our approach offers a new avenue for studying muscle coordination behaviour and has great potential for designing muscle-strengthening-based rehabilitation, sports training, and assistive devices.

Chapter 6. Conclusion and Future Work

6.1 Summary

This thesis is based on the optimal control theory and focuses on the prediction of human lower limb motion. Some innovative breakthroughs have been achieved, which are summarised as follows:

1) The first predictive study of sit-to-stand movement in unilateral transtibial amputees was completed. A multi-body dynamics model for predicting sit-to-stand motion was developed by combining the human model representing the unilateral transtibial amputee with the Hunt-Crossley contact model. To solve the problem of difficulty in determining the force equilibrium postures of the human model at the initial and final moments of the movement, the "free fall method" was creatively proposed. On this basis, the predictive problem of the sit-to-stand motion was formulated as the optimal control problem and solved by the direct collocation method. The predicted kinematic and kinetic results were able to effectively capture the main motion characteristics reflected in the experimental data, which verified the effectiveness of the established simulation framework. The results showed that the intact side bore greater peak knee extension moment and peak vertical ground reaction force than those in the amputated side, which may be the main reason why the knee joint in the intact side of the unilateral transtibial amputee is more susceptible to osteoarthritis. By utilising the established simulation framework, the

effects of changes in prosthetic stiffness on dynamic behaviour were further revealed, fully demonstrating the unique advantage of predictive simulation that does not require experimental data. The proposed simulation method has great potential in various fields such as prosthetic design.

2) The first predictive study of the sit-to-stand motion in patients with unilateral ankle dorsiflexion limitation was completed. Ankle dorsiflexion restriction is a common sequelae after ankle injury and surgery, but its negative effects on lower limb movement has not yet received attention in the field of human movement biomechanics. This thesis, for the first time, combines the proposed "free fall method" with optimal control theory to establish a simulation framework for predicting the sit-to-stand motion of patients with unilateral ankle dorsiflexion limitation. Based on the established simulation framework, the effects of different levels of ankle dorsiflexion limitation on dynamic behaviour were further explored, revealing the biomechanical compensation strategies that occur during the motion. This achievement provides a new approach for studying the pathological movement behaviour of patients with unilateral ankle dorsiflexion limitation.

3) The first inverse optimal control study of muscle-driven squat-to-stand motion was completed. By combining Bayesian optimisation with the Hermite-Simpson collocation method, a nested bilevel optimisation method for solving the inverse optimal control problem was established. The accuracy and robustness of the bilevel optimisation method were verified by testing the general case. The established

bilevel optimisation method was then applied to the human movement from squatting to standing, combined with a muscle-driven multi-body dynamics model to solve the inverse optimal control problem. The predicted kinematic trajectories were highly consistent with the experimental measurement results, verifying the effectiveness of the established bilevel optimisation method for solving complex inverse optimal control problems of human motion. In addition, the muscle coordination patterns during the squat-to-stand movement were also revealed. This study has reference significance for solving inverse optimal control problems in other human movements, and can provide technical support for rehabilitation medicine, the research and development of bionic robots and other fields.

6.2 Future Work

Although this thesis has made some breakthroughs in the prediction of human lower limb movements, it is impossible to cover and solve all the problems in this field. In the future, research work can be continued in the following directions:

1) Based on the simulation framework developed in this thesis, the torque-driven predictive simulation of sit-to-stand movement for unilateral lower limb amputees can be upgraded to muscle-driven predictive simulation, thereby obtaining richer biomechanical information. Although torque-driven predictive simulation can provide important insights in lower limb kinematics, ground reaction force, and total joint moments, it is unable to predict muscle-related quantities. In future research, by

introducing the muscle-driven multi-body dynamics model, more muscle-related biomechanical information can be predicted, such as muscle forces, muscle moments, and metabolic energy consumption. This will further enhance the understanding of the different muscle functions in unilateral transtibial amputees during the sit-to-stand movement and provide a more powerful reference for designing rehabilitation plans for disabled individuals.

2) In future research, the "free fall method" and simulation framework originally proposed in this thesis can be improved and extended to predict the sit-to-stand movement behaviour of lower limb amputees with various physical conditions such as ankle amputation and bilateral amputation. In addition, the prosthesis can be modelled in more detail based on the current work, so as to simulate the movement effect of the amputee after wearing the prosthesis more precisely. This will make up for the defect that the previous method of combining experience and trial and error to design prostheses requires a lot of time and money, shorten the research and development cycle of prosthetic products, and save research and development costs.

3) In order to more comprehensively understand the effect of unilateral ankle dorsiflexion limitation on patients' daily lives, optimal control theory can be used in the future to predict patients' behaviours in various movements other than sit-to-stand, such as walking, stand-to-sit, squatting, etc. This will deepen our understanding of the movement patterns of such patients and provide valuable theoretical references for their rehabilitation training.

4) To further enhance the functionality of the bilevel optimisation simulation framework. In this thesis, a bilevel optimisation simulation framework was established to solve the inverse optimal control problem of muscle-driven squat-to-stand movement based on a simple human model. However, due to the complexity of human movement, using only the simple human model for simulation cannot meet the higher demands of computational analysis and practical applications. Therefore, in future work, this framework can be considered for completing simulations based on human models with more degrees of freedom and a larger number of muscles. This will deepen our understanding of muscle coordination patterns in human movement, and further strengthen the support of bilevel optimisation simulation for practical applications such as sprots training, design of lower limb exoskeleton and bionic robot.

5) Develop digital design tools to provide personalised guidance for the selection of surgical plans and rehabilitation training programs in clinical medicine and rehabilitation treatment. Because each patient has unique physical conditions, clinically standardised surgical or treatment plans may not be universally applicable to all patients. The biomechanical simulation method can predict the effects of treatment in advance by providing personalised musculoskeletal modelling for patients and simulate treatment plans in computers, thereby providing the reference for designing more accurate surgical or treatment plans. In order to alleviate the burden on clinicians in learning biomechanical theory and using professional

simulation software, in future research, advanced software engineering technology can be used to design easy-to-use digital design tools according to the targeted needs of clinicians. This can be achieved through secondary development of open source software such as OpenSim. The introduction of digital design tools in clinical medicine and rehabilitation treatment will have significant and far-reaching impacts on these fields.

List of References

[1] Delp SL, Anderson FC, Arnold AS, et al. OpenSim: open-source software to create and analyze dynamic simulations of movement. *IEEE Trans Biomed Eng* 2007; 54: 1940–50.

[2] Seth A, Sherman M, Reinbolt JA, et al. OpenSim: a musculoskeletal modeling and simulation framework for in silico investigations and exchange. *Procedia IUTAM* 2011; 2: 212–232.

[3] Seth A, Hicks JL, Uchida TK, et al. OpenSim: Simulating musculoskeletal dynamics and neuromuscular control to study human and animal movement. *PLoS Comput Biol* 2018; 14: e1006223.

[4] Rasmussen J, Christensen ST. Musculoskeletal Modeling of Egress with the AnyBody Modeling System. SAE Technical Paper 2005.

[5] Damsgaard M, Rasmussen J, Christensen ST, et al. Analysis of musculoskeletal systems in the AnyBody Modeling System. *Simul Model Pract Theory* 2006; 14: 1100–1111.

[6] Shippen J, May B. BoB – biomechanics in MATLAB. In: *Proccedings of 11th International Conference Biomdlore 2016*. VGTU Technika, 2016.

[7] Cleather DJ, Bull AMJ. The development of a segment-based musculoskeletal model of the lower limb: introducing FreeBody. *R Soc Open Sci* 2015; 2: 140449.

[8] Zajac FE. Muscle and tendon: properties, models, scaling, and application to biomechanics and motor control. *Crit Rev Biomed Eng* 1989; 17: 359–411.

[9] Millard M, Uchida T, Seth A, et al. Flexing computational muscle: modeling and simulation of musculotendon dynamics. *J Biomech Eng* 2013; 135: 021005.

[10] De Groote F, Kinney AL, Rao A V., et al. Evaluation of Direct Collocation Optimal Control Problem Formulations for Solving the Muscle Redundancy Problem. *Ann Biomed Eng* 2016; 44: 2922–2936.

[11] Winters JM. An improved muscle-reflex actuator for use in large-scale neuromusculoskeletal models. *Ann Biomed Eng* 1995; 23: 359–374.

[12] Thelen DG. Adjustment of Muscle Mechanics Model Parameters to Simulate Dynamic Contractions in Older Adults. *J Biomech Eng* 2003; 125: 70–77.

[13] Hertz H. On the contact of elastic solids. *JourTialfur die reine und angewandte Matlumatilc* 1882; 156–171.

[14] Hunt KH, Crossley FRE. Coefficient of Restitution Interpreted as Damping in Vibroimpact. *J Appl Mech* 1975; 42: 440–445.

[15] Sherman MA, Seth A, Delp SL. Simbody: multibody dynamics for biomedical research. *Procedia IUTAM* 2011; 2: 241–261.

[16] Blankevoort L, Kuiper JH, Huiskes R, et al. Articular contact in a three-dimensional model of the knee. *J Biomech* 1991; 24: 1019–1031.

[17] Pérez-González A, Fenollosa-Esteve C, Sancho-Bru JL, et al. A modified elastic foundation contact model for application in 3D models of the prosthetic knee.

Med Eng Phys 2008; 30: 387–398.

[18] Serrancoli G, Falisse A, Dembia C, et al. Subject-Exoskeleton Contact Model Calibration Leads to Accurate Interaction Force Predictions. *IEEE Trans Neural Syst Rehabil Eng* 2019; 27: 1597–1605.

[19] Komura T, Prokopow P, Nagano A. Evaluation of the influence of muscle deactivation on other muscles and joints during gait motion. *J Biomech* 2004; 37: 425–436.

[20] Fraysse F, Dumas R, Cheze L, et al. Comparison of global and joint-to-joint methods for estimating the hip joint load and the muscle forces during walking. *J Biomech* 2009; 42: 2357–2362.

[21] Trinler U, Schwameder H, Baker R, et al. Muscle force estimation in clinical gait analysis using AnyBody and OpenSim. *J Biomech* 2019; 86: 55–63.

[22] Clancy CE, Gatti AA, Ong CF, et al. Muscle-driven simulations and experimental data of cycling. *Sci Rep* 2023; 13: 21534.

[23] Thelen DG, Anderson FC, Delp SL. Generating dynamic simulations of movement using computed muscle control. *J Biomech* 2003; 36: 321–328.

[24] Thelen DG, Anderson FC. Using computed muscle control to generate forward dynamic simulations of human walking from experimental data. *J Biomech* 2006; 39: 1107–1115.

[25] Lin Y-C, Pandy MG. Three-dimensional data-tracking dynamic optimization simulations of human locomotion generated by direct collocation. *J Biomech*

2017; 59: 1–8.

[26] Pandy MG, Garner BA, Anderson FC. Optimal control of non-ballistic muscular movements: a constraint-based performance criterion for rising from a chair. *J Biomech Eng* 1995; 117: 15–26.

[27] Kumar V, Yoshiike T, Shibata T. Predicting Sit-to-Stand Adaptations due to Muscle Strength Deficits and Assistance Trajectories to Complement Them. *Front Bioeng Biotechnol* 2022; 10: 799836.

[28] Gidley AD, Marsh AP, Umberger BR. Performance criteria for generating predictive optimal control simulations of bicycle pedaling. *Comput Methods Biomech Biomed Engin* 2019; 22: 11–20.

[29] Anderson FC, Pandy MG. Dynamic Optimization of Human Walking. *J Biomech Eng* 2001; 123: 381–390.

[30] Lin Y-C, Walter JP, Pandy MG. Predictive Simulations of Neuromuscular Coordination and Joint-Contact Loading in Human Gait. *Ann Biomed Eng* 2018; 46: 1216–1227.

[31] Ong CF, Geijtenbeek T, Hicks JL, et al. Predicting gait adaptations due to ankle plantarflexor muscle weakness and contracture using physics-based musculoskeletal simulations. *PLoS Comput Biol* 2019; 15: e1006993.

[32] Pariser KM, Higginson JS. Development and Validation of a Framework for Predictive Simulation of Treadmill Gait. *J Biomech Eng* 2022; 144(11): 114505.

[33] Miller RH, Umberger BR, Hamill J, et al. Evaluation of the minimum energy

hypothesis and other potential optimality criteria for human running. *Proc R Soc B-Biol Sci* 2012; 279: 1498–1505.

[34] Miller RH, Umberger BR, Caldwell GE. Sensitivity of maximum sprinting speed to characteristic parameters of the muscle force–velocity relationship. *J Biomech* 2012; 45: 1406–1413.

[35] LIN Y-C, PANDY MG. Predictive Simulations of Human Sprinting: Effects of Muscle–Tendon Properties on Sprint Performance. *Med Sci Sports Exerc* 2022; 54: 1961–1972.

[36] Pandy MG, Zajac FE, Sim E, et al. An optimal control model for maximum-height human jumping. *J Biomech* 1990; 23: 1185–1198.

[37] Porsa S, Lin Y-C, Pandy MG. Direct Methods for Predicting Movement Biomechanics Based Upon Optimal Control Theory with Implementation in OpenSim. *Ann Biomed Eng* 2016; 44: 2542–2557.

[38] Ostraich B, Riemer R. Design of a Multi-Joint Passive Exoskeleton for Vertical Jumping Using Optimal Control. *IEEE Trans Neural Syst Rehabil Eng* 2022; 30: 2815–2823.

[39] Nguyen VQ, Johnson RT, Sup FC, et al. Bilevel Optimization for Cost Function Determination in Dynamic Simulation of Human Gait. *IEEE Trans Neural Syst Rehabil Eng* 2019; 27: 1426–1435.

[40] Tang B, Peng Y, Luo J, et al. Cost Function Determination for Human Lifting Motion via the Bilevel Optimization Technology. *Front Bioeng Biotechnol* 2022;

10: 883633.

[41] Potra FA, Wright SJ. Interior-point methods. *J Comput Appl Math* 2000; 124: 281–302.

[42] Boggs PT, Tolle JW. Sequential Quadratic Programming. *Acta Numerica* 1995; 4: 1–51.

[43] Gill PE, Wong E. Sequential Quadratic Programming Methods. In: Mixed integer nonlinear programming 2012, pp. 147–224.

[44] Wächter A, Biegler LT. On the implementation of an interior-point filter line-search algorithm for large-scale nonlinear programming. *Math Program* 2006; 106: 25–57.

[45] Gill PE, Murray W, Saunders MA. SNOPT: An SQP Algorithm for Large-Scale Constrained Optimization. *SIAM J Optim* 2002; 12: 979–1006.

[46] Kirkpatrick S, Gelatt CD, Vecchi MP. Optimization by Simulated Annealing. *Science (1979)* 1983; 220: 671–680.

[47] Holland JH. Genetic Algorithms. *Sci Am* 1992; 267: 66–72.

[48] Katoch S, Chauhan SS, Kumar V. A review on genetic algorithm: past, present, and future. *Multimed Tools Appl* 2021; 80: 8091–8126.

[49] Kennedy J, Eberhart R. Particle swarm optimization. In: *Proceedings of ICNN'95 - International Conference on Neural Networks*. IEEE, 1995, pp. 1942–1948.

[50] Brochu E, Cora VM, de Freitas N. A Tutorial on Bayesian Optimization of

Expensive Cost Functions, with Application to Active User Modeling and Hierarchical Reinforcement Learning. arXiv preprint arXiv:1012.2599, 2010.

[51] Wu J, Chen XY, Zhang H, et al. Hyperparameter optimization for machine learning models based on Bayesian optimization. *Journal of Electronic Science and Technology* 2019; 17: 26–40.

[52] Victoria AH, Maragatham G. Automatic tuning of hyperparameters using Bayesian optimization. *Evol Syst* 2021; 12: 217–223.

[53] Betts JT. *Practical Methods for Optimal Control and Estimation Using Nonlinear Programming*. Society for Industrial and Applied Mathematics, 2010.

[54] Dembia CL, Bianco NA, Falisse A, et al. OpenSim Moco: Musculoskeletal optimal control. *PLoS Comput Biol* 2020; 16: e1008493.

[55] Kelly M. An Introduction to Trajectory Optimization: How to Do Your Own Direct Collocation. *SIAM Rev* 2017; 59: 849–904.

[56] Bohannon RW, Barreca SR, Shove ME, et al. Documentation of daily sit-to-stands performed by community-dwelling adults. *Physiother Theory Pract* 2008; 24: 437–442.

[57] Dall PM, Kerr A. Frequency of the sit to stand task: An observational study of free-living adults. *Appl Ergon* 2010; 41: 58–61.

[58] Agrawal V, Gailey R, Gaunaurd I, et al. Weight distribution symmetry during the sit-to-stand movement of unilateral transtibial amputees. *Ergonomics* 2011; 54: 656–664.

[59] Özyürek S, Demirbüken İ, Angın S. Altered movement strategies in sit-to-stand task in persons with transtibial amputation. *Prosthet Orthot Int* 2014; 38: 303–309.

[60] Kuželički J, Žefran M, Burger H, et al. Synthesis of standing-up trajectories using dynamic optimization. *Gait Posture* 2005; 21: 1–11.

[61] Willson A. *A Quasi-Passive Biarticular Prosthesis and Novel Musculoskeletal Model for Transtibial Amputees*. University of Washington, 2017.

[62] Miller RH, Russell Esposito E. Transtibial limb loss does not increase metabolic cost in three-dimensional computer simulations of human walking. *PeerJ* 2021; 9: e11960.

[63] Russell Esposito E, Miller RH. Maintenance of muscle strength retains a normal metabolic cost in simulated walking after transtibial limb loss. *PLoS One* 2018; 13: e0191310.

[64] Falisse A, Serrancolí G, Dembia CL, et al. Rapid predictive simulations with complex musculoskeletal models suggest that diverse healthy and pathological human gaits can emerge from similar control strategies. *J R Soc Interface* 2019; 16: 20190402.

[65] Ackermann M, van den Bogert AJ. Optimality principles for model-based prediction of human gait. *J Biomech* 2010; 43: 1055–60.

[66] Hu Y, Nori F, Mombaur K. Squat motion generation for the humanoid robot iCub with Series Elastic Actuators. In: *2016 6th IEEE International Conference on*

Biomedical Robotics and Biomechatronics (BioRob). IEEE, 2016, pp. 207–212.

[67] Ding Z, Henson DP, Sivapuratharasu B, et al. The effect of muscle atrophy in people with unilateral transtibial amputation for three activities: Gait alone does not tell the whole story. *J Biomech* 2023; 149: 111484.

[68] MELZER I, YEKUTIEL M, SUKENIK S. Comparative Study of Osteoarthritis of the Contralateral Knee Joint of Male Amputees Who Do and Do Not Play Volleyball. *J Rheumatol* 2001; 28: 169–172.

[69] Ding Z, Jarvis HL, Bennett AN, et al. Higher knee contact forces might underlie increased osteoarthritis rates in high functioning amputees: A pilot study. *J Orthop Res* 2021; 39: 850–860.

[70] Uchida TK, Delp SL. *Biomechanics of Movement: The Science of Sports, Robotics, and Rehabilitation*. Cambridge, MA: The MIT Press, 2021.

[71] Crosbie J, Green T, Refshauge K. Effects of reduced ankle dorsiflexion following lateral ligament sprain on temporal and spatial gait parameters. *Gait Posture* 1999; 9: 167–172.

[72] Bennell K, Talbot R, Wajswelner H, et al. Intra-rater and inter-rater reliability of a weight-bearing lunge measure of ankle dorsiflexion. *Aust J Physiother* 1998; 44: 175–180.

[73] Rajagopal A, Dembia CL, DeMers MS, et al. Full-Body Musculoskeletal Model for Muscle-Driven Simulation of Human Gait. *IEEE Trans Biomed Eng* 2016; 63: 2068–79.

[74] Farsetti P, Caterini R, Potenza V, et al. Immediate continuous passive motion after internal fixation of an ankle fracture. *J Orthop Traumatol* 2009; 10: 63–69.

[75] Escamilla RF. Knee biomechanics of the dynamic squat exercise. *Med Sci Sports Exerc* 2001; 33: 127–41.

[76] Hidayah R, Sui D, Wade KA, et al. Passive knee exoskeletons in functional tasks: Biomechanical effects of a *SpringExo* coil-spring on squats. *Wearable Technologies* 2021; 2: e7.

[77] Gams A, Petric T, Debevec T, et al. Effects of Robotic Knee Exoskeleton on Human Energy Expenditure. *IEEE Trans Biomed Eng* 2013; 60: 1636–1644.

[78] Mason S, Righetti L, Schaal S. Full dynamics LQR control of a humanoid robot: An experimental study on balancing and squatting. In: *2014 IEEE-RAS International Conference on Humanoid Robots*. IEEE, 2014, pp. 374–379.

[79] Zheng S, Li T, Li Q, et al. Different Phases in Manual Materials Handling Have Different Performance Criteria: Evidence From Multi-Objective Optimization. *J Biomech Eng* 2022; 144(9): 091004.

[80] Mombaur K, Truong A, Laumond J-P. From human to humanoid locomotion—an inverse optimal control approach. *Auton Robots* 2010; 28: 369–383.

[81] Becanovic F, Bonnet V, Dumas R, et al. Force Sharing Problem During Gait Using Inverse Optimal Control. *IEEE Robot Autom Lett* 2023; 8: 872–879.

[82] Sinha A, Malo P, Deb K. A Review on Bilevel Optimization: From Classical to Evolutionary Approaches and Applications. *IEEE Trans Evol Comput* 2018; 22:

276–295.

[83] Snoek J, Larochelle H, Adams RP. Practical Bayesian Optimization of Machine Learning Algorithms. arXiv preprint arXiv:1206.2944, 2012.

[84] Bull AD. Convergence rates of efficient global optimization algorithms. arXiv preprint arXiv: 1101.3501, 2011.

[85] Gelbart MA, Snoek J, Adams RP. Bayesian Optimization with Unknown Constraints. arXiv preprint arXiv:1403.5607, 2014.

[86] Johnson M, Aghasadeghi N, Bretl T. Inverse optimal control for deterministic continuous-time nonlinear systems. In: *52nd IEEE Conference on Decision and Control*. IEEE, 2013, pp. 2906–2913.

[87] Pandy MG, Lin Y-C, Kim HJ. Muscle coordination of mediolateral balance in normal walking. *J Biomech* 2010; 43: 2055–2064.